行政院國家科學委員會專題研究計畫 成果報告

抑制克雷伯氏菌複製叉重啟活性之研究
研究成果報告(完整版)

計 畫 類 別 ：個別型
計 畫 編 號 ：NSC 100-3112-B-040-001-
執 行 期 間 ：100 年 05 月 01 日至 101 年 07 月 31 日
執 行 單 位 ：中山醫學大學生物醫學科學學系（所）

計 畫 主 持 人：黃晟洋

計畫參與人員：碩士級-專任助理人員：黃彥華
碩士級-專任助理人員：陳彥君
碩士班研究生-兼任助理人員：黃彥華
碩士班研究生-兼任助理人員：莊立勤
大專生-兼任助理人員：林欣賢
大專生-兼任助理人員：宋秋嫻
大專生-兼任助理人員：何雅燁
大專生-兼任助理人員：廖仁弗
大專生-兼任助理人員：賴瑩縈
大專生-兼任助理人員：丁之絜

報 告 附 件 ：出席國際會議研究心得報告及發表論文

公 開 資 訊 ：本計畫可公開查詢

中 華 民 國 101 年 11 月 05 日

中 文 摘 要 ： 細菌利用 DNA 複製重啟之引子合成體 (DNA replication restart primosome) 來重新啟動 DNA 複製對其存活而言已被確認為必需，此蛋白質-核酸複合體包含八個蛋白質有次序的互相結合於停滯的複製叉上，分別為 PriA、PriB、PriC、SSB、DnaB、DnaC、DnaG 與 DnaT。克雷伯氏肺炎桿菌是台灣最常被分離出的病原菌之一，為了對抗被克雷伯氏肺炎桿菌感染的威脅，阻斷其 DNA 複製叉重啟的能力也許可行。在此計劃我們找到類黃酮具有抑制細菌引子合成體活性的潛力，而這個一年期的計畫目前已發表 4 篇 SCI 論文以及一篇在專書內之章節。希望這些結果在未來能對各種抗藥性細菌提供初步的標靶藥物設計之建議。

中文關鍵詞： 克雷伯氏肺炎桿菌，PriA，PriB，PriC，SSB，DnaB，DnaC，DnaG，DnaT，引子合成體，DNA 複製重啟體，複製重啟，複製叉，類黃酮，以結構為依據的藥物設計，單股 DNA 結合模式，蛋白質-蛋白質交互作用，蛋白質-DNA 交互作用，巨分子組裝，蛋白質結晶結構

英 文 摘 要 ： It has been recognized that the ability of DNA replication restart primosome is essential for bacterial survival. These primosomal proteins, PriA, PriB, PriC, SSB, DnaB, DnaC, DnaG and DnaT, sequentially associated together and then restart arrested DNA replication forks. Klebsiella pneumoniae (KP) is one of the most commonly isolated bacterial pathogens in Taiwan. To combat the threat of KP infections, blocking the restart of replication fork of KP may be useful. In this project, we have found that several flavonols can inhibit the primosomal activity, and these results have been published in 4 SCI papers and 1 chapter in a book. We hope these results will provide a new target for drug design for bacterial antibiotics resistances.

英文關鍵詞： Klebsiella pneumoniae, PriA, PriB, PriC, SSB, DnaB, DnaC, DnaG, DnaT, primosome, DNA replication restart primosome, DNA replication restart, replication forks, flavonols, structure-based drug design, single-strand DNA binding mode, protein-protein interactions, protein-DNA interactions, macromolecular assembly, protein crystal structure.

目　　錄

一、計畫摘要

1a. 中文摘要

關鍵詞：克雷伯氏肺炎桿菌，PriA，PriB，PriC，SSB，DnaB，DnaC，DnaG，DnaT，引子合成體，DNA 複製重啟體，複製重啟，複製叉，類黃酮，以結構為依據的藥物設計，單股 DNA 結合模式，蛋白質-蛋白質交互作用，蛋白質-DNA 交互作用，巨分子組裝，蛋白質結晶結構。

細菌利用 DNA 複製重啟之引子合成體 (DNA replication restart primosome) 來重新啟動 DNA 複製對其存活而言已被確認為必需，此蛋白質-核酸複合體包含八個蛋白質有次序的互相結合於停滯的複製叉上，分別為 PriA、PriB、PriC、SSB、DnaB、DnaC、DnaG 與 DnaT。克雷伯氏肺炎桿菌是台灣最常被分離出的病原菌之一，為了對抗被克雷伯氏肺炎桿菌感染的威脅，阻斷其 DNA 複製叉重啟的能力也許可行。在此計劃我們找到類黃酮具有抑制細菌引子合成體活性的潛力，而這個一年期的計畫目前已發表 4 篇 SCI 論文以及一篇在專書內之章節。希望這些結果在未來能對各種抗藥性細菌提供初步的標靶藥物設計之建議。

一、計畫摘要

1b. 英文摘要

Keywords: *Klebsiella pneumoniae*, PriA, PriB, PriC, SSB, DnaB, DnaC, DnaG, DnaT, primosome, DNA replication restart primosome, DNA replication restart, replication forks, flavonols, structure-based drug design, single-strand DNA binding mode, protein-protein interactions, protein-DNA interactions, macromolecular assembly, protein crystal structure.

It has been recognized that the ability of DNA replication restart primosome is essential for bacterial survival. These primosomal proteins, PriA, PriB, PriC, SSB, DnaB, DnaC, DnaG and DnaT, sequentially associated together and then restart arrested DNA replication forks. *Klebsiella pneumoniae* (KP) is one of the most commonly isolated bacterial pathogens in Taiwan. To combat the threat of KP infections, blocking the restart of replication fork of KP may be useful. In this project, we have found that several flavonols can inhibit the primosomal activity, and these results have been published in 4 SCI papers and 1 chapter in a book. We hope these results will provide a new target for drug design for bacterial antibiotics resistances.

二、背景介紹

2a. 前言

2b. 研究目的

2c. 文獻探討

This report focuses on "**Characterization of flavonol inhibition of DnaB helicase: real-time monitoring, structural modeling, and proposed mechanism**."

DNA helicases are motor proteins that play essential roles in DNA replication, repair, and recombination [1,2]. In the replicative hexameric helicase, the fundamental reaction is the unwinding of double-stranded DNA (dsDNA) into single-stranded DNA (ssDNA) intermediates to provide ssDNA templates for DNA polymerases at the replication fork [3]. The most widely studied replicative helicase is *Escherichia coli* DnaB helicase (*Ec*DnaB) [4]. *Ec*DnaB participates in the initiation of DNA replication once the *oriC* region of *E. coli* is bound by the DnaA initiator protein [5,6]. It continues to act during the priming and elongation phases of DNA replication, and it catalyzes ATP hydrolysis and migrates on the DNA template with a strict 5′-3′ direction [5]. ATP hydrolysis may drive the movement of the helicase toward the 3′ end of the lagging strand [7].

Currently, infections occur that are resistant to all antibacterial options [8]. Few therapies are effective against the six antibiotic-resistant ESKAPE pathogens (*Enterococcus faecium*, *Staphylococcus aureus*, *Klebsiella pneumoniae*, *Acinetobacter baumannii*, *Pseudomonas aeruginosa*, and *Enterobacter species*) [9,10]. *K. pneumoniae* (*Kp*) is a ubiquitous opportunistic pathogen that causes severe diseases such as septicemia, pneumonia, urinary tract infections, and soft tissue infections [11]. Since DnaB helicase is required for DNA replication, blocking the activity of DnaB helicase would be detrimental to bacterial survival [12]. In addition, because the structure and function between eukaryotic and prokaryotic DnaB-like helicases are different [5,12], the *K. pneumoniae* DnaB helicase (*Kp*DnaB) and other bacterial DnaB-like proteins may be a promising target in developing antibiotics.

Previously, we determined the three-dimensional structures of the *Geobacillus kaustophilus* DnaB-family protein (*Gk*DnaB) and its complex with ssDNA [7]. Although the overall structure of the apo and the complex forms of *Gk*DnaB is similar, the largest difference is found in their loop I region, which undergoes a strong conformational change during the helicase's action [7]. These structural and functional analyses are useful in helping our understanding of the mechanism of DNA translocation in replication forks, and the resulting information may be useful in designing compounds that target bacterial DnaB helicases. Recently, we established that the 4 flavonols (Fig. 1) myricetin (Myr), quercetin (Que), kaempferol (Kae), and galangin (Gal) can interact with *Kp*DnaB and prevent dNTP binding [13]. Flavonoids are the most common group of plant polyphenols, and are responsible for much of the flavor and color of fruits and vegetables [14]. Over 5000 different flavonoids have been described; many of these compounds display structure-dependent biological and pharmacological activities [15]. The 6 major subclasses of flavonoids are: flavonols, flavones, flavanones, flavanols, anthocyanidins, and isoflavones [14]. Flavonols, composed of 2 aromatic rings linked by a heterocyclic pyran-4-one ring, are known to have antioxidant [16], antiradical [17], and antibacterial activities [18]. In the present study, we further investigated the effect of flavonols on the inhibition of the ssDNA binding, ATPase activity, and dsDNA-unwinding activity of *Kp*DnaB. A new assay that enables the real-time measurement of DNA helicase activity was also developed. This assay may be useful for screening helicase inhibitors at high throughput.

三、研究方法

Materials.

All restriction enzymes and DNA-modifying enzymes were purchased from New England Biolabs (Ipswich, MA, USA) unless explicitly stated otherwise. All custom oligonucleotide primers were obtained from Invitrogen Corporation (Carlsbad, CA, USA). All chemicals were purchased from Sigma-Aldrich (St. Louis, MO, USA) unless explicitly stated otherwise.

Protein Expression and Purification.

The encoding region of *Kp*DnaB was put on pET21e expression vector and expressed with a hexahistidine tag at the C-terminus of the recombinant protein. The pET21e vector [19] was engineered from the pET21b vector (Novagen Inc., Madison, WI, USA), to avoid having the N-terminal T7 tag fused with the gene product. Details of the construction of pET21e-*Kp*DnaB expression vector and protein purification have been described previously [13]. The purified protein was dialyzed against Buffer B (20 mM HEPES, 100 mM NaCl; pH 7.0), and concentrated to 5 mg/mL. Protein purity remained greater than 95% as determined by Coomassie-stained SDS-PAGE (Fig. 2).

Gel Shifts.

EMSA for *Kp*DnaB was carried out using the same protocol as described previously for SSB proteins [20-22], with a minor modification. ssDNA oligonucleotides were custom synthesized by MdBio, Inc., Frederick, MD. Radiolabeling was carried out with [γ^{32}P]ATP (6000 Ci/mmol; PerkinElmer Life Sciences) and T4 polynucleotide kinase (Promega, Madison, WI, USA). *Kp*DnaB (0, 90, 170, 340, 680, 1360, 2730, and 5450 nM) was incubated for 30 min at 25°C with 1.7 nM ssDNA substrate (dT30) and 16.7 μM flavonol in a total volume of 10 μL in 20 mM HEPES (pH 7.0) and 100 mM NaCl. Aliquots (5 μL) were removed from each reaction solution and added to 2 μL of gel-loading solution (0.25% bromophenol blue and 40% sucrose, w/v). The resulting samples were resolved on a native 8% polyacrylamide gel (8.3 × 7.3 cm) at 4°C in TBE buffer (89 mM Tris borate and 1 mM EDTA) for 1 h at 100 V and visualized by phosphorimaging. The phosphor storage plate was scanned, and the data for complexed and free DNA bands were digitized for quantitative analysis. The ssDNA binding ability ($K_{d,app}$ value) for the protein was estimated from the protein concentration that binds 50% of the input DNA [23-25]. Each K_d value is calculated as the average of at least three measurements ± S.D.

FRET-based dsDNA Unwinding Activity Assay.

To monitor the 5′-3′ DNA helicase activity of *Kp*DnaB in real-time, we developed an assay on the basis of fluorescence resonance energy transfer (FRET) method. The dsDNA substrate was prepared with the fluorescent strand, 5′-TAGTACCGCCACCCTCAGAACC-3′ with Alexa Fluor 488 (maximum excitation/emission = 495/519 nm) coupled to the 5′-end, and the complementary quencher strand, 3′-ATCATGGCGGTGGGAGTCTTGGTTTTTTTTTTTTTT-5′ with BHQ1 coupled to the 3′-end, at a 1:1.2 concentration ratio. The dsDNA substrate was formed in 20 mM HEPES (pH 7.0) and 100 mM NaCl, by brief heating at 95 °C for 5 min and then followed by slow cooling to room temperature overnight. The fluorescence helicase assay was performed in 20 mM HEPES (pH 7.0), 100 mM NaCl, 3 mM $MgCl_2$, 50 nM dsDNA substrate, and 5 mM ATP in 2.0 mL of reaction volume. The unwinding reaction was started by adding *Kp*DnaB (200 nM) and was carried out at 37 °C for 60 min using a spectrofluorimeter (Hitachi F-2700; Hitachi High-Technologies, Tokyo, Japan). The fluorescence intensity was recorded every 5 s. The DNA helicase activity was calculated as the initial reaction velocity from the linear part of the progress curve using the linear regression method.

ATPase Activity Assay.

The protocol for measuring the ATPase activity of purified *Kp*DnaB is based on the colorimetric determination of inorganic phosphate (Pi) released by the hydrolysis of ATP [26]. The ATPase activity assay for *Kp*DnaB (20–50 ng) was performed in 20 mM HEPES (pH 7.0),

100 pmol of X-ssDNA, 10 μM flavonol, 100 mM NaCl, 3 mM $MgCl_2$, and 5 mM ATP in 100 μL of reaction volume. Liberated Pi was detected using ammonium molybdate and malachite green solutions, and absorbance was measured at 610 nm using a UV/vis spectrophotometer (Thermo Scientific Helios Omega; Thermo Fisher Scientific Inc., Waltham, MA, USA). The ATPase activity of *Kp*DnaB was calibrated with sodium phosphate (NaH_2PO_4) of known concentrations.

Bioinformatics.

The amino acid sequences of *Kp*DnaB, *Ec*DnaB, *Gs*DnaB, *Gk*DnaB were aligned using CLUSTALW2 [27]. The model of *Kp*DnaB was built from the coordinates of 2R6D (crystal structure of *Gs*DnaB), 2VYF (crystal structure of *Gk*DnaB), and 2VYE (crystal structure of *Gk*DnaB in complex with ssDNA) by using SWISS-MODEL, http://swissmodel.expasy.org/ [28]. The coordinate and topology file of the flavonols, Myr, Que, Kae, and Gal, was found in DrugBank, http://drugbank.ca/ [29]. The flavonol was individually computationally docked into the three-dimensional models of *Kp*DnaB by using PatchDock, http://bioinfo3d.cs.tau.ac.il/PatchDock/ [30]. The structures were visualized by using the program PyMol.

四、結果與討論

Sequence Analysis

The gene *KPN04439*, encoding *K. pneumoniae* DnaB helicase, was initially found using a database search through the National Center for Biotechnology Information (NCBI). Based on the known nucleotide sequence, the predicted *Kp*DnaB monomer protein has a length of 471 amino acid residues and a molecular mass of 52.5 kDa, with a pI of 4.93. Analysis of the primary structure of *Kp*DnaB revealed the presence of the putative Walker A motif (aa 232–238), Walker B motif (aa 340–343), ATP binding sites (aa 237–238, 343, 384, 420, 442, and 453), and DNA binding sites (348–349, 356–358, 383–391, 419–420, and 432–433); these are common in all known DnaB helicases. Figure 3 shows an alignment of the amino acid sequences of *K. pneumoniae* [13], *E. coli* [31], *Geobacillus stearothermophilus* [32], and *Geobacillus kaustophilus* DnaB helicases [7]; their ATP (boxed) and DNA binding sites (shaded in gray) are highly conserved.

ssDNA-dependent ATPase Activity of KpDnaB.

The ATPase activity of purified *Kp*DnaB is based on the vanadate-sensitive colorimetric determination of inorganic phosphate released by the hydrolysis of ATP [26]. Figure 4A shows a standard linear regression curve generated by plotting the optical density (OD) at 610 nm against the concentrations of sodium phosphate (NaH_2PO_4). After some preliminary experiments to establish a suitable range of concentrations for the reagents (including *Kp*DnaB) used for the assay, 3 mM $MgCl_2$, 5 mM ATP, 10 μM flavonol, and 20–50 ng of *Kp*DnaB were chosen for analysis of inhibition of *Kp*DnaB ATPase activity by the flavonol. In the absence of the flavonol and ϕX-ssDNA, the specific activity of *Kp*DnaB was 0.42 ± 0.09 $\mu mol \cdot min^{-1} \cdot mg^{-1}$. In the presence of ϕX-ssDNA, the specific activity of *Kp*DnaB was increased to 5.5 ± 0.6 $\mu mol \cdot min^{-1} \cdot mg^{-1}$. These data are similar to reported values for *Ec*DnaB; the activity of *Ec*DnaB is 3.3×10^5 (without M13 ssDNA) and 6.4×10^6 $pmol \cdot min^{-1} \cdot mg^{-1}$ (with M13 ssDNA), respectively [33]. Thus, the ATPase activity of *Kp*DnaB was stimulated by ssDNA, a property common to all DnaB helicases.

ATPase Activity of KpDnaB Is Inhibited by Flavonols.

Previously, we showed that the binding of *Kp*DnaB to dNTP is inhibited by the flavonols Myr, Kae, Gal, and Que [13]. Here, as shown in Fig. 4B, the ATP hydrolysis activity of *Kp*DnaB was also inhibited by the flavonols. In the presence of Myr, Que, Kae, or Gal, the specific activity of *Kp*DnaB was decreased to 59%, 75%, 65%, and 57%, respectively, meaning that Gal exhibited the strongest inhibitory effect on the ATP hydrolysis of *Kp*DnaB in the presence of ϕX-ssDNA.

Inhibitory Effects of Flavonols on ssDNA Binding of KpDnaB.

To investigate whether the ssDNA-binding ability of *Kp*DnaB is inhibited by the flavonol, we used EMSA to study the binding of *Kp*DnaB to dT30 (Fig. 5) when mixed with Myr, Que, Kae, or Gal. In the absence of any flavonol, *Kp*DnaB formed a stable complex with dT30, as shown by electrophoresis (Fig. 5A). In the presence of 16.7 μM Gal (Fig. 5B), Kae (Fig. 5C), Que (Fig. 5D), or Myr (Fig. 5E), *Kp*DnaB still bound to dT30, but the binding activity was slightly decreased. The apparent dissociation constant ($K_{d,app}$) values of *Kp*DnaB bound to dT30 in the absence of any flavonol or presence of Myr, Que, Kae, or Gal, as determined from the titration curves, were 0.97 ± 0.07, 1.11 ± 0.05, 1.03 ± 0.07, 1.10 ± 0.05, and 1.03 ± 0.06 μM, respectively. It should be noted that the observed inhibition was dependent on protein concentration (Fig. 5F); the disruption of formation of the *Kp*DnaB-dT30 complex did disappear when its concentration was increased to 2.72 μM, a value that the [flavonol]/[*Kp*DnaB monomer] ratio is ~6.1 (16.7/2.73 = 6.14).

Real-time Monitoring of KpDnaB Helicase Activity Based on FRET.

To investigate whether the helicase activity of *Kp*DnaB is also inhibited by flavonols, the fluorescence helicase assay was carried out in the absence or presence of Myr or Gal. This assay,

modified from that for HCV NS3 3′–5′ RNA helicase [34], was found to be useful for *Kp*DnaB. The dsDNA substrate was prepared by annealing 2 oligonucleotides, a 5′ fluorophore-labeled (Alexa Fluor 488) 22-nucleotide donor and a 3′ quencher-labeled (BHQ1) 36-nucleotide quencher (Fig. 6A). When the dsDNA substrate is unwound by the helicase, the fluorophore (F) emits upon its release from the quencher (Q). The fluorescence quenching efficiency (signal-to-background ratio) for this substrate was >90%, suggesting high sensitivity for monitoring helicase activity, similar to that for HCV NS3 RNA helicase [34].

Because of its high inhibitory effects on the ATPase activity of *Kp*DnaB (Fig. 4B), Myr and Gal were selected for this assay. When *Kp*DnaB was added, fluorescence was continuously emitted, whereas no increase in fluorescence occurred in the absence of *Kp*DnaB (as the negative control). These results indicate that the observed fluorescence emission arose from the unwinding of the dsDNA substrate by purified *Kp*DnaB (Fig. 6B). When assaying the helicase activity of *Kp*DnaB in the presence of Myr or Gal, a linear increase in fluorescence emission was also observed. In addition, the initial velocity for *Kp*DnaB helicase activity was nearly identical with or without flavonol (~1×10^{-3} fluorescence intensity/s). In contrast, unlike fluorescence emission of *Kp*DnaB that continued to increase, the fluorescence emission of *Kp*DnaB assayed in the presence of the flavonol Myr or Gal soon reached its maximal point. The magnitude of fluorescence activity for *Kp*DnaB was in the following order: no flavonol added > Myr present > Gal present.

Homology Modeling.

The most thoroughly studied replicative DnaB helicase from bacteria is that of *E. coli*. Although *Kp*DnaB shows a high degree of sequence identity with *Ec*DnaB, its crystal structure is not yet reported. To deeply understand the structure-function relationship of the flavonol-*Kp*DnaB-ssDNA complex(es), we decided to model its three-dimensional structure by homology modeling. The model of *Kp*DnaB was built from the coordinates of 2R6D (crystal structure of *Gs*DnaB), 2VYF (crystal structure of *Gk*DnaB) and 2VYE (crystal structure of *Gk*DnaB in complex with ssDNA) by using SWISS-MODEL, http://swissmodel.expasy.org/ [28]. *Kp*DnaB and *Gk*DnaB share 47% identity and 69% similarity, and *Kp*DnaB and *Gs*DnaB share 46% identity and 69% similarity respectively, in the amino acid sequences level. The three-dimensional model of the hexameric *Kp*DnaBs all forms a ring structure (Fig. 7A), of which the loop I position in *Gk*DnaB-ssDNA complex based model was different. We propose that, as in the *Gk*DnaB complexes [7], loop I of *Kp*DnaB undergoes a conformational change, and thereby playing an important role in stabilizing DNA binding. It should be noted that the NTP-binding site, Walker A and B motifs, is adjacent to the DNA interaction site loop I (Fig. 7B).

Docking Study Using PatchDock.

The flavonol, found in DrugBank, was individually computationally docked into the three-dimensional models of *Kp*DnaB by using PatchDock, http://bioinfo3d.cs.tau.ac.il/PatchDock/ [30]. After uploading the coordinate and topology file of the flavonol and *Kp*DnaB, the docking was automatically performed. The docking results for *Kp*DnaB (*Gk*DnaB based model) interacting with Myr or Que are shown in Fig. 8 and Table 1. Myr (Fig. 8A) and Que (Fig. 8B) were found to be docked in the ATP-binding pocket of *Kp*DnaB; however, there were also a few binding poses docked outside the pocket (Fig. 8B). Despite a similar structure, these flavonols were found to be docked with distinct binding poses in the ATP-binding pocket of both DNA-unbound and DNA-bound models of *Kp*DnaB. For example, the binding pose of *Kp*DnaB to Myr is different from that of Que (Fig. 9A). Que, the compound with 2 hydroxyl groups on the B ring, interacts with L214 and N215, whereas Myr (3 hydroxyl groups) interacts with L214, N247, and F460. In addition, the same compound is also found to be docked in different positions of the ATP-binding pocket of both DNA-unbound and DNA-bound models of *Kp*DnaB. For instance, Myr interacts with L214, N247, and F460 in the DNA-unbound model, and interacts with L214 and N462 in the DNA-bound model of *Kp*DnaB, respectively (Fig. 9B). Generally, L214 is a key residue in all DNA-unbound and DNA-bound modeled structures

regardless of which flavonol was used.

Discussion.

The development of clinically useful small molecule antibiotics has been a seminal event in the world of infectious diseases [35]. DNA replication is one of the most basic biological functions and should be a prime target in antibiotic development. For example, some novel inhibitors were discovered to target topoisomerase [36,37], DNA gyrase [38], RNA polymerase [39], helicase-primase [40], and retroviral reverse transcriptase [41,42]. Since DNA helicases are important components of the cellular replication machinery in all organisms, inhibition of helicase activity would be detrimental to bacterial survival as well. Previously, we have shown that some flavonoid compounds can directly bind to *Kp*DnaB and inhibit its binding ability to nucleotides, thus interfering with the growth of *K. pneumoniae* [13]. Flavonoids [14] are the most common group of plant polyphenols with antioxidant [16], antiradical [17], and antibacterial activities [18]. It is now clear that some flavonoids are ATP-inhibiting agents as competitors for ATP-binding proteins. For example, several flavonoid derivatives have been developed as therapeutic agents for cancer [43]. In this study, we used several assays to analyze the effects of 4 flavonols, namely, Myr, Que, Kae, and Gal—which contain different numbers of hydroxyl substituents on the aromatic rings—on the ssDNA binding, ATP hydrolysis, and dsDNA unwinding abilities of *Kp*DnaB. For the first time, our results demonstrated that these flavonols were capable of inhibiting the unwinding activity of the helicase.

DnaB helicase is an ssDNA-dependent ATPase. Previously, we showed that the binding of *Kp*DnaB to dNTP is inhibited by the flavonols Myr, Kae, Gal, and Que. This study further investigated the flavonol-mediated inhibition of *Kp*DnaB binding to dNTP, which may have led to the associated decrease in ATPase activity in the presence of ssDNA (Fig. 4). The ATP-hydrolyzing activity of *Kp*DnaB was inhibited by flavonols in the following order of decreasing efficiency: Gal > Myr > Kae > Que. Although it is well established that flavonoids have several hydroxyl groups, and thus have marked potentials to bind any protein, the strength of inhibition of *Kp*DnaB ATP-hydrolyzing activity did not correlate with the number of hydroxyl substituents on the flavonol aromatic rings. In addition, the structural model of *Kp*DnaB shows that these flavonols bind to *Kp*DnaB with distinct binding poses in the ATP-binding pocket (Fig. 9). This situation is also found in several ATP-binding proteins that bind to different flavonoids. Crystal structures of PIM1 kinase in complex with quercetagetin and Myr reveal 2 distinct binding poses in the ATP-binding pocket, namely, orientations I and II [44]. Myr, adopting orientation II, has flipped 180^{o} in PIM1 kinase, in contrast to quercetagetin (orientation I), such that the B ring is oriented toward the entrance of the ATP pocket. These orientations in PIM1 are also found to closely resemble those of Que and Myr in phosphatidylinositol 3-kinase [45]. Although the ATP-binding pocket in these proteins, including *Kp*DnaB, is different, cases of PIM1 and phosphatidylinositol 3-kinase with different binding poses, are very similar to that of *Kp*DnaB. Despite a very similar structure, flavonols may bind to *Kp*DnaB by using different mechanisms, as shown in the structural models (Figs. 8 and 9). This may explain why the strength of inhibition in *Kp*DnaB ATPase activity was not correlated with the number of hydroxyl substituents on the flavonol aromatic rings.

Other studies showed that Myr non-competitively inhibits *E. coli* DnaB helicase with an IC_{50} of approximately 10 μM [46]; however, we have recently discovered that Gal, Kae, Que, and Myr can inhibit dNTP binding to *Kp*DnaB, indicating a specific inhibitory process. Furthermore, these flavonols can be docked into the *Kp*DnaB ATP-binding pocket. It is not known whether this disparity is due to the inherent differences among the species, or an alternative (allosteric) binding site(s) in DnaB helicase. However, the docking results also show that a few binding poses of the flavonol outside the ATP-binding pocket (Fig. 8), suggesting that there may be more than one site for flavonol binding in the DnaB helicase. This may explain why Myr non-competitively inhibits *Ec*DnaB. In addition, we also showed flavonol-mediated inhibition of *Kp*DnaB-ssDNA complex formation, which depended on the [flavonol]/[*Kp*DnaB monomer] ratio; at a ~6 fold ratio, the inhibitory effect did disappear (Fig. 5). Since these flavonols inhibited not only the ATPase activity of *Kp*DnaB but also the ssDNA-binding ability, we believe that there may be

more than one site in *Kp*DnaB for flavonol binding. However, this speculation must be confirmed by further biochemical experiments.

In this study, we describe a new in vitro fluorescence assay for measuring 5′–3′ DNA helicase activity by using dsDNA substrate (Fig. 6). Alexa Fluor 488 and BHQ1 were selected as the fluorophore-quencher pair. This assay enables the real-time, high-throughput measurement of DNA helicase activity, and does not require time-consuming procedures like the conventional gel-based assays. For example, on the basis of this assay, we observed that the initial velocity of *Kp*DnaB for the unwinding activity assayed in the absence of the flavonol, or with Myr or Gal were very similar; however, their maximal activities were different. While fluorescence was continuously emitted without the addition of flavonol to the *Kp*DnaB solution, the fluorescence increase stopped at ~300 s and ~600 s for Myr and Gal, respectively (Fig. 6B). This real-time unwinding kinetics of the DNA helicase cannot be easily observed by the conventional gel-based assays. Our laboratory is currently screening DNA helicase inhibitors using this high-throughput method.

All DNA-unbound and DNA-bound modeled structures showed flavonols binding to *Kp*DnaB with distinct poses. However, these models all displayed a key residue involved in the flavonol binding, namely, L214. The L214 residue in DnaB helicases is highly conserved (Fig. 3), but its role has not yet been determined. On the basis of these results, we propose that these flavonols may inhibit *Kp*DnaB in 2 possible ways. First, since DnaB helicase binding to dNTP causes a large conformational change [31,47,48] to become a translocase [7], these flavonols may partially occupy the ATP-binding pocket of the DnaB helicase and inhibit conformational change, thereby causing varying degrees of inhibition. This is a possible inhibition mechanism because the L214 residue of *Kp*DnaB is not involved in ATP binding (Fig. 3), but most structural models indicate its importance in binding flavonols (Fig. 10). Second, more than one flavonol binds to *Kp*DnaB; 1 is at the active site, and the other(s) is at an unknown site. The overall inhibition possibly results from the interactions between the flavonols and the enzyme. This may be a reason why flavonols not only bind at the ATP pocket of the DNA helicase, but can also non-competitively inhibit the ATPase activity of the DNA helicase [46]. Our crystal structure of *Gk*DnaB in complex with ssDNA previously suggested that ATP hydrolysis may drive the movement of the helicase toward the 3′ end of the lagging strand [7]. In addition, the dNTP-binding site of the helicase at loop I, part of the Walker B motif, is adjacent to the DNA interaction site. In conclusion, the flavonol likely inhibits the DNA helicase (translocase) activity by affecting the ATP binding of *Kp*DnaB, to ultimately shut down and lock the enzyme in the ATP-unbound state.

References.

[1] R. Reyes-Lamothe, D. J. Sherratt, and M.C. Leake, “Stoichiometry and architecture of active DNA replication machinery in *Escherichia coli*,” *Science*, vol. 328, no. 5977, pp. 498-501, 2010.
[2] M. L. Mott and J. M. Berger, “DNA replication initiation: mechanisms and regulation in bacteria,” *Nature Reviews Microbiology*, vol. 5, no. 5, pp. 343-354, 2007.
[3] K. J. Marians, “Prokaryotic DNA replication,” *Annual Review of Biochemistry*, vol. 61, pp. 673-719, 1992.
[4] T. A. Baker and S. P. Bell, “Polymerases and the replisome: machines within machines,” *Cell*, vol. 92, no. 3, pp. 295-305, 1998.
[5] M. R. Singleton, M. S. Dillingham, and D. B. Wigley, “Structure and mechanism of helicases and nucleic acid translocases,” *Annual Review of Biochemistry*, vol. 76, pp. 23-50, 2007.
[6] S. S. Patel and K. M. Picha, “Structure and function of hexameric helicases,” *Annual Review of Biochemistry*, vol. 69, pp. 651-697, 2000.
[7] Y. H. Lo, K. L. Tsai, Y. J. Sun et al., “The crystal structure of a replicative hexameric helicase DnaC and its complex with single-stranded DNA,” *Nucleic Acids Research*, vol. 37, no. 3, pp. 804-814, 2009.
[8] H. W. Boucher, G. H. Talbot, J. S. Bradley et al., “Bad bugs, no drugs: no ESKAPE! An update from the Infectious Diseases Society of America,” *Clinical Infectious Diseases*, vol. 48, no. 1, pp. 1-12, 2009.

[9] K. K. Kumarasamy, M. A. Toleman, T. R. Walsh et al., "Emergence of a new antibiotic resistance mechanism in India, Pakistan, and the UK: a molecular, biological, and epidemiological study," *Lancet Infectious Diseases*, vol. 10, no. 9, pp. 597-602, 2010.
[10] K. Bush, "Alarming beta-lactamase-mediated resistance in multidrug-resistant *Enterobacteriaceae*," *Current Opinion in Microbiology*, vol. 13, no. 5, pp. 558-564, 2010.
[11] R. Podschun and U. Ullmann, "*Klebsiella* spp. as nosocomial pathogens: epidemiology, taxonomy, typing methods, and pathogenicity factors," *Clinical Microbiology Reviews*, vol. 11, no. 4, pp. 589-603, 1998.
[12] P. Soultanas, "The bacterial helicase-primase interaction: a common structural/functional module," *Structure*, vol. 13, no. 6, pp. 839-844, 2005.
[13] C. C. Chen and C. Y. Huang, "Inhibition of *Klebsiella pneumoniae* DnaB helicase by the flavonol galangin," *Protein Journal*, vol. 30, no. 1, pp. 59-65, 2011.
[14] J. A. Ross and C. M. Kasum, "Dietary flavonoids: bioavailability, metabolic effects, and safety," *Annual Review of Nutrition*, vol. 22, pp. 19-34, 2002.
[15] F. Teillet, A. Boumendjel, J. Boutonnat, and X. Ronot, "Flavonoids as RTK inhibitors and potential anticancer agents," *Medicinal Research Reviews*, vol. 28, no. 5, pp. 715-745, 2008.
[16] K. L. Wolfe and R. H. Liu, "Structure-activity relationships of flavonoids in the cellular antioxidant activity assay," *Journal of agricultural and food chemistry*, vol. 56, no. 18, pp. 8404-8411, 2008.
[17] S. Burda and W. Oleszek, "Antioxidant and antiradical activities of flavonoids," *Journal of agricultural and food chemistry*, vol. 49, no. 6, pp. 2774-2779, 2001.
[18] T. P. Cushnie and A. J. Lamb, "Antimicrobial activity of flavonoids," *International journal of antimicrobial agents*, vol. 26, no. 5, pp. 343-356, 2005.
[19] C. C. Wang, H. W. Tsau, W. T. Chen, and C.Y. Huang, "Identification and characterization of a putative dihydroorotase, KPN01074, from *Klebsiella pneumoniae*," *Protein Journal*, vol. 29, no. 6, pp. 445-452, 2010.
[20] H. C. Jan, Y. L. Lee, and C. Y. Huang, "Characterization of a single-stranded DNA-binding protein from *Pseudomonas aeruginosa* PAO1," *Protein Journal*, vol. 30, no. 1, pp. 20-26, 2011.
[21] Y. H. Huang, Y. L. Lee, and C. Y. Huang, "Characterization of a single-stranded DNA binding protein from *Salmonella enterica* Serovar Typhimurium LT2," *Protein Journal*, vol. 30, no. 2, pp. 102-108, 2011.
[22] Y. H. Huang and C. Y. Huang, "Characterization of a single-stranded DNA binding protein from *Klebsiella pneumoniae*: mutation at either Arg73 or Ser76 causes a less cooperative complex on DNA," *Genes to Cells*, vol. 17, pp. 146-157, 2012.
[23] H. C. Hsieh and C. Y. Huang, "Identification of a novel protein, PriB, in *Klebsiella pneumoniae*," *Biochemical and biophysical research communications*, vol. 404, no. 1, pp. 546-551, 2011.
[24] C. Y. Huang, C. H. Hsu, Y. J. Sun, H. N. Wu, and C. D. Hsiao, "Complexed crystal structure of replication restart primosome protein PriB reveals a novel single-stranded DNA-binding mode," *Nucleic Acids Research*, vol. 34, no. 14, pp. 3878-3886, 2006.
[25] J. H. Liu, T. W. Chang, C. Y. Huang et al., "Crystal structure of PriB, a primosomal DNA replication protein of *Escherichia coli*," *Journal of Biological Chemistry*, vol. 279, no. 48, pp. 50465-50471, 2004.
[26] P. P. Van Veldhoven and G. P. Mannaerts, "Inorganic and organic phosphate measurements in the nanomolar range," *Analytical Biochemistry*, vol. 161, no. 1, pp. 45-48, 1987.
[27] M. A. Larkin, G. Blackshields, N. P. Brown et al., "Clustal W and Clustal X version 2.0," *Bioinformatics*, vol. 23, no. 21, pp. 2947-2948, 2007.
[28] K. Arnold, L. Bordoli, J. Kopp, and T. Schwede, "The SWISS-MODEL workspace: a web-based environment for protein structure homology modelling," *Bioinformatics*, vol. 22, no. 2, pp. 195-201, 2006.
[29] C. Knox, V. Law, T. Jewison et al., "DrugBank 3.0: a comprehensive resource for 'omics' research on drugs," *Nucleic Acids Research*, vol. 39, pp. D1035-1041, 2011.
[30] D. Schneidman-Duhovny, Y. Inbar, R. Nussinov, and H.J. Wolfson, "PatchDock and SymmDock: servers for rigid and symmetric docking," *Nucleic Acids Research*, vol. 33, pp.

W363-367, 2005.
[31] A. Roychowdhury, M. R. Szymanski, M. J. Jezewska, and W. Bujalowski, “Mechanism of NTP hydrolysis by the *Escherichia coli* primary replicative helicase DnaB protein. 2. Nucleotide and nucleic acid specificities,” *Biochemistry*, vol. 48, no. 29, pp. 6730-6746, 2009.
[32] S. Bailey, W. K. Eliason, and T. A. Steitz, “Structure of hexameric DnaB helicase and its complex with a domain of DnaG primase,” *Science*, vol. 318, no. 5849, pp. 459-463, 2007.
[33] E. E. Biswas and S. B. Biswas, “Mechanism of DnaB helicase of *Escherichia coli*: structural domains involved in ATP hydrolysis, DNA binding, and oligomerization,” *Biochemistry*, vol. 38, no. 34, pp. 10919-10928, 1999.
[34] H. Tani, O. Fujita, A. Furuta et al., “Real-time monitoring of RNA helicase activity using fluorescence resonance energy transfer in vitro,” *Biochemical and biophysical research communications*, vol. 393, no. 1, pp. 131-136, 2010.
[35] A. Koul, E. Arnoult, N. Lounis, J. Guillemont, and K. Andries, “The challenge of new drug discovery for tuberculosis,” *Nature*, vol. 469, no. 7331, pp. 483-490, 2011.
[36] B. D. Bax, P. F. Chan, D. S. Eggleston et al., “Type IIA topoisomerase inhibition by a new class of antibacterial agents,” *Nature*, vol. 466, no. 7309, pp. 935-940, 2010.
[37] M. T. Black and K. Coleman, “New inhibitors of bacterial topoisomerase GyrA/ParC subunits,” *Current Opinion in Investigational Drugs*, vol. 10, no. 8, pp. 804-810, 2009.
[38] K. L. Hopkins, R. H. Davies, and E. J. Threlfall, “Mechanisms of quinolone resistance in *Escherichia coli* and *Salmonella*: recent developments,” *International journal of antimicrobial agents*, vol. 25, no. 5, pp. 358-373, 2005.
[39] A. Srivastava, M. Talaue, S. Liu et al., “New target for inhibition of bacterial RNA polymerase: 'switch region'. *Current Opinion in Microbiology*, vol. 14, no. 5, pp. 532-543, 2011.
[40] K. Chono, K. Katsumata, T. Kontani et al., “ASP2151, a novel helicase-primase inhibitor, possesses antiviral activity against varicella-zoster virus and herpes simplex virus types 1 and 2,” *Journal of antimicrobial chemotherapy*, vol. 65, no. 8, pp. 1733-1741, 2010.
[41] S. Li, T. Hattori, and E. N. Kodama, “Epigallocatechin gallate inhibits the HIV reverse transcription step,” *Antiviral Chemistry and Chemotherapy*, vol. 21, no. 6, pp. 239-243, 2011.
[42] S. C. Chu, Y. S. Hsieh, and J. Y. Lin, “Inhibitory effects of flavonoids on Moloney murine leukemia virus reverse transcriptase activity,” *Journal of natural products*, vol. 55, no. 2, pp. 179-183, 1992.
[43] M. K. Chahar, N. Sharma, M. P. Dobhal, and Y. C. Joshi, “Flavonoids: A versatile source of anticancer drugs,” *Pharmacognosy Reviews*, vol. 5, no. 9, pp. 1-12, 2011.
[44] S. Holder, M. Zemskova, C. Zhang et al., “Characterization of a potent and selective small-molecule inhibitor of the PIM1 kinase,” *Molecular Cancer Therapeutics*, vol. 6, no. 1, pp. 163-172, 2007.
[45] E. H. Walker, M. E. Pacold, O. Perisic et al, “Structural determinants of phosphoinositide 3-kinase inhibition by wortmannin, LY294002, quercetin, myricetin, and staurosporine,” *Molecular Cell*, vol. 6, no. 4, pp. 909-919, 2000.
[46] M. A. Griep, S. Blood, M. A. Larson, S. A. Koepsell, and S. H. Hinrichs, “Myricetin inhibits *Escherichia coli* DnaB helicase but not primase,” *Bioorganic and medicinal chemistry*, vol. 15, no. 22, pp. 7203-7208, 2007.
[47] M. J. Jezewska, U. S. Kim, and W. Bujalowski, “Interactions of *Escherichia coli* primary replicative helicase DnaB protein with nucleotide cofactors,” *Biophysical journal*, vol. 71, no. 4, pp. 2075-2086, 1996.
[48] M. J. Jezewska and W. Bujalowski, “Global conformational transitions in *Escherichia coli* primary replicative helicase DnaB protein induced by ATP, ADP, and single-stranded DNA binding. Multiple conformational states of the helicase hexamer,” *Journal of Biological Chemistry*, vol. 271, no. 8, pp. 4261-4265, 1996.

Figure legends

Fig. 1 Molecular structure of myricetin (Myr), quercetin (Que), kaempferol (Kae), and galangin (Gal).

Fig. 2 Coomassie Blue-stained SDS-PAGE (12%) of the purified *Kp*DnaB and molecular mass standards. The sizes of the standard proteins, from the top down, are as follows: 170, 130, 100, 70, 55, 40, 35, 25, and 15 kDa.

Fig. 3 Multiple amino acid sequence alignment of DnaB helicases. Alignment was carried out using CLUSTALW2. Amino acid residues displaying 100% homology are highlighted in red, and those displaying similarity are highlighted in blue. The amino acids that are involved in ATP binding are boxed. The amino acids that are involved in ssDNA binding are shaded in gray. For clarity, only 4 bacterial stains are shown. Abbreviations: *Kp*, *K. pneumoniae*; *Ec*, *E. coli*; *Gs*, *Geobacillus stearothermophilus* [32]; *Gk*, *Geobacillus kaustophilus* [7].

Fig. 4 ssDNA-dependent ATPase activity of *Kp*DnaB. (A) The vanadate-sensitive colorimetric determination of inorganic phosphate released by the hydrolysis of ATP. A standard linear regression curve was generated by plotting the optical density (OD) at 610 nm against the concentrations of sodium phosphate (NaH_2PO_4). (B) ATPase activity of *Kp*DnaB is inhibited by flavonols. In the presence of Myr, Que, Kae, or Gal, the specific activity of *Kp*DnaB was decreased to 59%, 75%, 65%, and 57%, respectively.

Fig. 5 Inhibitory effects of flavonols on ssDNA binding of *Kp*DnaB. EMSA of *Kp*DnaB bound to dT30 (A) in the absence of any flavonol or presence of (B) Gal, (C) Kae, (D) Que, or (E) Myr. (F) The titration curves for ssDNA binding of *Kp*DnaB. The apparent dissociation constant ($K_{d,app}$) values of *Kp*DnaB bound to dT30 in the absence of any flavonol or presence of Myr, Que, Kae, or Gal, as determined from the titration curves, were 0.97 ± 0.07, 1.11 ± 0.05, 1.03 ± 0.07, 1.10 ± 0.05, and 1.03 ± 0.06 μM, respectively.

Fig. 6 Real-time monitoring of *Kp*DnaB helicase activity. (A) Schematic representation of fluorescence helicase assay based on FRET. The dsDNA substrate was prepared by annealing 2 oligonucleotides, a 5′ fluorophore-labeled (Alexa Fluor 488) 22-nucleotide donor and a 3′ quencher-labeled (BHQ1) 36-nucleotide quencher. When the dsDNA substrate is unwound by the helicase, the fluorophore (F) emits upon its release from the quencher (Q). (B) Inhibitory effects of flavonols on *Kp*DnaB helicase activity. Myr and Gal were selected for this assay.

Fig. 7 Homology modeling. (A) The three-dimensional models of the hexameric *Kp*DnaB form a ring structure. The monomers are colored differently. ssDNA is colored in black. (B) The structural model of the *Kp*DnaB-ssDNA complex. The NTP-binding site, Walker A and B motifs, is adjacent to the DNA interaction site loop I (green). There are synergistic effects between the nucleotide and ssDNA binding [7]. The Walker A and B motifs are colored in red and blue, respectively. ssDNA is colored in gold.

Fig. 8 Representation of the docking models from PatchDock. The six docking models with the highest score for *Kp*DnaB (*Gk*DnaB based model) interacting with (A) Myr and (B) Que are shown. The Walker A motif (aa 232-238), a nucleotide binding site, is colored in red.

Fig. 9 (A) The binding pose of *Kp*DnaB to Myr is different from that of Que. Que interacts with L214 and N215, whereas Myr interacts with L214, N247, and F460. (B) Myr was docked in different positions of the ATP-binding pocket of both DNA-unbound and DNA-bound models of *Kp*DnaB. Myr interacts with L214, N247, and F460 in the DNA-unbound model, and interacts with L214 and N462 in the DNA-bound model of *Kp*DnaB, respectively.

Table 1. Docking results of *Kp*DnaB with Myr and Que from PatchDock.

	Score	
Solution Number	Myr	Que
1	4142	4170
2	3938	4096
3	3802	3994
4	3796	3962
5	3752	3766
6	3722	3694

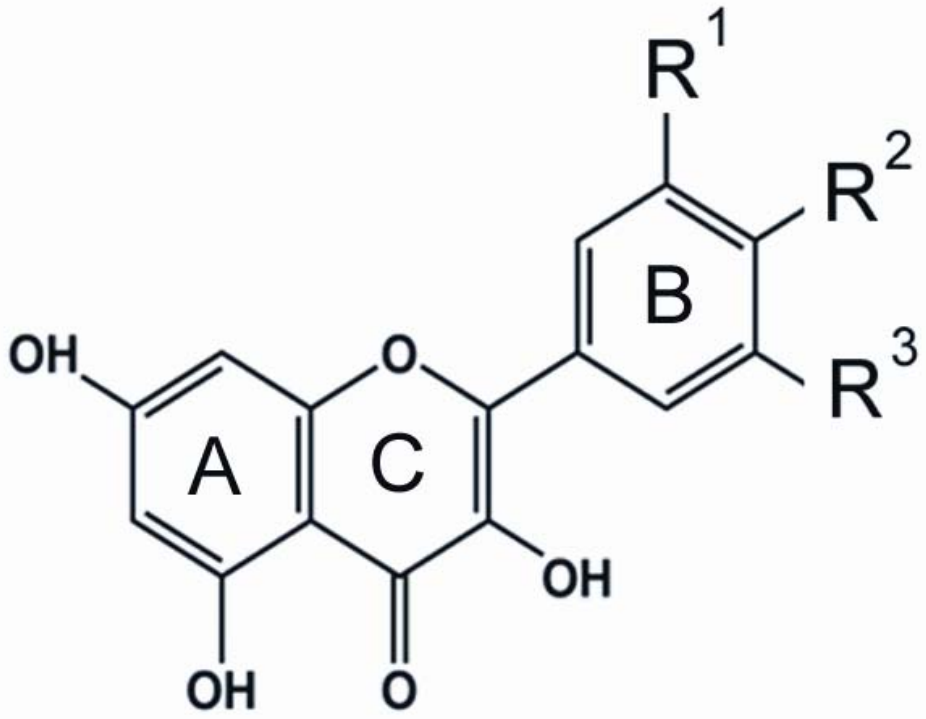

	R^1	R^2	R^3
Galangin	H	H	H
Kaempferol	H	OH	H
Quercetin	OH	OH	H
Myricetin	OH	OH	OH

Figure 1

Figure 2

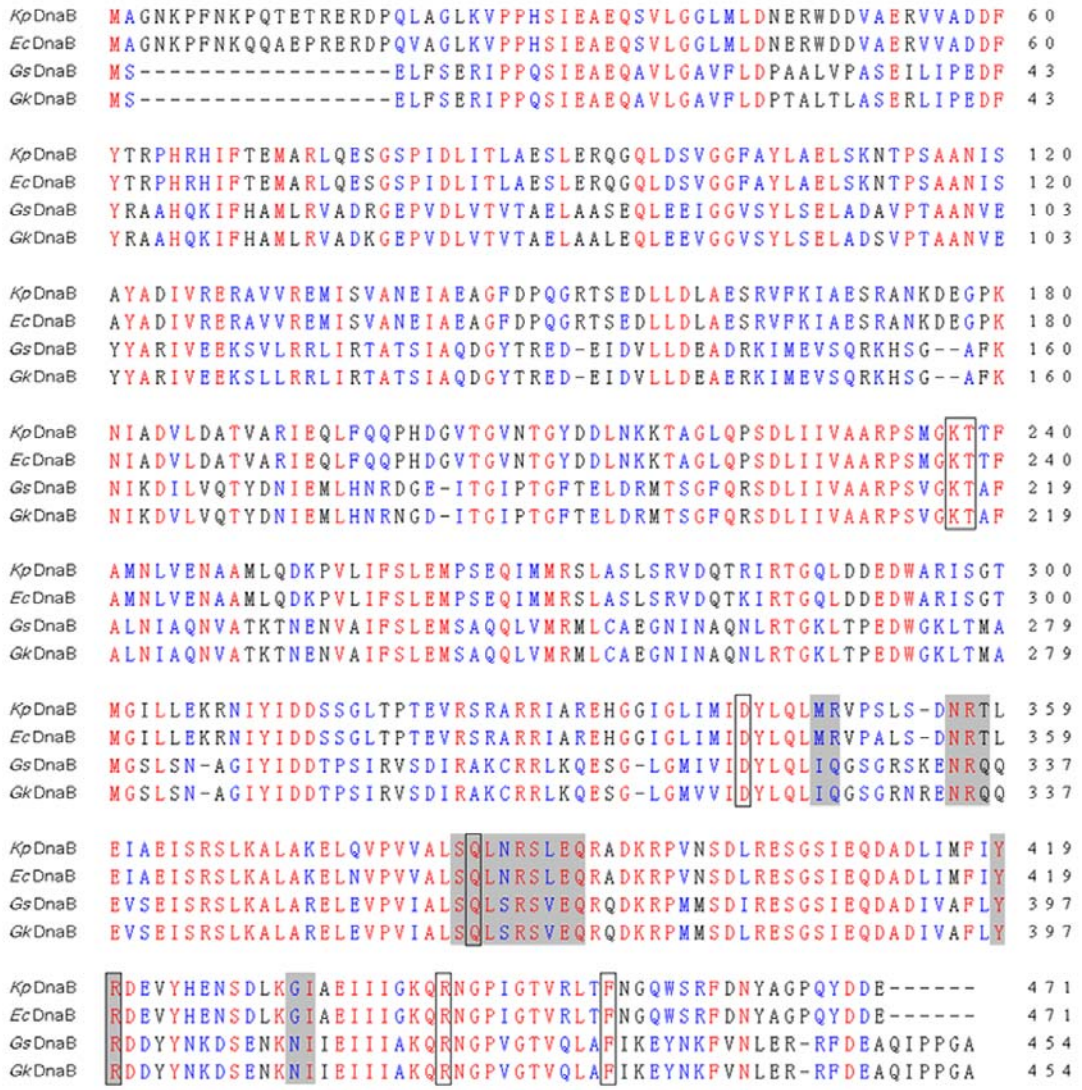
KpDnaB MAGNKPFNKPQTETRERDPQLAGLKVPPHSIEAEQSVLGGLMLDNERWDDVAERVVADDF 60
EcDnaB MAGNKPFNKQQAEPRERDPQVAGLKVPPHSIEAEQSVLGGLMLDNERWDDVAERVVADDF 60
GsDnaB MS----------ELFSERIPPQSIEAEQAVLGAVFLDPAALVPASEILIPEDF 43
GkDnaB MS----------ELFSERIPPQSIEAEQAVLGAVFLDPTALTLASERLIPEDF 43
KpDnaB YTRPHRHIFTEMARLQESGSPIDLITLAESLERQGQLDSVGGFAYLAELSKNTPSAANIS 120
EcDnaB YTRPHRHIFTEMARLQESGSPIDLITLAESLERQGQLDSVGGFAYLAELSKNTPSAANIS 120
GsDnaB YRAAHQKIFHAMLRVADRGEPVDLVTVTAELAASEQLEEIGGVSYLSELADAVPTAANVE 103
GkDnaB YRAAHQKIFHAMLRVADKGEPVDLVTVTAELAALEQLEEVGGVSYLSELADSVPTAANVE 103
KpDnaB AYADIVRERAVVREMISVANEIAEAGFDPQGRTSEDLLDLAESRVFKIAESRANKDEGPK 180
EcDnaB AYADIVRERAVVREMISVANEIAEAGFDPQGRTSEDLLDLAESRVFKIAESRANKDEGPK 180
GsDnaB YYARIVEEKSVLRRLIRTATSIAQDGYTRED-EIDVLLDEADRKIMEVSQRKHSG--AFK 160
GkDnaB YYARIVEEKSLLRRLIRTATSIAQDGYTRED-EIDVLLDEAERKIMEVSQRKHSG--AFK 160
KpDnaB NIADVLDATVARIEQLFQQPHDGVTGVNTGYDDLNKKTAGLQPSDLIIVAARPSMGKTTF 240
EcDnaB NIADVLDATVARIEQLFQQPHDGVTGVNTGYDDLNKKTAGLQPSDLIIVAARPSMGKTTF 240
GsDnaB NIKDILVQTYDNIEMLHNRDGE-ITGIPTGFTELDRMTSGFQRSDLIIVAARPSVGKTAF 219
GkDnaB NIKDVLVQTYDNIEMLHNRNGD-ITGIPTGFTELDRMTSGFQRSDLIIVAARPSVGKTAF 219
KpDnaB AMNLVENAAMLQDKPVLIFSLEMPSEQIMMRSLASLSRVDQTRIRTGQLDDEDWARISGT 300
EcDnaB AMNLVENAAMLQDKPVLIFSLEMPSEQIMMRSLASLSRVDQTKIRTGQLDDEDWARISGT 300
GsDnaB ALNIAQNVATKTNENVAIFSLEMSAQQLVMRMLCAEGNINAQNLRTGKLTPEDWGKLTMA 279
GkDnaB ALNIAQNVATKTNENVAIFSLEMSAQQLVMRMLCAEGNINAQNLRTGKLTPEDWGKLTMA 279
KpDnaB MGILLEKRNIYIDDSSGLTPTEVRSRARRIAREHGGIGLIMIDYLQLMRVPSLS-DNRTL 359
EcDnaB MGILLEKRNIYIDDSSGLTPTEVRSRARRIAREHGGIGLIMIDYLQLMRVPALS-DNRTL 359
GsDnaB MGSLSN-AGIYIDDTPSIRVSDIRAKCRRLKQESG-LGMIVIDYLQLIQGSGRSKENRQQ 337
GkDnaB MGSLSN-AGIYIDDTPSIRVSDIRAKCRRLKQESG-LGMVVIDYLQLIQGSGRNRENRQQ 337
KpDnaB EIAEISRSLKALAKELQVPVVALSQLNRSLEQRADKRPVNSDLRESGSIEQDADLIMFIY 419
EcDnaB EIAEISRSLKALAKELNVPVVALSQLNRSLEQRADKRPVNSDLRESGSIEQDADLIMFIY 419
GsDnaB EVSEISRSLKALARELEVPVIALSQLSRSVEQRQDKRPMMSDIRESGSIEQDADIVAFLY 397
GkDnaB EVSEISRSLKALARELEVPVIALSQLSRSVEQRQDKRPMMSDLRESGSIEQDADIVAFLY 397
KpDnaB RDEVYHENSDLKGIAEIIIGKQRNGPIGTVRLTFNGQWSRFDNYAGPQYDDE------ 471
EcDnaB RDEVYHENSDLKGIAEIIIGKQRNGPIGTVRLTFNGQWSRFDNYAGPQYDDE------ 471
GsDnaB RDDYYNKDSENKNIIEIIIAKQRNGPVGTVQLAFIKEYNKFVNLER-RFDEAQIPPGA 454
GkDnaB RDDYYNKDSENKNIIEIIIAKQRNGPVGTVQLAFIKEYNKFVNLER-RFDEAQIPPGA 454

Figure 3

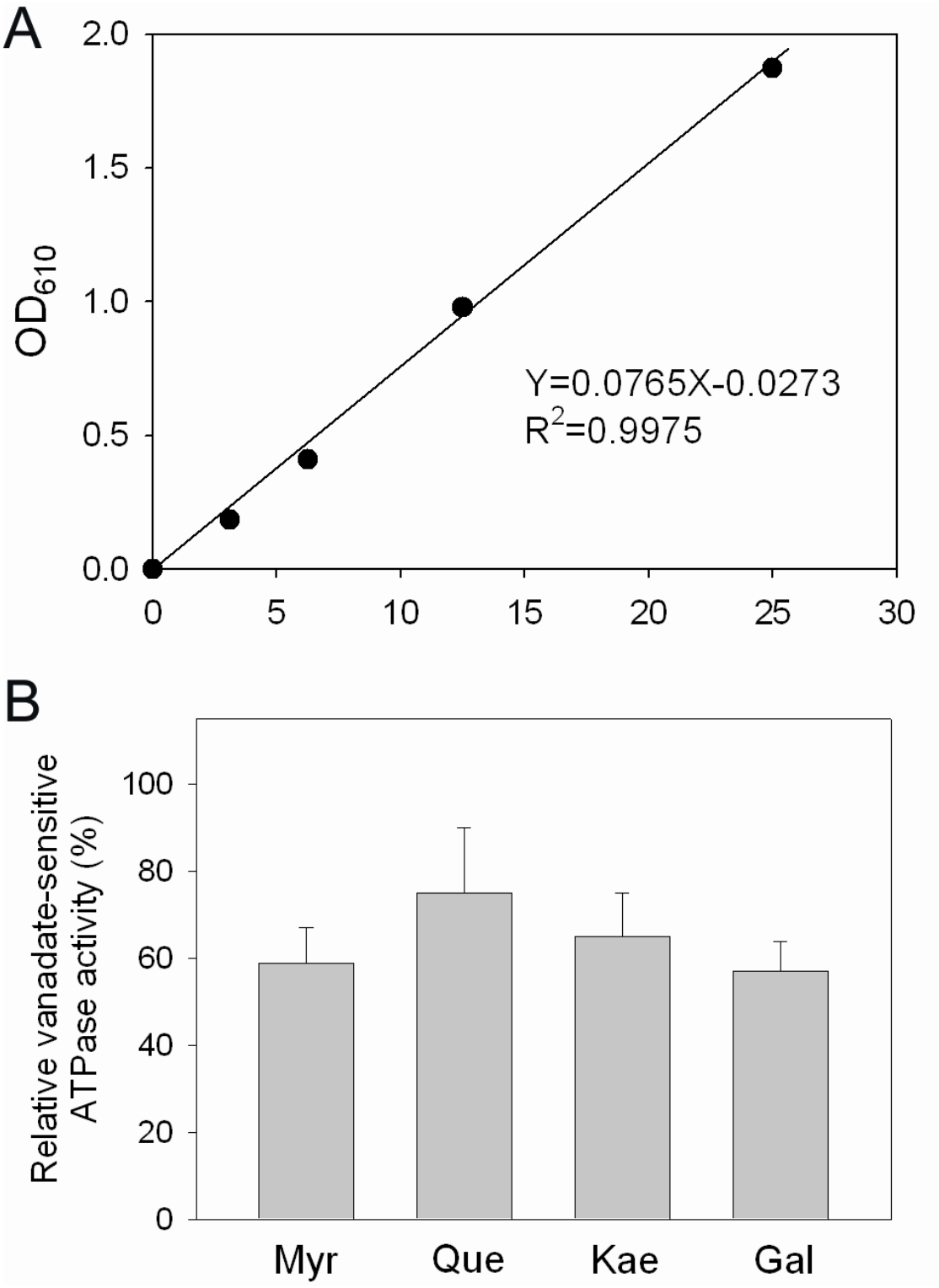
A
2.0
1.5
1.0
0.5
0.0
OD610
Y=0.0765X-0.0273
R2=0.9975
0
5
10
15
20
25
30
B
Relative vanadate-sensitive ATPase activity (%)
100
80
60
40
20
0
Myr
Que
Kae
Gal

Figure 4

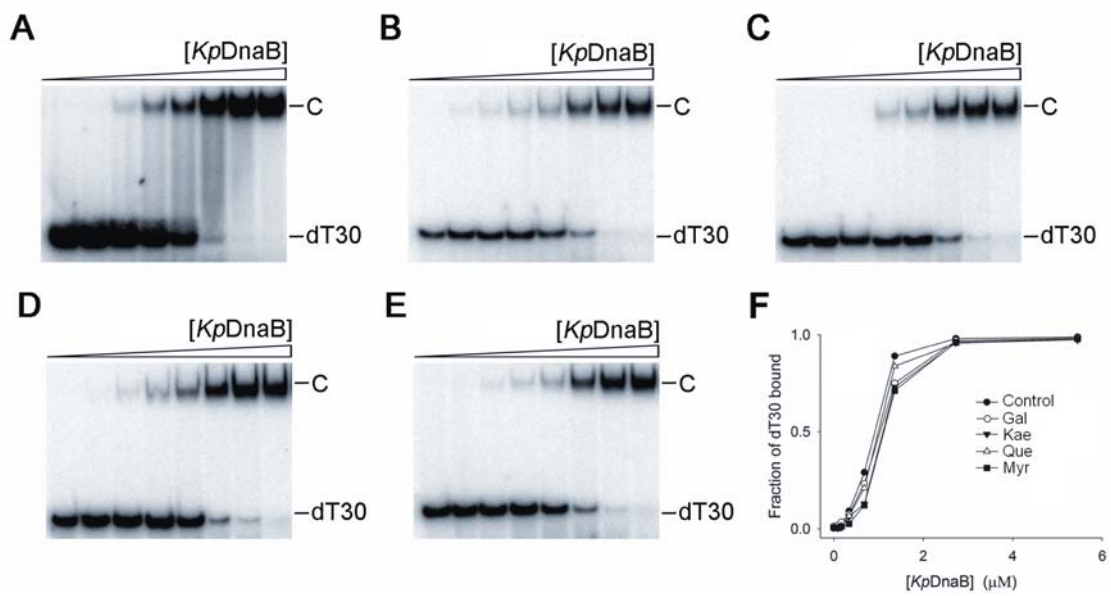
A
[KpDnaB]
C
dT30
B
[KpDnaB]
C
dT30
C
[KpDnaB]
C
dT30
D
[KpDnaB]
C
dT30
E
[KpDnaB]
C
dT30
F
Fraction of dT30 bound
1.0
0.5
0.0
0
2
4
6
[KpDnaB] (μM)
Control
Gal
Kae
Que
Myr

Figure 5

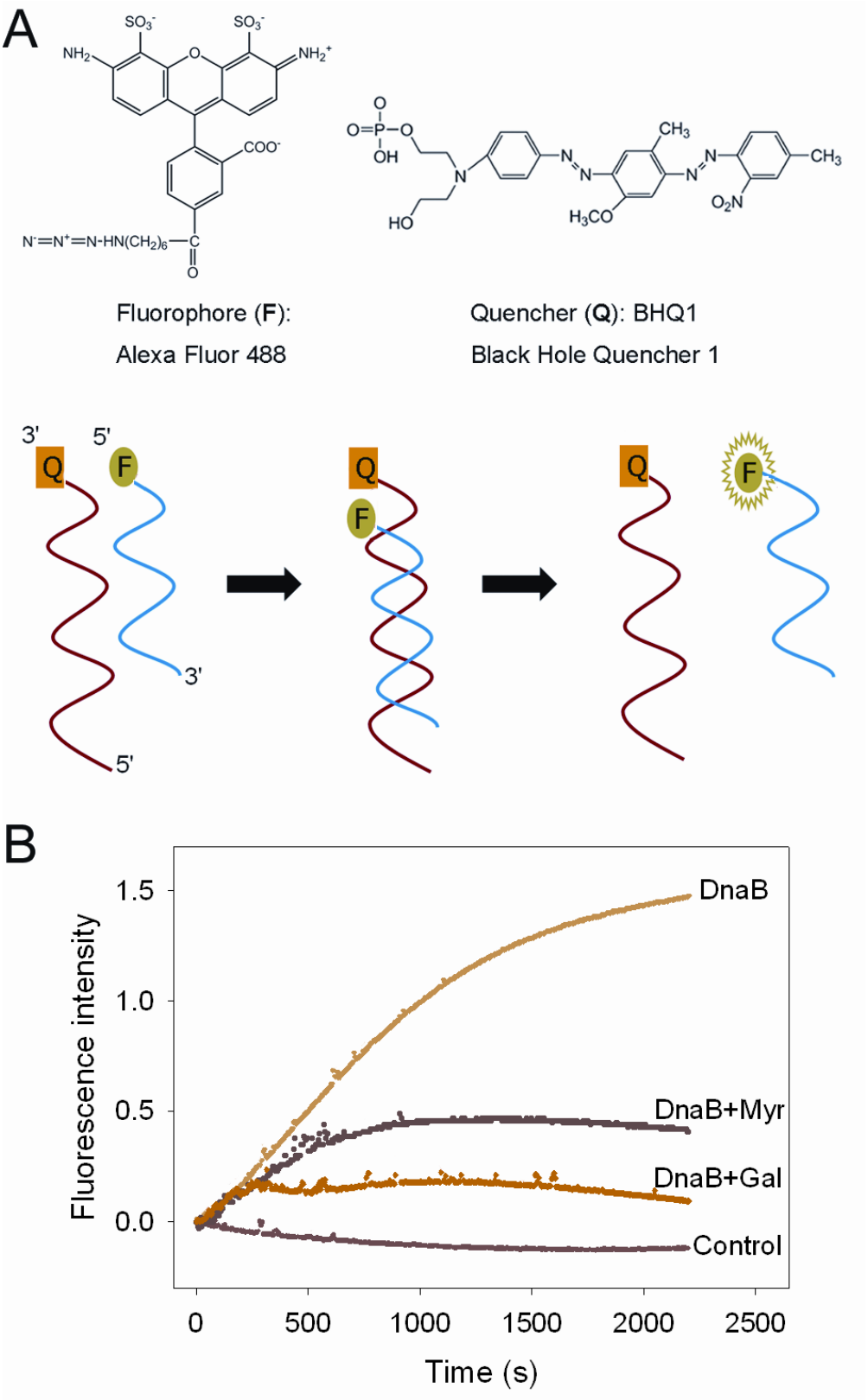
A
Fluorophore (F):
Alexa Fluor 488
Quencher (Q): BHQ1
Black Hole Quencher 1
3'
5'
Q
F
B
Fluorescence intensity
1.5
1.0
0.5
0.0
0
500
1000
1500
2000
2500
Time (s)
DnaB
DnaB+Myr
DnaB+Gal
Control

Figure 6

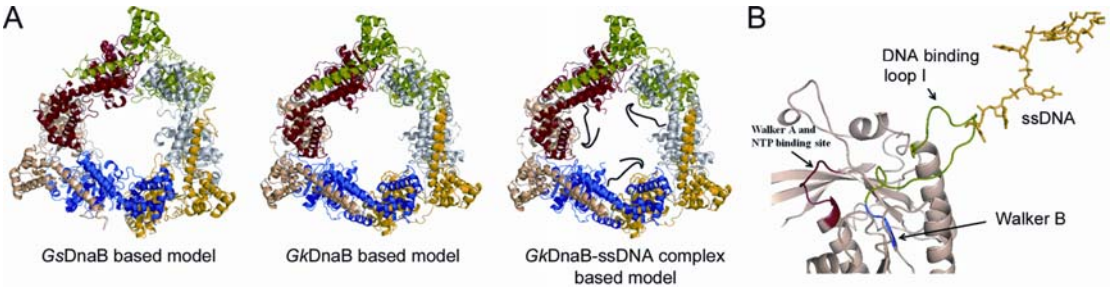
A
GsDnaB based model
GkDnaB based model
GkDnaB-ssDNA complex based model
B
DNA binding loop I
ssDNA
Walker A and NTP binding site
Walker B

Figure 7

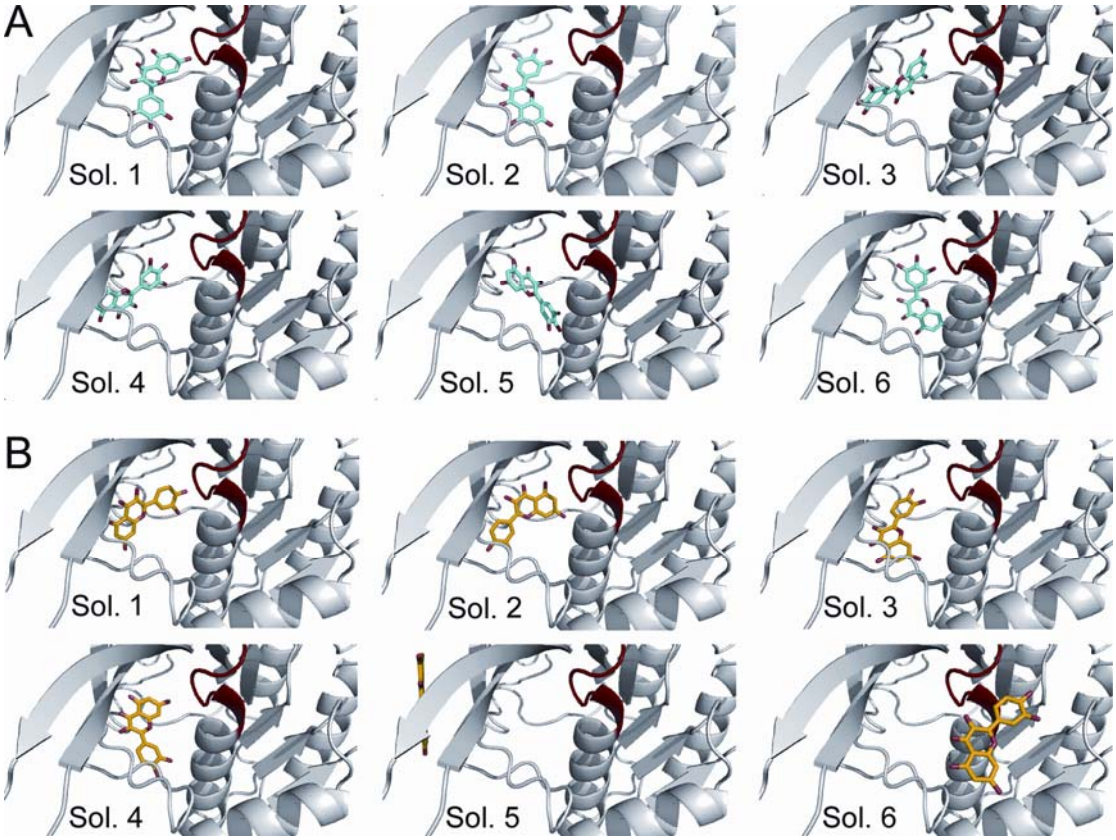
A
Sol. 1
Sol. 2
Sol. 3
Sol. 4
Sol. 5
Sol. 6
B
Sol. 1
Sol. 2
Sol. 3
Sol. 4
Sol. 5
Sol. 6

Figure 8

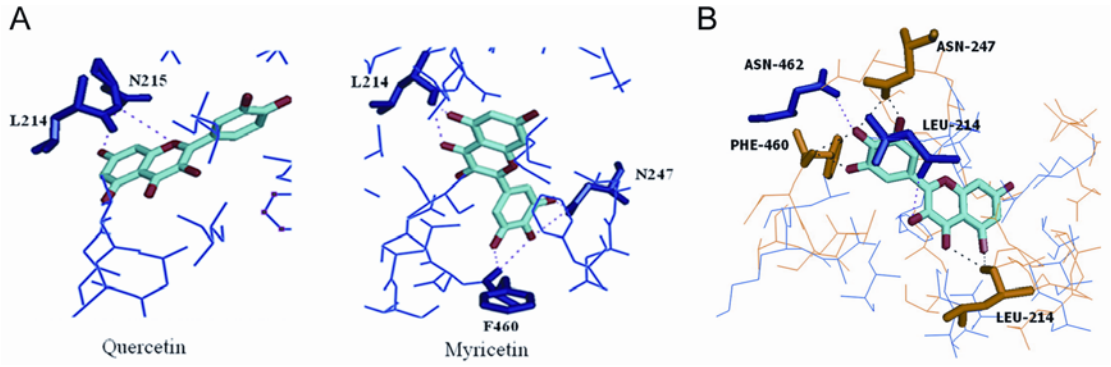
A
N215
L214
Quercetin
L214
N247
F460
Myricetin
B
ASN-462
ASN-247
LEU-214
PHE-460
LEU-214

Figure 9

五、附件(學術論文)

5a Huang, Y.H., Lo, Y.H., Huang, W., **Huang, C.Y.*** (2012) Crystal structure and DNA-binding mode of *Klebsiella pneumoniae* primosomal PriB protein. ***Genes Cells***, 17, 837-849. (SCI)

5b Lin, H.H., **Huang, C.Y.*** (2012) Characterization of flavonol inhibition of DnaB helicase: real-time monitoring, structural modeling, and proposed mechanism. ***J. Biomed. Biotechnol.***, 2012, 735368. (SCI)

5c Huang, Y.H., **Huang, C.Y.*** (2012) Characterization of a single-stranded DNA binding protein from *Klebsiella pneumoniae*: mutation at either Arg73 or Ser76 causes a less cooperative complex on DNA. ***Genes Cells***, 17, 146-157. (SCI)

5d Huang, Y.H., Lin, H.H., **Huang, C.Y.*** (2012) A single residue determines the cooperative binding property of a primosomal DNA replication protein, PriB, to single-stranded DNA. ***Biosci. Biotechnol. Biochem.***, 76, 1110-1115. (SCI)

5e **Huang, C.Y.*** (2012) Determination of the binding site-size of the protein-DNA complex by use of the electrophoretic mobility shift assay, an invited review in a book chapter: ***Stoichiometry and Research - The Importance of Quantity in Biomedicine*** (ISBN 978-953-51-0198-7), Chapter 10, pp. 235-242, edited by Innocenti, A., InTech Press Inc.

Genes to Cells

Crystal structure and DNA-binding mode of *Klebsiella pneumoniae* primosomal PriB protein

Yen-Hua Huang[1], Yu-Hua Lo[2], Wenya Huang[3] and Cheng-Yang Huang[1,4]*

[1]*Department of Biomedical Sciences, Chung Shan Medical University, No. 110, Sec. 1, Chien-Kuo N. Rd, Taichung City, Taiwan*
[2]*Institute of Molecular Biology, Academia Sinica, Taipei, Taiwan*
[3]*Department of Medical Laboratory Science and Biotechnology, Center for Gene Regulation and Signal Transduction Research, College of Medicine, National Cheng Kung University, No. 1, University Rd, Tainan City, Taiwan*
[4]*Department of Medical Research, Chung Shan Medical University Hospital, No. 110, Sec. 1, Chien-Kuo N. Rd, Taichung City, Taiwan*

PriB is a primosomal DNA replication protein required for the re-initiation of replication in bacteria. In this study, we investigated the gene expression of PriB in *Klebsiella pneumoniae* (*Kp*PriB) and characterized the gene product through crystal structural and functional analyses. Quantitative polymerase chain reaction analysis (Q-PCR) indicated that the 104-aa *priB* was expressed in *K. pneumoniae* with a C_T value of 22.4. The crystal structure of *Kp*PriB (Protein Data Bank entry: 4APV) determined at a resolution of 2.1 Å was similar to that of *Escherichia coli* PriB (*Ec*PriB). *Kp*PriB formed a single complex with single-stranded DNA (ssDNA) of different lengths, suggesting a highly cooperative process. Structure-based mutational analysis revealed that substitution at K18, F42, R44, W47, K82, K84, or K89 but not R34 in *Kp*PriB had a significant effect on both ssDNA and double-stranded DNA (dsDNA) binding. Based on these findings, the known ssDNA interaction sites of PriB were expanded to include R44 and F42, thus allowing nucleic acids to wrap around the whole PriB protein.

Introduction

The initiation and re-initiation of chromosomal DNA replication in bacteria for genome duplication is a complex process that relies on divergent multi-protein assembly for entry of the replicative DNA helicase (Benkovic *et al.* 2001). In *Escherichia coli*, replication starts with the loading of DnaB helicase at the unique *oriC* site – a process accomplished by DnaA (an *oriC*-specific recognition protein) and DnaC (a loader protein) (Mott & Berger 2007). However, the replication fork initiated at *oriC* can be arrested anywhere along the DNA, leading to failure of replication (Cox *et al.* 2000; McGlynn & Lloyd 2002; Masai *et al.* 2010). Thus, a reloading DnaB helicase for *oriC*-independent DNA replication is required for bacterial survival (Gabbai & Marians 2010). The replication restart primosome is a multi-protein complex that reactivates stalled DNA replication at the forks after DNA damage (Masai *et al.* 2010). To date, at least two DnaB helicase-recruiting pathways are known: the PriA-PriB-DnaT-DnaC-dependent reactions are the most effective on fork structures with no gaps in the leading strand, whereas the PriC-DnaC-dependent system preferentially uses fork structures with large gaps in the leading strand (Heller & Marians 2006a,b). In the PriA-directed pathway, PriB is the second protein to be assembled in the protein-DNA complex (Marians 2000), where it then stimulates PriA helicase activity (Cadman *et al.* 2005). PriB also stabilizes the binding of PriA to DNA hairpins, therefore facilitating the association of DnaT with the primosome (Liu *et al.* 1996). In an ATP- and DnaC-dependent manner, DnaB helicase is then loaded onto the complex and forms the complete primosome upon binding to DnaG primase (Bailey *et al.* 2007; Lo *et al.* 2009). Recruitment of

Communicated by: Hisao Masai
**Correspondence*: cyhuang@csmu.edu.tw

DOI: 10.1111/gtc.12001

DnaB helicase to the DNA results in reactivation of the repaired replication forks, allowing bidirectional DNA synthesis to resume.

Escherichia coli PriB exists as a homodimer, with each PriB monomer (104 aa) possessing an oligonucleotide/oligosaccharide-binding (OB)-fold structure (Liu *et al.* 2004; Lopper *et al.* 2004; Shioi *et al.* 2005). The single-stranded DNA (ssDNA)-binding site of PriB is located centrally in L_{45} loop within the dimer (Huang *et al.* 2006) and occupies 12 ± 1 nt of the total site size (Szymanski *et al.* 2010). The N-terminal (1–49 aa) region of PriB is crucial for dimerization, whereas the C-terminal (50–104 aa) region is crucial for ssDNA binding (Hsieh & Huang 2011). Although a dimer, PriB has only one ssDNA-binding site (Huang *et al.* 2006; Szymanski *et al.* 2010). PriB shares structural similarity with the DNA-binding domain of *E. coli* ssDNA-binding protein (*Ec*SSB) (Raghunathan *et al.* 2000), except for differences in their ssDNA-binding modes (Huang *et al.* 2006).

Recently, several small proteins possessing ssDNA-binding activity have been discovered (Aravind *et al.* 2003; Jelinska *et al.* 2005; Luo *et al.* 2007; Paytubi *et al.* 2012), including a shorter 55-aa *Klebsiella pneumoniae* PriB (*Kp*PriBc) documented by the NCBI (Hsieh & Huang 2011). Some of these small DNA-binding proteins have similar properties. For instance, similar to *Kp*PriBc, CC1 is a 6-kDa, monomeric, basic protein adopting an OB-fold-like structure (Luo *et al.* 2007). However, a recent study using sequence alignment indicated that *Kp*PriBc, which is much shorter in length than the well-studied *Ec*PriB, probably resulted from the use of the wrong ATG as the *priB* start codon (Berg & Lopper 2011). Although gel filtration and some ssDNA-binding analyses suggest that *Kp*PriB (104-aa) is similar to *Ec*PriB in structure and function (Berg & Lopper 2011), the gene expression of *Kp*PriB has never been analyzed and identified. As many prokaryotic genomes do not contain a recognizable homologue of *priB* (Dong *et al.* 2010), the expression of *Kp*PriB should be analyzed carefully. In this study, we identified the expression of the *priB* gene in *K. pneumoniae* and characterized the gene product by crystal structural and mutational analyses.

Results

Expression of *priB* gene in *K. pneumoniae*

To date, gene expression of the "putative" 104-aa PriB in *K. pneumoniae* has never been analyzed and identified. To test whether the 104-aa PriB could be expressed in *K. pneumoniae*, total RNA was extracted and reverse transcribed and then analyzed by Q-PCR using specific primers. We found that the 104-aa PriB was expressed with a C_T value of 22.4 (Fig. 1). This low C_T value suggests that PriB is a nonhousekeeping gene. Results experimentally confirmed that the 104-aa PriB was actually expressed in *K. pneumoniae*. The original version of *K. pneumoniae* PriB, *KPN_04595* (NCBI), probably resulted from the use of the wrong ATG as the *priB* start codon (residue Met50 in *Kp*PriB).

*Kp*PriB binds to ssDNA

Electrophoretic mobility shift assay (EMSA) is a popular and well-established approach in molecular biology that allows the detection of distinct complexes (Huang 2012). In this study, EMSA of the binding of *Kp*PriB to dT20–dT60 with different protein concentrations revealed that *Kp*PriB could not form a stable complex with dT20 during electrophoresis (Fig. 2). Because some smears were observed, it appears that *Kp*PriB can interact with dT20. In contrast, the longer dT homopolymers (i.e., dT25, dT30, dT35, dT40, dT45, dT50, dT55, and dT60) bind to *Kp*PriB to form a single complex. These interactions appear to be highly cooperative because only one complex of *Kp*PriB molecules bound per ssDNA was visible; no other obvious and distinctive complex or intermediate form was detected. Our findings indicate that the length of ssDNA required to enable the formation of a stable complex with the *Kp*PriB molecule(s) is approximately 25 nt, as determined using EMSA.

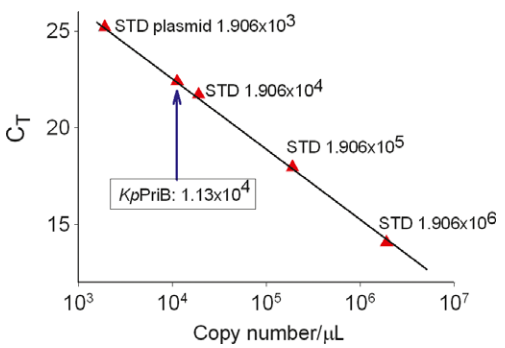

Figure 1 Expression of *priB* gene in *K. pneumoniae* analyzed by Q-PCR. The expression plasmid pET21b-*Kp*PriB served as quantitative standard. *Kp*PriB was expressed with a C_T value of 22.4.

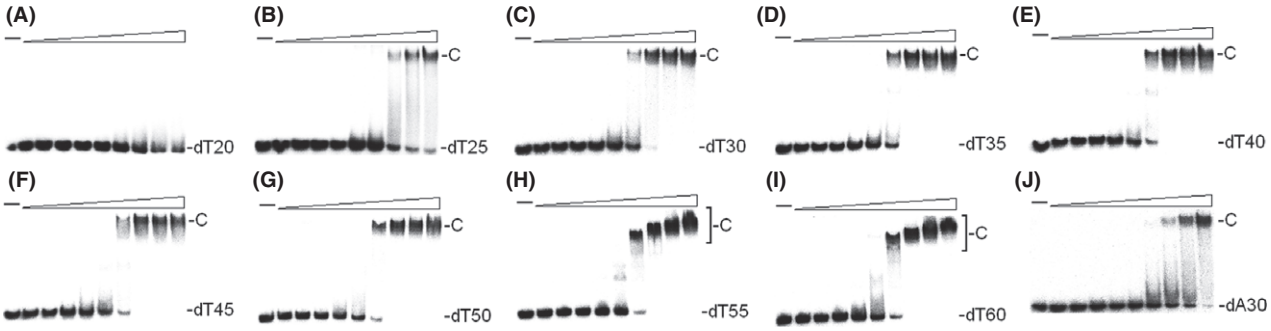

Figure 2 Binding of *Kp*PriB to ssDNA. *Kp*PriB (0, 0.2, 0.4, 0.8, 1.6, 3.2, 6.4, 12.5, 25, and 50 μM) was incubated for 30 min at 25 °C with 1.7 nM of (A) dT20, (B) dT25, (C) dT30, (D) dT35, (E) dT40, (F) dT45, (G) dT50, (H) dT55, (I) dT60, or (J) dA30 in a total volume of 10 μL in 20 mM Tris–HCl pH 8.0 and 100 mM NaCl. Aliquots (5 μL) were removed from each reaction solution and added to 2 μL of gel-loading solution (0.25% bromophenol blue and 40% sucrose). The resulting samples were resolved on a native 8% polyacrylamide gel at 4 °C in TBE buffer (89 mM Tris borate and 1 mM EDTA) for 1 h at 100 V and visualized by autoradiography. Complexed and free DNA bands were scanned and quantified.

ssDNA-binding ability of *Kp*PriB

To compare the binding ability of *Kp*PriB to ssDNA of different lengths, the midpoint values for input ssDNA binding, calculated from the titration curves of EMSA and referred to as $[\text{Protein}]_{50}$, were quantified. They are summarized in Table 1. In general, the binding ability of *Kp*PriB to ssDNA increased with length. However, the ability of *Kp*PriB to bind ssDNA does not significantly change when the length of the dT homopolymer is furthermore increased to 50 nt.

There is a conflicting report on the binding abilities of *Kp*PriB protein. The concentration of *Kp*PriB required for 50% of the 15–45-mer fluorescein-labeled ssDNA to be bound, determined using fluorescence polarization spectroscopy, is 45–62 nM (Berg & Lopper 2011). In addition, we also noted that the binding ability of *Kp*PriB to a longer 45-base ssDNA is lower than that to a shorter 30-base ssDNA (Berg & Lopper 2011). To compare their results, we also studied the DNA binding by *Kp*PriB under the same conditions using EMSA (Fig. 3). As expected, *Kp*PriB could not form a stable complex with the 15-mer ssDNA substrate, and the longer 30-mer and 45-mer ssDNA substrates can bind to *Kp*PriB to form a single complex, as in the case using the dT homopolymers (Fig. 2). However, the $[Kp\text{PriB}]_{50}$ for the 30-mer and 45-mer ssDNA substrates are 9–12 μM, a significantly lower value (~ 2–3 orders of magnitude) than that reported previously using fluorescence polarization spectroscopy (Berg & Lopper 2011). The lower values from EMSA are also found in other protein-DNA complexes (Wang *et al.* 2003) and probably due to the dissociation of the DNA-protein complexes during gel electrophoresis.

Table 1 ssDNA-binding properties of *Kp*PriB analyzed using electrophoretic mobility shift assay

ssDNA substrate	$[Kp\text{PriB}]_{50}$ (μM)
dT20	ND
dT25	18 ± 2
dT30	9 ± 2
dT35	8 ± 1
dT40	6 ± 1
dT45	6 ± 0.8
dT50	4 ± 0.5
dT55	4 ± 0.5
dT60	4 ± 0.5
The 15-mer ssDNA	ND
The 30-mer ssDNA	12 ± 1
The 45-mer ssDNA	9 ± 1
dA30	16 ± 2

Errors are standard deviations determined using three independent titration experiments.

Base preference for ssDNA binding of *Kp*PriB

We used dT30 (Fig. 2C) and dA30 (Fig. 2J) to test the base preference for *Kp*PriB binding to purine and pyrimidine (Table 1). Similar to *Ec*PriB (Liu *et al.* 2004) and *Kp*PriBc (Hsieh & Huang 2011), *Kp*PriB showed a preference for dT30 than dA30, indicating that *Kp*PriB preferentially binds to pyrimidine than purine. However, the *in vitro* base preference of PriB, as well as other SSBs, is still unknown (Lohman & Ferrari 1994).

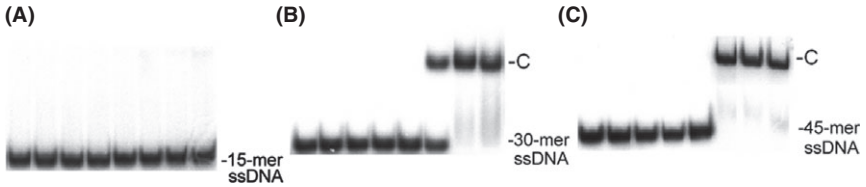

Figure 3 Binding of *Kp*PriB to the 15-mer, 30-mer, and 45-mer ssDNA. For comparison (Berg & Lopper 2011), other DNA substrates (15-mer, 30-mer, and 45-mer) and conditions were also used for EMSA. *Kp*PriB (0, 0.8, 1.6, 3.2, 6.4, 12.5, 25, and 50 μM) was incubated with 1 nM of the (A) 15-mer, (B) 30-mer, or (C) 45-mer ssDNA substrate, 20 mM Tris-HCl pH 8.0, 50 mM NaCl, 4% glycerol, 1 mM $MgCl_2$, 1 mM β-mercaptoethanol, 0.1 mg/mL bovine serum albumin to a total volume of 10 μL for 30 min at 25 °C. Aliquots (5 μL) were removed from each reaction solution and added to 2 μL of gel-loading solution (0.25% bromophenol blue and 40% sucrose). The resulting samples were resolved on a native 8% polyacrylamide gel at 4 °C in TBE buffer (89 mM Tris borate and 1 mM EDTA) for 1 h at 100 V and visualized by autoradiography. Complexed and free DNA bands were scanned and quantified.

Crystal structure of *Kp*PriB

*Kp*PriB was crystallized and its structure was determined at a resolution of 2.1 Å (Table 2). The cell unit contains only one monomer of *Kp*PriB, but its oligomerization state in solution is dimeric (Berg & Lopper 2011). The *Kp*PriB monomer has an OB-fold domain, similar to *Ec*PriB and *Neisseria gonorrhoeae* PriB (*Ng*PriB) (Fig. 4). The majority of the electron density for *Kp*PriB is of good quality, but a discontinuity is observed for residues 84–86 (K84, N85, and G86), and these three residues are absent from the model, suggesting that this region is highly dynamic.

ssDNA-binding mode of *Kp*PriB

Previously, we described the crystal structure of *Ec*PriB in complex with ssDNA dT15; a single dT15 periodically interacts with two OB-fold from 2 symmetrically related PriB dimers in the crystal (Huang *et al.* 2006). Although the DNA-binding site is known to be located centrally in loop L_{45} of *Ec*PriB, the length of DNA in the cocrystal structure is not long enough to wrap the nucleic acid around the protein dimer. Thus, the ssDNA-binding mode of PriB is still not completely clear. Based on the structure of the *Ec*PriB-DNA complex, we manually superimposed the location of ssDNA with the structure of *Kp*PriB (Fig. 5A). ssDNA-binding sites R13, K18, W47, K82, K84, and K89 that were revealed by *Ec*PriB-DNA complex and functional analyses were well conserved in *Kp*PriB (Fig. 5B). In order for nucleic acid to wrap around the whole *Kp*PriB protein, there are two significant grooves that may serve as potential ssDNA-binding pocket on the protein surface (Fig. 5C): one is mediated by F42-R44 (Model I) and the other involved R34-R44 (Model II).

Table 2 Data collection and refinement statistics

Data collection		
Crystal	*Kp*PriB	
Wavelength (Å)	0.97622	
Resolution (Å)	36.1–2.1	
Space group	C2	
Cell dimension (Å)	a = 64.8	
	b = 36.9	β = 113.8
	c = 39.5	
Completeness (%)	95.6 (99.8)★	
$<I/\sigma I>$	40.7 (6.4)	
R_{sym}† (%)	6.4 (25.9)	
Redundancy	3.4 (3.6)	
Refinement		
Resolution (Å)	29.5–2.1	
No. reflections	4899	
R_{work}/R_{free}	0.205/0.274	
No. atoms		
Protein	755	
Water	10	
R.m.s deviation		
Bond lengths (Å)	0.007	
Bond angles (°)	1.001	
Ramachandran Plot		
In preferred regions	91 (96.8%)	
In allowed regions	3 (3.2%)	
Outliers	0 (0%)	
PDB entry	4APV	

★Values in parentheses are for the highest resolution shell.
†$R_{sym} = \Sigma_h\Sigma_i |I_i - I|\Sigma_h\Sigma_I I$, where I is the mean intensity of the i observations of reflection h.

To determine which of the two models is used for *Kp*PriB binding to ssDNA, alanine substitution mutants (i.e. K18A, R34A, F42A, R44A, W47A, K82A, K84A, and K89A) and the double mutant W47A/K82A were constructed and analyzed by

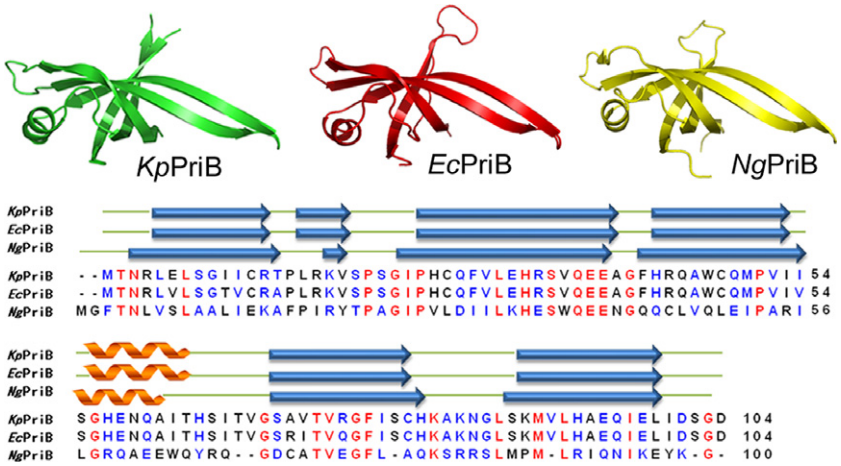

Figure 4 Crystal structure of *Kp*PriB. Sequence alignment and ribbon diagram of *Kp*PriB (PDB code 4APV), *Ec*PriB (PDB code 1V1Q), and *Ng*PriB (PDB code 3K8A) monomer. The secondary structural elements of these PriBs are shown above the sequences. Amino acid residues displaying 100% homology are highlighted in red, and those displaying similarity are highlighted in blue. Three residues, K84, N85, and G86 are absent from the model of *Kp*PriB.

EMSA (Fig. 6). The $[\text{Protein}]_{50}$ values for the binding of these *Kp*PriB variants to dT30 are summarized in Table 3. F42A has a $[Kp\text{PriB}]_{50}$ value that was 2.3-fold higher than that of wild-type *Kp*PriB, whereas substitution at R34 had very little effect (~1.0-fold) on ssDNA binding compared with wild-type *Kp*PriB. Results suggest that Model I is most likely used as the ssDNA-binding mode of *Kp*PriB (Fig. 5C). The DNA interaction sites of PriB (i.e., K84, R13, K82, K89, W47, and K18) that were previously investigated using the crystal structure of *Ec*PriB-ssDNA complex has been expanded to include R44 and F42 to allow for nucleic acid to fully wrap around the whole *Kp*PriB protein.

To strengthen the conclusion that Model I is the DNA-binding mode of PriB, two mutant proteins containing the double mutations, F42A/R44A and R34A/R44A, were constructed and analyzed by EMSA (Fig. 6J,K). F42A/R44A has a $[Kp\text{PriB}]_{50}$ value that was significantly higher than that of either F42A or R44A, whereas R34/R44A had very little effect on ssDNA binding compared with R44A. These results may firmly rule out the role of R34 for ssDNA binding (Table 3). Furthermore, a quadruple mutant, F42A/R44A/W47A/K82A was also generated and no band shift of this quadruple mutant was observed, indicating a dramatically impaired ability for ssDNA binding of this mutant. Previous report has demonstrated that K82A/K84A/K89A in *Ec*PriB plays a very important role in ssDNA binding (Huang *et al.* 2006). Taken together, these results showed that not only the highly electropositive region in L_{45} loop, the aromatic residues F42 and W47 are also very critical for ssDNA binding by PriB. However, it should be noted that the Model I is still not a fully convincing model at this time. The length of ssDNA used in this model is only 18 nt (15 nt in the complex structure of 2CCZ plus 3 nt manually added) and in fact, 18 nt long ssDNA did not bind to *Kp*PriB (Fig. 2).

Double-stranded DNA (dsDNA) binding of *Kp*PriB

Despite the fact that both PriB and SSB have a classical OB-fold ssDNA-binding surface, they bind ssDNA using different strategies. Unlike SSB (Raghunathan *et al.* 2000), PriB binds ssDNA with the highly electrostatic positive L_{45} loop surface (Huang *et al.* 2006). This feature leads us to assess whether *Kp*PriB binds dsDNA. The 22 base pairs (bp) dsDNA substrate for EMSA was prepared by annealing two oligonucleotides, of which one DNA strand was radiolabeled. As expected, *Kp*PriB can bind this dsDNA (Fig. 7A). However, unexpectedly, we found that the $[Kp\text{PriB}]_{50}$ for this dsDNA binding is 5 ± 0.5 μM, a value higher than that for ssDNA dT30 binding of *Kp*PriB (9 ± 2 μM).

To investigate the contribution of individual amino acid residues to dsDNA binding, alanine substitution mutants were constructed and analyzed by EMSA (Fig. 7), similarly to our study on ssDNA

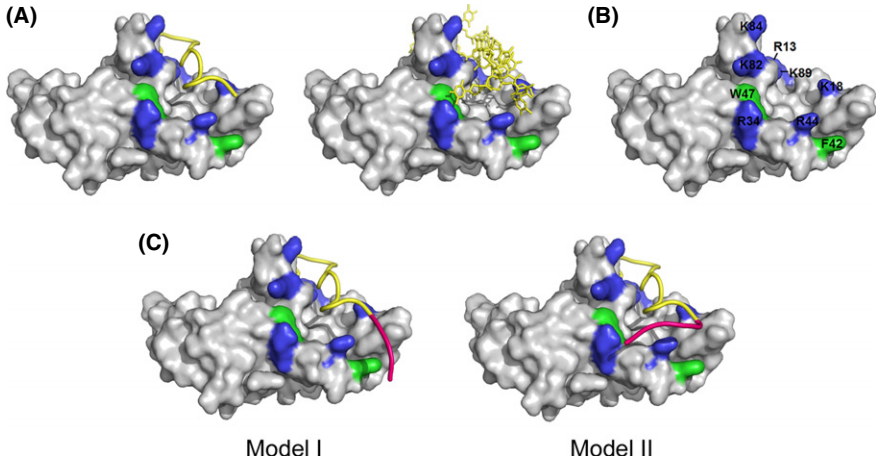

Figure 5 ssDNA-binding mode of *Kp*PriB. (A) A model of the ssDNA-*Kp*PriB complex. Dimeric *Kp*PriB structure was generated from the symmetry-related molecules. The model was directly constructed by superimposing the *Kp*PriB dimeric form (determined in this study) with the crystal structure of the ssDNA-*Ec*PriB complex (PDB code 2CCZ) (Huang *et al.* 2006). The ssDNA generated from the ssDNA-*Ec*PriB complex is shown in gold. The hydrophobic (green) and basic residues (blue) of *Kp*PriB located on the potential ssDNA-binding surface are indicated. (B) The putative ssDNA-binding sites of *Kp*PriB, R13, K18, R34, R44, F42, W47, K82, K84, and K89, are indicated. (C) *Kp*PriB binds to ssDNA in two possible ways: one is mediated by F42-R44 (Model I), and another is involved in R34-R44 (Model II). The length of manually modeled ssDNA interacting with either F42-R44 or R34-R44, shown in hot pink, is 3 nt.

binding (Fig. 6). For the first time, the dsDNA-binding mode of PriB was assessed. The $[Protein]_{50}$ values for the binding of these *Kp*PriB variants to dsDNA are summarized in Table 4. Like ssDNA binding, these mutant proteins F42, R44, W47, K82, K84, and K89 but not R34 of *Kp*PriB had low $[Protein]_{50}$ values (approximately 1.8- to- 3.8-folds) compared with wild-type *Kp*PriB for dsDNA binding. In addition, the mutant proteins containing the double mutations W47A/K82A and F42A/R44A, and the quadruple mutations F42A/R44A/W47A/K82A, exhibited significantly impaired ability for dsDNA binding of *Kp*PriB. Thus, results from these structure-based mutational analyses indicated that the amino acid residues important for ssDNA binding were also crucial for dsDNA binding in *Kp*PriB (see Discussion).

Discussion

In this study, we investigated the crystal structure and DNA-binding mode of *Kp*PriB, in which several results extend the knowledge in the field of PriB family. We also confirmed that the 104-aa PriB was expressed in *K. pneumoniae* (Fig. 1), but not the 55-aa *Kp*PriBc (*KPN_04595*) (Hsieh & Huang 2011), originally documented in NCBI. Although a recent study using sequence alignment suggests that *Kp*PriBc, which is much shorter in length than the well-studied *Ec*PriB, resulted from the use of the wrong ATG as the *priB* start codon (Berg & Lopper 2011), we believe that the expression of the 104-aa *Kp*PriB still needs to be carefully analyzed. As PriB is such a small protein, we do not know whether some prokaryotic genomes without a recognizable homologue of *priB* resulted from the use of the wrong ATG as the *priB* start codon, such as in the case of *K. pneumoniae*. This problem could be addressed by investigation using RT-PCR, as demonstrated in this study.

Many SSB proteins bind to ssDNA with some degree of positive cooperativity (Lohman & Ferrari 1994). In this study, we found differing EMSA behaviors between PriB and SSB proteins. SSB proteins form multiple distinct complexes with ssDNA of different lengths (Olszewski *et al.* 2008, 2010; Huang *et al.* 2011; Jan *et al.* 2011; Huang & Huang 2012), whereas *Kp*PriB binding to ssDNA dT20-dT60 forms a single complex only (Fig. 2). EMSA is a useful technology in molecular biology that allows the detection of distinct complexes (Huang 2012). These findings strongly suggest that *Kp*PriB binds to ssDNA with higher cooperativity than SSB proteins. However, it should be noted that ssDNA-binding affinity of PriB is significantly lower (>2–3 orders of magnitude) than that of SSB proteins (Huang *et al.* 2011; Jan *et al.* 2011; Huang & Huang 2012). Inter-

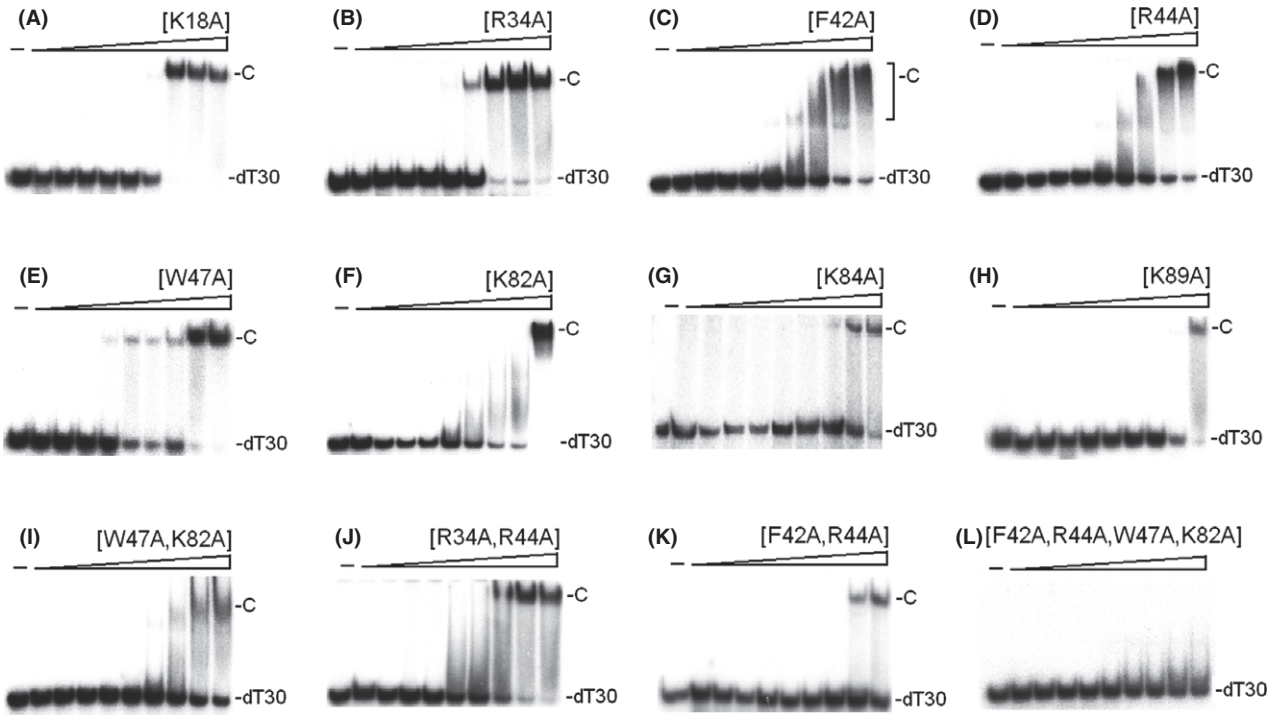

Figure 6 Mutational analysis of *Kp*PriB for ssDNA binding. Binding of *Kp*PriB mutant protein, (A) K18A, (B) R34A, (C) F42A, (D) R44A, (E) W47A, (F) K82A, (G) K84A, (H) K89A, (I) W47A/K82A, (J) R34A/R44A, (K) F42A/R44A, or (L) F42A/R44A/W47A/K82A, to dT30. The mutant protein (0, 0.2, 0.4, 0.8, 1.6, 3.2, 6.4, 12.5, 25, and 50 μM) was incubated for 30 min at 25 °C with 1.7 nM of dT30 in a total volume of 10 μL in 20 mM Tris–HCl pH 8.0 and 100 mM NaCl. Aliquots (5 μL) were removed from each reaction solution and added to 2 μL of gel-loading solution (0.25% bromophenol blue and 40% sucrose). The resulting samples were resolved on a native 8% polyacrylamide gel at 4 °C in TBE buffer (89 mM Tris borate and 1 mM EDTA) for 1 h at 100 V and visualized by autoradiography. Complexed and free DNA bands were scanned and quantified.

Table 3 ssDNA-binding affinities for *Kp*PriB variants to dT30

*Kp*PriB variants	$[KpPriB]_{50}$ (μM)	Fold
Wild type	9 ± 2	1.0
K18A	10 ± 2	1.1
R34A	9 ± 2	1.0
F42A	21 ± 3	2.3
R44A	21 ± 4	2.3
W47A	17 ± 3	1.9
K82A	35 ± 5	3.9
K84A	32 ± 4	3.6
K89A	35 ± 6	3.9
W47A, K82A	>50	>5.6
R34A, R44A	19 ± 3	2.1
F42A, R44A	>50	>5.6
F42A,R44A, W47A,K82A	>>50	>>5.6

Errors are standard deviations determined using three independent titration experiments.

estingly, sequence comparisons and operon organization analyses have shown that PriB evolved from SSB via gene duplication with subsequent rapid sequence diversification (Ponomarev *et al.* 2003). These findings raises several questions as to why PriB has become a kind of SSB with lower ssDNA-binding ability and higher cooperativity, and how PriB participates in DNA replication differently from its ancestor. Previous investigations have demonstrated that aromatic stacking plays an important role in ssDNA binding of SSB (Raghunathan *et al.* 2000), whereas PriB binds to the phosphate backbone of ssDNA via its highly electropositive region in L_{45} loops of the OB-fold (Huang *et al.* 2006). SSB possesses conserved aromatic residues (W40, W54, and F60) in L_{45} loop of the OB-fold; in contrast, two of these residues (W40 and F60) are replaced with nonconserved amino acids in the PriB family. A possible explanation is that during evolution, the conserved

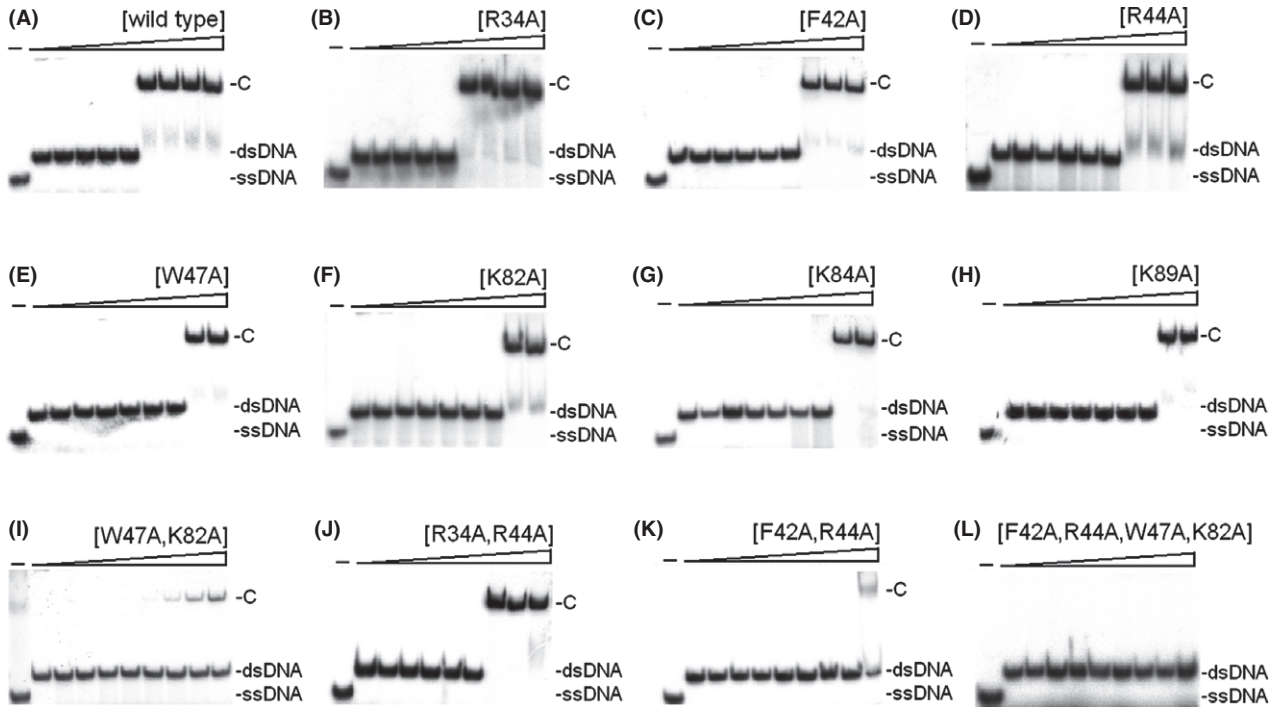

Figure 7 Mutational analysis of *Kp*PriB for dsDNA binding. Binding of *Kp*PriB protein, (A) the wild type, (B) R34A, (C) F42A, (D) R44A, (E) W47A, (F) K82A, (G) K84A, (H) K89A, (I) W47A/K82A, (J) R34A/R44A, (K) F42A/R44A, or (L) F42A/R44A/W47A/K82A, to the dsDNA substrate (22 bp). The mutant protein (0, 0.4, 0.8, 1.6, 3.2, 6.4, 12.5, 25, and 50 μM) was incubated for 30 min at 25 °C with 1.7 nM of dT30 in a total volume of 10 μL in 20 mM Tris–HCl pH 8.0 and 100 mM NaCl. Aliquots (5 μL) were removed from each reaction solution and added to 2 μL of gel-loading solution (0.25% bromophenol blue and 40% sucrose). The resulting samples were resolved on a native 8% polyacrylamide gel at 4 °C in TBE buffer (89 mM Tris borate and 1 mM EDTA) for 1 h at 100 V and visualized by autoradiography. Complexed and free DNA bands were scanned and quantified. A radiolabeled ssDNA is shown in left lane as a control.

Table 4 Binding affinities for *Kp*PriB variants to dsDNA

*Kp*PriB variants	$[KpPriB]_{50}$ (μM)	Fold
Wild type	5 ± 0.5	1.0
R34A	5 ± 0.5	1.0
F42A	9 ± 1	1.8
R44A	9 ± 1	1.8
W47A	18 ± 1	3.6
K82A	19 ± 2	3.8
K84A	18 ± 1	3.6
K89A	18 ± 1	3.6
W47A, K82A	>50	>10
R34A, R44A	10 ± 1	2.0
F42A, R44A	>50	>10
F42A, R44A, W47A, K82A	>>50	>>10

Errors are standard deviations determined using three independent titration experiments.

aromatic and other residues in L_{45} loop of the OB-fold in SSB were changed into positively charged residues in PriB in order to more precisely fit the requirement for assembly of the replication re-initiation primosome at the stalled DNA forks.

Results from the mutational analysis (Fig. 6) and the crystal structural information (Fig. 4) demonstrated that Model I was most likely used for ssDNA binding of *Kp*PriB (Fig. 5C). Thus, the ssDNA interaction sites of PriB that were previously investigated using the crystal structure of *Ec*PriB-ssDNA complex has been expanded to include R44 and F42 in order to allow for nucleic acid to fully wrap around the whole *Kp*PriB protein. Although PriB uses a different DNA-binding strategy compared with other SSBs, including human replication protein A (Bochkarev *et al.* 1997; Huang *et al.* 2006), all SSB proteins still follow a similar DNA-binding path (i.e., loop L_{45} to loop L_{23}) of OB-fold proteins (Murzin 1993; Theobald *et al.* 2003).

There are conflicting reports on the binding ability of residue 34 in PriB proteins. Substitution of K34 in *Ng*PriB with alanine, the position structurally corresponding to R34 in *Kp*PriB, significantly reduces the protein's ssDNA-binding activity (Dong *et al.* 2010). Results indicate that K34 probably plays an important role in *Ng*PriB, whereas R34 in *Kp*PriB does not. In addition, the binding ability of *Ng*PriB to a (longer) 45-base ssDNA is ~2-fold lower than that to a (shorter) 36-base ssDNA (Dong *et al.* 2010). In contrast, the binding ability of *Kp*PriB to oligonucleotides generally increases with greater length (Table 1). As the mechanisms for participating in assembly of the replication re-initiation primosome should be distinct (Dong *et al.* 2010; Feng *et al.* 2011), *Ng*PriB and *Kp*PriB may bind DNA differently. The crystal structure of *Ng*PriB complexed with DNA is highly needed in helping our understanding of the primosome assembly mechanism(s).

In this study, we also found that *Kp*PriB can bind both ssDNA and dsDNA with comparable affinity (Tables 1 and 4). According to crystal structures of some dimeric proteins complexed with dsDNA found in Protein Data Bank (PDB), as well as results from mutational analysis (Fig. 7), we speculate that *Kp*PriB binds dsDNA in two possible ways (Fig. 8). First, *Kp*PriB may bind to dsDNA via the HU-binding mode (Swinger *et al.* 2003; Kamashev *et al.* 2008). HU, a dimeric nucleoid-associated protein, mainly uses the two β sheets to bind the dsDNA (Fig. 8A). According to the structure of HU-DNA complex, we manually superimpose the location of dsDNA with our *Kp*PriB structure and find that this complex structure seems to match the residues important for dsDNA binding (Fig. 7 and Table 4). Secondly, *Kp*PriB may bind dsDNA in a manner similar to bind ssDNA (Fig. 8B). The structure-based mutational analysis indicated that residues in *Kp*PriB crucial for ssDNA binding were also crucial for dsDNA binding (Tables 3 and 4). As these residues responsible for ssDNA and dsDNA binding were almost overlapped, *Kp*PriB may use a similar way to bind to the phosphate backbone of ssDNA and dsDNA via several positively charged residues. This may be a reason for the comparable binding affinities of *Kp*PriB with ssDNA and dsDNA. This might also explain why SSB can bind dsDNA but with far less affinity than ssDNA (Meyer & Laine 1990): several important residues in L_{45} loop of the OB-fold of SSB are aromatic residues (W40, W54, and F60), not the positively charged residues like in PriB. Taken together, we believe that both these two possible ways to bind dsDNA for *Kp*PriB, namely the HU binding mode or ssDNA-binding mode of *Kp*PriB, cannot be ruled out at this time.

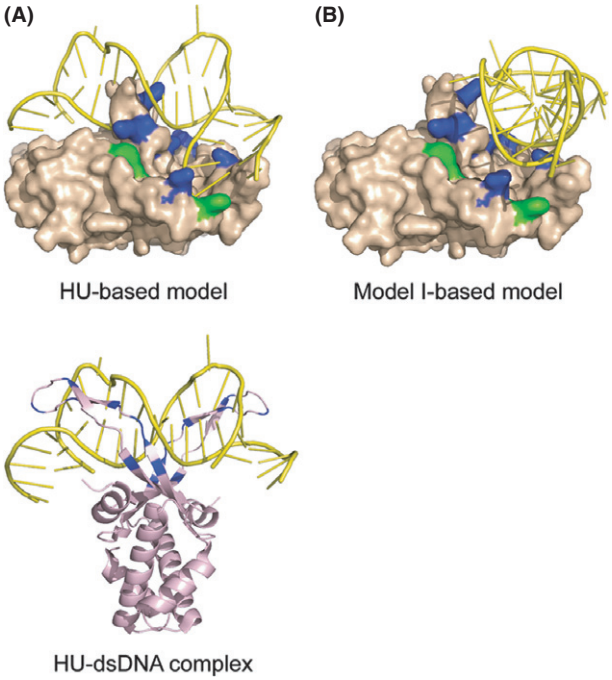

Figure 8 dsDNA-binding mode of *Kp*PriB. (A) A HU-based model of the dsDNA-*Kp*PriB complex. The model was directly constructed by manually superimposing the *Kp*PriB dimeric form with the crystal structure of the dsDNA-HU complex (Swinger *et al.* 2003) (PDB code 1P51). The basic residues R53, R55, K56, R58, R61, K64, K68, and R75 of HU located on its potential dsDNA-binding surface are indicated. (B) A ssDNA-*Kp*PriB complex based model for the dsDNA-*Kp*PriB complex. The model, based on the Model I in Fig. 5C, was constructed by manually superimposing the B-form dsDNA with *Kp*PriB dimeric form.

The binding site on PriB for ssDNA overlaps the binding sites for PriA and DnaT, suggesting a dynamic primosome assembly process in which ssDNA is handed off from one primosome protein to another as a repaired replication fork is reactivated (Lopper *et al.* 2007). However, the complexed structure (Huang *et al.* 2006) and the thermodynamic analysis (Szymanski *et al.* 2010) indicate that the PriB dimer behaves like a protein with half-site reactivity, where only one monomer of the dimer can engage in interactions with the DNA and the partner protein(s) (Szymanski *et al.* 2010). Thus, it still remains to be explored whether the binding site on PriB for ssDNA is necessary to overlap the binding sites for PriA and DnaT.

The activity mediated by the replication primosomal proteins, including PriB, to reinitiate replication

after DNA damage is essential for bacterial survival. There are some conflicting reports on the proposed binding mode of PriB to DNA and its partner proteins (Liu *et al.* 2004; Cadman *et al.* 2005; Huang *et al.* 2006; Lopper *et al.* 2007; Dong *et al.* 2010). It is not known whether this disparity is because of inherent differences among the species, use of different assay methods, or the effect of different investigators. This study reports the structural and functional analysis of *Kp*PriB and discusses why PriB evolved from SSB to become a new DNA-binding protein during evolution. The more complex structures of PriB are useful in helping our understanding of the primosome assembly mechanism(s).

Experimental procedures

Materials

All restriction enzymes and DNA-modifying enzymes were purchased from New England Biolabs (Ipswich, MA, USA) unless explicitly stated otherwise. All chemicals were purchased from Sigma-Aldrich (St. Louis, MO, USA) unless explicitly stated otherwise. The *E. coli* strains TOP10F' (Invitrogen, USA) and BL21(DE3)pLysS (Novagen, UK) were used for genetic construction and protein expression, respectively.

RNA purification and cDNA synthesis

Klebsiella pneumoniae subsp. *pneumoniae* MGH 78578 was grown to an OD_{600} of 1.0 at 37 °C in Luria-Bertani medium. RNA of *K. pneumoniae* was extracted from 4 mL cell cultures using RNAprotect Bacteria Reagent and Qiagen RNeasy Mini Columns (Qiagen), according to the manufacturer's instructions. Total RNA was treated with DNaseI and reverse transcribed using high-capacity cDNA reverse transcription kit (PE Applied Biosystems) and random primers according to the manufacturer's instructions.

Quantitative real-time PCR

Quantitative real-time PCR (Q-PCR) analysis was carried out using PowerSYBR Green Master Mix on a 7900 Real-Time PCR system (PE Applied Biosystems) as recommended by the manufacturer. Briefly, cDNA (25.4 ng) and primers (300 nM) were used in the amplification reactions: one cycle of 50 °C for 2 min; one cycle of 95 °C for 10 min; 45 cycles of 95 °C for 15 s and 60 °C for 20 s; and one cycle of 95 °C for 15 s, 60 °C for 1 min, and 95 °C for 15 s. Primer 1 (5′-CACTGC CAGTTCGTGCTTGA-3′) and Primer 2 (5′-ACTGTGAGT AATGGCCTGGTTCTC-3′) were used. Product formation was monitored by the increase in fluorescence from SYBR Green intercalation. The threshold cycle (C_T) is the first cycle for which a statistically significance increase in the amount of product is detected. C_T values are inversely proportional to the cDNA amount in the sample. The expression plasmid pET21b-*Kp*PriB served as quantitative standard.

Cloning, protein expression, and purification

The gene encoding the putative *Kp*PriB was PCR-amplified using cDNA from the reverse transcribed RNA as template. The forward (GAAGGGGCATATGCCCGTTATTATTAG CGGTCATGAG) and reverse primers (GGGCTCGAGGTC TCCAGAATCTATCAATTCAAT) were designed to introduce unique NdeI and XhoI restriction sites into *Kp*PriB, thus allowing the insertion of the amplified genes into the pET21b vector (Novagen Inc., Madison, WI, USA). The recombinant *Kp*PriB protein was expressed and purified using the protocol used for *Ec*PriB (Liu *et al.* 2004). Briefly, *E. coli* cells were transformed with the expression vector and grown to OD_{600} of 0.9 at 37 °C in Luria-Bertani medium containing 250 μg/mL ampicillin. Over-expression of *Kp*PriB construct was induced with 1 mM isopropyl thiogalactoside (IPTG) for 3 h at 37 °C. The cells overexpressing the protein were chilled on ice, harvested by centrifugation, resuspended in Buffer A (20 mM Tris-HCl, 5 mM imidazole, 0.5 M NaCl; pH 7.9) and disrupted by sonication with ice cooling between pulses. The *Kp*PriB protein was then purified from the soluble supernatant by Ni^{2+}-affinity chromatography (HiTrap HP; GE Healthcare Bio-Sciences, Piscataway, NJ, USA). Protein purity was greater than 97% as determined by Coomassie-stained SDS-PAGE.

Preparation of dsDNA substrates

The dsDNA substrate (22 bp) was prepared with a radiolabeled strand (3′-GGGCTTAAGCTCGAGCCATGGG-5′) and an unlabeled strand (5′-CCCGAATTCGAGCTCGGTA CCC-3′) at a 1 : 1 concentration ratio. The dsDNA substrate was formed in 20 mM HEPES (pH 7.0) and 100 mM NaCl, by brief heating at 95 °C for 5 min and then followed by slow cooling to room temperature overnight.

Electrophoretic mobility shift assay

Electrophoretic mobility shift assay for *Kp*PriB was carried out according to the protocol described for SSB proteins (Huang *et al.* 2011; Jan *et al.* 2011; Huang & Huang 2012). Briefly, [γ^{32}P]ATP (6000 Ci/mmol; PerkinElmer Life Sciences) and T4 polynucleotide kinase (Promega, Madison, WI, USA) were used for radiolabeling of various lengths of ssDNA oligonucleotides. *Kp*PriB (0, 0.2, 0.4, 0.8, 1.6, 3.2, 6.4, 12.5, 25, and 50 μM) was incubated with 1.7 nM DNA, 20 mM Tris-HCl pH 8.0, and 100 mM NaCl to a total volume of 10 μL for 30 min at 25 °C. Aliquots (5 μL) were removed from each reaction solution and added to 2 μL of gel-loading solution (0.25% bromophenol blue and 40% sucrose). The resulting samples were resolved on a native 8% polyacrylamide gel at

4 °C in TBE buffer (89 mM Tris borate and 1 mM EDTA) for 1 h at 100 V and visualized by autoradiography. Complexed and free DNA bands were scanned and quantified. For dsDNA, *Kp*PriB (0, 0.4, 0.8, 1.6, 3.2, 6.4, 12.5, 25, and 50 μM) was used, and a radiolabeled ssDNA is shown in left lane as a control.

Other DNA substrates and conditions were also tried for comparison (Berg & Lopper 2011). *Kp*PriB (0, 0.8, 1.6, 3.2, 6.4, 12.5, 25, and 50 μM) was incubated with 1 nM DNA (15-mer: 5′-TAGCAATGTAATCGT-3′; 30-mer: 5′-GCG TGGGTAATTGTGCTTCAATGGACTGAC-3′; 45-mer: 5′-GCCGTGATCACCAATGCAGATTGACGAACCTTTG CTCCAGTAACC-3′), 20 mM Tris–HCl pH 8.0, 50 mM NaCl, 4% glycerol, 1 mM $MgCl_2$, 1 mM β-mercaptoethanol, 0.1 mg/mL bovine serum albumin to a total volume of 10 μL for 30 min at 25 °C, and then assayed using the protocol described earlier.

Site-directed mutagenesis

*Kp*PriB mutants were generated according to the QuikChange Site-Directed Mutagenesis kit protocol (Stratagene, LaJolla, CA, USA) using the primers and wild-type plasmid pET21b-*Kp*PriB as template. The presence of the mutation was verified by DNA sequencing.

DNA-binding ability

The DNA-binding ability ($[Protein]_{50}$) for the protein was estimated from the protein concentration that binds 50% of the input DNA. Each $[Protein]_{50}$ is calculated as the average of at least three measurements ± SD.

Crystallography

Before crystallization, *Kp*PriB was concentrated to 10 mg/mL in 20 mM sodium citrate and 100 mM NaCl (pH 5). Crystals were grown at room temperature by hanging drop vapor diffusion in 50% ethanol and 10 mM sodium acetate. Data collection and refinement statistics for the crystal of *Kp*PriB are shown in Table 2. Data were collected using an ADSC Quantum-315r CCD area detector at SPXF beamline BL13C1 at NSRRC (Taiwan, ROC). All data integration and scaling were carried out using HKL-2000 (Otwinowski & Minor 1997). There was only one *Kp*PriB molecule per asymmetric unit. The crystal structure of *Kp*PriB was solved at 2.1 Å resolution with the molecular replacement software AMoRe (Navaza 1994) using *Ec*PriB (Liu *et al*. 2004) as model (1V1Q). After molecular replacement, model building was carried out using XtalView (McRee 1999). CNS was used for molecular dynamic refinement (Brünger *et al*. 1998). The final structure was refined to an *R*-factor of 0.205 and an R_{free} of 0.274. Atomic coordinates and related structure factors have been deposited in the PDB with accession code 4APV.

Acknowledgements

We would like to thank two anonymous reviewers and the editor for their comments. We also thank Prof. Chwan-Deng Hsiao (IMB of Academia Sinica) for technological support of this work. Portions of this study were carried out at the National Synchrotron Radiation Research Center, a national user facility supported by the National Science Council of Taiwan, ROC. The Synchrotron Radiation Protein Crystallography Facility is supported by the National Core Facility Program for Biotechnology. This research was supported by a grant from the National Research Program for Genome Medicine, Taiwan (NSC 100-3112-B-040-001 to C.Y. Huang).

References

Aravind, L., Iyer, L.M. & Anantharaman, V. (2003) The two faces of Alba: the evolutionary connection between proteins participating in chromatin structure and RNA metabolism. *Genome Biol*. **4**, R64.

Bailey, S., Eliason, W.K. & Steitz, T.A. (2007) Structure of hexameric DnaB helicase and its complex with a domain of DnaG primase. *Science* **318**, 459–463.

Benkovic, S.J., Valentine, A.M. & Salinas, F. (2001) Replisome-mediated DNA replication. *Annu. Rev. Biochem*. **70**, 181–208.

Berg, L. & Lopper, M.E. (2011) The *priB* Gene of *Klebsiella pneumoniae* encodes a 104-amino acid protein that is similar in structure and function to *Escherichia coli* PriB. *PLoS One* **6**, e24494.

Bochkarev, A., Pfuetzner, R.A., Edwards, A.M. & Frappier, L. (1997) Structure of the single-stranded-DNA-binding domain of replication protein A bound to DNA. *Nature* **385**, 176–181.

Brünger, A.T., Adams, P.D., Clore, G.M., DeLano, W.L., Gros, P., Grosse-Kunstleve, R.W., Jiang, J.S., Kuszewski, J., Nilges, M., Pannu, N.S., Read, R.J., Rice, L.M., Simonson, T. & Warren, G.L. (1998) Crystallography & NMR system: a new software suite for macromolecular structure determination. *Acta Crystallogr.* **54**, 905–921.

Cadman, C.J., Lopper, M., Moon, P.B., Keck, J.L. & McGlynn, P. (2005) PriB stimulates PriA helicase via an interaction with single-stranded DNA. *J. Biol. Chem*. **280**, 39693–39700.

Cox, M.M., Goodman, M.F., Kreuzer, K.N., Sherratt, D.J., Sandler, S.J. & Marians, K.J. (2000) The importance of repairing stalled replication forks. *Nature* **404**, 37–41.

Dong, J., George, N.P., Duckett, K.L., DeBeer, M.A. & Lopper, M.E. (2010) The crystal structure of *Neisseria gonorrhoeae* PriB reveals mechanistic differences among bacterial DNA replication restart pathways. *Nucleic Acids Res*. **38**, 499–509.

Feng, C., Sunchu, B., Greenwood, M.E. & Lopper, M.E. (2011) A bacterial PriB with weak single-stranded DNA binding activity can stimulate the DNA unwinding activity of its cognate PriA helicase. *BMC Microbiol*. **11**, 189.

Gabbai, C.B. & Marians, K.J. (2010) Recruitment to stalled replication forks of the PriA DNA helicase and replisome-loading activities is essential for survival. *DNA Repair* **9**, 202–209.

Heller, R.C. & Marians, K.J. (2006a) Replication fork reactivation downstream of a blocked nascent leading strand. *Nature* **439**, 557–562.

Heller, R.C. & Marians, K.J. (2006b) Replisome assembly and the direct restart of stalled replication forks. *Nat. Rev. Mol. Cell Biol.* **7**, 932–943.

Hsieh, H.C. & Huang, C.Y. (2011) Identification of a novel protein, PriB, in *Klebsiella pneumoniae*. *Biochem. Biophys. Res. Commun.* **404**, 546–551.

Huang, C.Y., Hsu, C.H., Sun, Y.J., Wu, H.N. & Hsiao, C. D. (2006) Complexed crystal structure of replication restart primosome protein PriB reveals a novel single-stranded DNA-binding mode. *Nucleic Acids Res.* **34**, 3878–3886.

Huang, C.Y. (2012) Determination of the binding site-size of the protein-DNA complex by use of the electrophoretic mobility shift assay. In: *Stoichiometry and Research – The Importance of Quantity in Biomedicine* (ed. A. Innocenti), pp. 235–242. Rijeka, Croatia: InTech Press.

Huang, Y.H. & Huang, C.Y. (2012) Characterization of a single-stranded DNA-binding protein from *Klebsiella pneumoniae*: mutation at either Arg73 or Ser76 causes a less cooperative complex on DNA. *Genes Cells* **17**, 146–157.

Huang, Y.H., Lee, Y.L. & Huang, C.Y. (2011) Characterization of a single-stranded DNA binding protein from *Salmonella enterica* Serovar Typhimurium LT2 . *Protein J.* **30**, 102–108.

Jan, H.C., Lee, Y.L. & Huang, C.Y. (2011) Characterization of a single-stranded DNA-binding protein from *Pseudomonas aeruginosa* PAO1. *Protein J.* **30**, 20–26.

Jelinska, C., Conroy, M.J., Craven, C.J., Hounslow, A.M., Bullough, P.A., Waltho, J.P., Taylor, G.L. & White, M.F. (2005) Obligate heterodimerization of the archaeal Alba2 protein with Alba1 provides a mechanism for control of DNA packaging. *Structure* **13**, 963–971.

Kamashev, D., Balandina, A., Mazur, A.K., Arimondo, P.B. & Rouviere-Yaniv, J. (2008) HU binds and folds single-stranded DNA. *Nucleic Acids Res.* **36**, 1026–1036.

Liu, J., Nurse, P. & Marians, K.J. (1996) The ordered assembly of the phiX174-type primosome. III. PriB facilitates complex formation between PriA and DnaT. *J. Biol. Chem.* **271**, 15656–15661.

Liu, J.H., Chang, T.W., Huang, C.Y., Chen, S.U., Wu, H. N., Chang, M.C. & Hsiao, C.D. (2004) Crystal structure of PriB, a primosomal DNA replication protein of *Escherichia coli*. *J. Biol. Chem.* **279**, 50465–50471.

Lo, Y.H., Tsai, K.L., Sun, Y.J., Chen, W.T., Huang, C.Y. & Hsiao, C.D. (2009) The crystal structure of a replicative hexameric helicase DnaC and its complex with single-stranded DNA. *Nucleic Acids Res.* **37**, 804–814.

Lohman, T.M. & Ferrari, M.E. (1994) *Escherichia coli* single-stranded DNA-binding protein: multiple DNA-binding modes and cooperativities. *Annu. Rev. Biochem.* **63**, 527–570.

Lopper, M., Boonsombat, R., Sandler, S.J. & Keck, J.L. (2007) A hand-off mechanism for primosome assembly in replication restart. *Mol. Cell* **26**, 781–793.

Lopper, M., Holton, J.M. & Keck, J.L. (2004) Crystal structure of PriB, a component of the *Escherichia coli* replication restart primosome. *Structure* **12**, 1967–1975.

Luo, X., Schwarz-Linek, U., Botting, C.H., Hensel, R., Siebers, B. & White, M.F. (2007) CC1, a novel crenarchaeal DNA binding protein. *J. Bacteriol.* **189**, 403–409.

Marians, K.J. (2000) PriA-directed replication fork restart in *Escherichia coli*. *Trends Biochem. Sci.* **25**, 185–189.

Masai, H., Tanaka, T. & Kohda, D. (2010) Stalled replication forks: making ends meet for recognition and stabilization. *BioEssays* **32**, 687–697.

McGlynn, P. & Lloyd, R.G. (2002) Recombinational repair and restart of damaged replication forks. *Nat. Rev. Mol. Cell Biol.* **3**, 859–870.

McRee, D.E. (1999) XtalView/Xfit–A versatile program for manipulating atomic coordinates and electron density. *J. Struct. Biol.* **125**, 156–165.

Meyer, R.R. & Laine, P.S. (1990) The single-stranded DNA-binding protein of *Escherichia coli*. *Microbiol. Rev.* **54**, 342–380.

Mott, M.L. & Berger, J.M. (2007) DNA replication initiation: mechanisms and regulation in bacteria. *Nat. Rev. Microbiol.* **5**, 343–354.

Murzin, A.G. (1993) OB(oligonucleotide/oligosaccharide binding)-fold: common structural and functional solution for non-homologous sequences. *EMBO J.* **12**, 861–867.

Navaza, J. (1994) AMoRe: an automated package for molecular replacement. *Acta Crystallogr.* **50**, 157–163.

Olszewski, M., Grot, A., Wojciechowski, M., Nowak, M., Mickiewicz, M. & Kur, J. (2010) Characterization of exceptionally thermostable single-stranded DNA-binding proteins from *Thermotoga maritima* and *Thermotoga neapolitana*. *BMC Microbiol.* **10**, 260.

Olszewski, M., Mickiewicz, M. & Kur, J. (2008) Two highly thermostable paralogous single-stranded DNA-binding proteins from *Thermoanaerobacter tengcongensis*. *Arch. Microbiol.* **190**, 79–87.

Otwinowski, Z. & Minor, W. (1997) Processing of X-ray diffraction data collected in oscillation mode. *Methods Enzymol.* **276**, 307–326.

Paytubi, S., McMahon, S.A., Graham, S., Liu, H., Botting, C. H., Makarova, K.S., Koonin, E.V., Naismith, J.H. & White, M.F. (2012) Displacement of the canonical single-stranded DNA-binding protein in the Thermoproteales. *Proc. Natl Acad. Sci. USA* **109**, E398–E405.

Ponomarev, V.A., Makarova, K.S., Aravind, L. & Koonin, E. V. (2003) Gene duplication with displacement and rearrangement: origin of the bacterial replication protein PriB from the single-stranded DNA-binding protein Ssb. *J. Mol. Microbiol. Biotechnol.* **5**, 225–229.

Raghunathan, S., Kozlov, A.G., Lohman, T.M. & Waksman, G. (2000) Structure of the DNA binding domain of *E. coli* SSB bound to ssDNA. *Nat. Struct. Biol.* **7**, 648–652.

Shioi, S., Ose, T., Maenaka, K., Shiroishi, M., Abe, Y., Kohda, D., Katayama, T. & Ueda, T. (2005) Crystal structure of a biologically functional form of PriB from *Escherichia coli* reveals a potential single-stranded DNA-binding site. *Biochem. Biophys. Res. Commun.* **326**, 766–776.

Swinger, K.K., Lemberg, K.M., Zhang, Y. & Rice, P.A. (2003) Flexible DNA bending in HU-DNA cocrystal structures. *EMBO J.* **22**, 3749–3760.

Szymanski, M.R., Jezewska, M.J. & Bujalowski, W. (2010) Interactions of the *Escherichia coli* primosomal PriB protein with the single-stranded DNA. Stoichiometries, intrinsic affinities, cooperativities, and base specificities. *J. Mol. Biol.* **398**, 8–25.

Theobald, D.L., Mitton-Fry, R.M. & Wuttke, D.S. (2003) Nucleic acid recognition by OB-fold proteins. *Annu. Rev. Biophys. Biomol. Struct.* **32**, 115–133.

Wang, C.C., Chang, T.C., Lin, C.W., Tsui, H.L., Chu, P.B., Chen, B.S., Huang, Z.S. & Wu, H.N. (2003) Nucleic acid binding properties of the nucleic acid chaperone domain of hepatitis delta antigen. *Nucleic Acids Res.* **31**, 6481–6492.

Received: 23 February 2012
Accepted: 28 July 2012

Hindawi Publishing Corporation
Journal of Biomedicine and Biotechnology
Volume 2012, Article ID 735368, 11 pages
doi:10.1155/2012/735368

Research Article

Characterization of Flavonol Inhibition of DnaB Helicase: Real-Time Monitoring, Structural Modeling, and Proposed Mechanism

Hsin-Hsien Lin[1] and Cheng-Yang Huang[1,2]

[1] *Department of Biomedical Sciences, Chung Shan Medical University, No. 110, Section 1, Chien-Kuo N. Road, Taichung City 40201, Taiwan*
[2] *Department of Medical Research, Chung Shan Medical University Hospital, No. 110, Section 1, Chien-Kuo N. Road, Taichung City 40201, Taiwan*

Correspondence should be addressed to Cheng-Yang Huang, cyhuang@csmu.edu.tw

Received 1 February 2012; Revised 18 April 2012; Accepted 22 May 2012

Academic Editor: S. L. Mowbray

DnaB helicases are motor proteins essential for DNA replication, repair, and recombination and may be a promising target for developing new drugs for antibiotic-resistant bacteria. Previously, we established that flavonols significantly decreased the binding ability of *Klebsiella pneumoniae* DnaB helicase (*Kp*DnaB) to dNTP. Here, we further investigated the effect of flavonols on the inhibition of the ssDNA binding, ATPase activity, and dsDNA-unwinding activity of *Kp*DnaB. The ssDNA-stimulated ATPase activity of *Kp*DnaB was decreased to 59%, 75%, 65%, and 57%, in the presence of myricetin, quercetin, kaempferol, and galangin, respectively. The ssDNA-binding activity of *Kp*DnaB was only slightly decreased by flavonols. We used a continuous fluorescence assay, based on fluorescence resonance energy transfer (FRET), for real-time monitoring of *Kp*DnaB helicase activity in the absence and presence of flavonols. Using this assay, the flavonol-mediated inhibition of the dsDNA-unwinding activity of *Kp*DnaB was observed. Modeled structures of bound and unbound DNA showed flavonols binding to *Kp*DnaB with distinct poses. In addition, these structural models indicated that L214 is a key residue in binding any flavonol. On the basis of these results, we proposed mechanisms for flavonol inhibition of DNA helicase. The resulting information may be useful in designing compounds that target *K. pneumoniae* and other bacterial DnaB helicases.

1. Introduction

DNA helicases are motor proteins that play essential roles in DNA replication, repair, and recombination [1, 2]. In the replicative hexameric helicase, the fundamental reaction is the unwinding of double-stranded DNA (dsDNA) into single-stranded DNA (ssDNA) intermediates to provide ssDNA templates for DNA polymerases at the replication fork [3]. The most widely studied replicative helicase is *Escherichia coli* DnaB helicase (*Ec*DnaB) [4]. *Ec*DnaB participates in the initiation of DNA replication once the *oriC* region of *E. coli* is bound by the DnaA initiator protein [5, 6]. It continues to act during the priming and elongation phases of DNA replication, and it catalyzes ATP hydrolysis and migrates on the DNA template with a strict 5′-3′ direction [5]. ATP hydrolysis may drive the movement of the helicase toward the 3′ end of the lagging strand [7].

Currently, infections occur that are resistant to all antibacterial options [8]. Few therapies are effective against the six antibiotic-resistant ESKAPE pathogens (*Enterococcus faecium*, *Staphylococcus aureus*, *Klebsiella pneumoniae*, *Acinetobacter baumannii*, *Pseudomonas aeruginosa*, and *Enterobacter* species) [9, 10]. *K. pneumoniae* (*Kp*) is a ubiquitous opportunistic pathogen that causes severe diseases such as septicemia, pneumonia, urinary tract infections, and soft tissue infections [11]. Since DnaB helicase is required for DNA replication, blocking the activity of DnaB helicase would be detrimental to bacterial survival [12]. In addition,

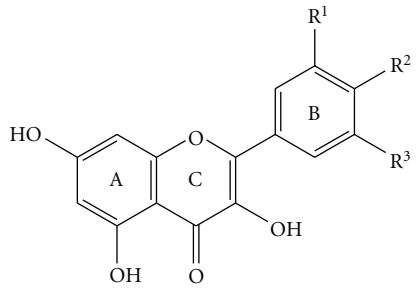

	R^1	R^2	R^3
Galangin	H	H	H
Kaempferol	H	OH	H
Quercetin	OH	OH	H
Myricetin	OH	OH	OH

Figure 1: Molecular structure of myricetin (Myr), quercetin (Que), kaempferol (Kae), and galangin (Gal).

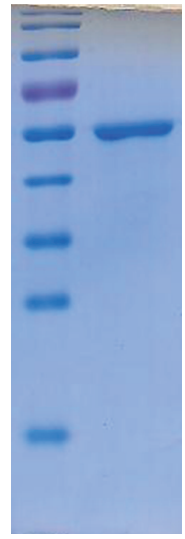

Figure 2: Coomassie Blue-stained SDS-PAGE (12%) of the purified *Kp*DnaB and molecular mass standards. The sizes of the standard proteins, from the top down, are as follows: 170, 130, 100, 70, 55, 40, 35, 25, and 15 kDa.

because the structure and function between eukaryotic and prokaryotic DnaB-like helicases are different [5, 12], the *K. pneumoniae* DnaB helicase (*Kp*DnaB) and other bacterial DnaB-like proteins may be a promising target in developing antibiotics.

Previously, we determined the three-dimensional structures of the *Geobacillus kaustophilus* DnaB-family protein (*Gk*DnaB) and its complex with ssDNA [7]. Although the overall structure of the apo and the complex forms of *Gk*DnaB is similar, the largest difference is found in their loop I region, which undergoes a strong conformational change during the helicase's action [7]. These structural and functional analyses are useful in helping our understanding of the mechanism of DNA translocation in replication forks, and the resulting information may be useful in designing compounds that target bacterial DnaB helicases. Recently, we established that the 4 flavonols (Figure 1) myricetin (Myr), quercetin (Que), kaempferol (Kae), and galangin (Gal) can interact with *Kp*DnaB and prevent dNTP binding [13]. Flavonoids are the most common group of plant polyphenols, and are responsible for much of the flavor and color of fruits and vegetables [14]. Over 5000 different flavonoids have been described; many of these compounds display structure-dependent biological and pharmacological activities [15]. The 6 major subclasses of flavonoids are flavonols, flavones, flavanones, flavanols, anthocyanidins, and isoflavones [14]. Flavonols, composed of 2 aromatic rings linked by a heterocyclic pyran-4-one ring, are known to have antioxidant [16], antiradical [17], and antibacterial activities [18]. In the present study, we further investigated the effect of flavonols on the inhibition of the ssDNA binding, ATPase activity, and dsDNA-unwinding activity of *Kp*DnaB. A new assay that enables the real-time measurement of DNA helicase activity was also developed. This assay may be useful for screening helicase inhibitors at high throughput.

2. Materials and Method

2.1. Materials. All restriction enzymes and DNA-modifying enzymes were purchased from New England Biolabs (Ipswich, MA, USA) unless explicitly stated otherwise. All custom oligonucleotide primers were obtained from Invitrogen Corporation (Carlsbad, CA, USA). All chemicals were purchased from Sigma-Aldrich (St. Louis, MO, USA) unless explicitly stated otherwise.

2.2. Protein Expression and Purification. The encoding region of *Kp*DnaB was put on pET21e expression vector and expressed with a hexahistidine tag at the C-terminus of the recombinant protein. The pET21e vector [19] was engineered from the pET21b vector (Novagen Inc., Madison, WI, USA), to avoid having the N-terminal T7 tag fused with the gene product. Details of the construction of pET21e-*Kp*DnaB expression vector and protein purification have been described previously [13]. The purified protein was dialyzed against Buffer B (20 mM HEPES, 100 mM NaCl; pH 7.0), and concentrated to 5 mg/mL. Protein purity remained greater than 95% as determined by Coomassie-stained SDS-PAGE (Figure 2).

2.3. Gel Shifts. EMSA for *Kp*DnaB was carried out using the same protocol as described previously for SSB proteins [20–22], with a minor modification. ssDNA oligonucleotides were custom synthesized by MdBio, Inc., Frederick, MD, USA. Radiolabeling was carried out with [γ^{32}P]ATP (6000 Ci/mmol; PerkinElmer Life Sciences) and T4 polynucleotide kinase (Promega, Madison, WI, USA). *Kp*DnaB (0, 90, 170, 340, 680, 1360, 2730, and 5450 nM) was incubated for 30 min at 25°C with 1.7 nM ssDNA substrate (dT30) and 16.7 μM flavonol in a total volume of 10 μL in 20 mM HEPES (pH 7.0) and 100 mM NaCl. Aliquots (5 μL) were

removed from each reaction solution and added to 2 μL of gel-loading solution (0.25% bromophenol blue and 40% sucrose, w/v). The resulting samples were resolved on a native 8% polyacrylamide gel (8.3 × 7.3 cm) at 4°C in TBE buffer (89 mM Tris borate and 1 mM EDTA) for 1 h at 100 V and visualized by phosphorimaging. The phosphor storage plate was scanned, and the data for complexed and free DNA bands were digitized for quantitative analysis. The ssDNA binding ability ($K_{d,app}$ value) for the protein was estimated from the protein concentration that binds 50% of the input DNA [23–25]. Each K_d value is calculated as the average of at least three measurements ± S.D.

2.4. FRET-Based dsDNA Unwinding Activity Assay. To monitor the 5′-3′ DNA helicase activity of *Kp*DnaB in real-time, we developed an assay on the basis of fluorescence resonance energy transfer (FRET) method. The dsDNA substrate was prepared with the fluorescent strand, 5′-TAGTACCGCCACCCTCAGAACC-3′ with Alexa Fluor 488 (maximum excitation/emission = 495/519 nm) coupled to the 5′-end, and the complementary quencher strand, 3′-ATCATGGCGGTGGGAGTCTTGGTTTTTTTTTTTTTT-5′ with BHQ1 coupled to the 3′-end, at a 1 : 1.2 concentration ratio. The dsDNA substrate was formed in 20 mM HEPES (pH 7.0) and 100 mM NaCl, by brief heating at 95°C for 5 min and then followed by slow cooling to room temperature overnight. The fluorescence helicase assay was performed in 20 mM HEPES (pH 7.0), 100 mM NaCl, 3 mM $MgCl_2$, 50 nM dsDNA substrate, and 5 mM ATP in 2.0 mL of reaction volume. The unwinding reaction was started by adding *Kp*DnaB (200 nM) and was carried out at 37°C for 60 min using a spectrofluorimeter (Hitachi F-2700; Hitachi High-Technologies, Tokyo, Japan). The fluorescence intensity was recorded every 5 s. The DNA helicase activity was calculated as the initial reaction velocity from the linear part of the progress curve using the linear regression method.

2.5. ATPase Activity Assay. The protocol for measuring the ATPase activity of purified *Kp*DnaB is based on the colorimetric determination of inorganic phosphate (Pi) released by the hydrolysis of ATP [26]. The ATPase activity assay for *Kp*DnaB (20–50 ng) was performed in 20 mM HEPES (pH 7.0), 100 pmol of ϕX-ssDNA, 10 μM flavonol, 100 mM NaCl, 3 mM $MgCl_2$, and 5 mM ATP in 100 μL of reaction volume. Liberated Pi was detected using ammonium molybdate and malachite green solutions, and absorbance was measured at 610 nm using a UV/vis spectrophotometer (Thermo Scientific Helios Omega; Thermo Fisher Scientific Inc., Waltham, MA, USA). The ATPase activity of *Kp*DnaB was calibrated with sodium phosphate (NaH_2PO_4) of known concentrations.

2.6. Bioinformatics. The amino acid sequences of *Kp*DnaB, *Ec*DnaB, *Gs*DnaB, and *Gk*DnaB were aligned using CLUSTALW2 [27]. The model of *Kp*DnaB was built from the coordinates of 2R6D (crystal structure of *Gs*DnaB), 2VYF (crystal structure of *Gk*DnaB), and 2VYE (crystal structure of *Gk*DnaB in complex with ssDNA) by using SWISS-MODEL, http://swissmodel.expasy.org/ [28]. The coordinate and topology file of the flavonols, Myr, Que, Kae, and Gal, was found in DrugBank, http://www.drugbank.ca/ [29]. The flavonol was individually computationally docked into the three-dimensional models of *Kp*DnaB by using PatchDock, http://bioinfo3d.cs.tau.ac.il/PatchDock/ [30]. The structures were visualized by using the program PyMol.

3. Results

3.1. Sequence Analysis. The gene *KPN04439*, encoding *K. pneumoniae* DnaB helicase, was initially found using a database search through the National Center for Biotechnology Information (NCBI). Based on the known nucleotide sequence, the predicted *Kp*DnaB monomer protein has a length of 471 amino acid residues and a molecular mass of 52.5 kDa, with a pI of 4.93. Analysis of the primary structure of *Kp*DnaB revealed the presence of the putative Walker A motif (aa 232–238), Walker B motif (aa 340–343), ATP binding sites (aa 237–238, 343, 384, 420, 442, and 453), and DNA binding sites (348, 349, 356–358, 383–391, 419-420, and 432-433); these are common in all known DnaB helicases. Figure 3 shows an alignment of the amino acid sequences of *K. pneumoniae* [13], *E. coli* [31], *Geobacillus stearothermophilus* [32], and *Geobacillus kaustophilus* DnaB helicases [7]; their ATP (boxed) and DNA binding sites (shaded in gray) are highly conserved.

3.2. ssDNA-Dependent ATPase Activity of KpDnaB. The ATPase activity of purified *Kp*DnaB is based on the vanadate-sensitive colorimetric determination of inorganic phosphate released by the hydrolysis of ATP [26]. Figure 4(a) shows a standard linear regression curve generated by plotting the optical density (OD) at 610 nm against the concentrations of sodium phosphate (NaH_2PO_4). After some preliminary experiments to establish a suitable range of concentrations for the reagents (including *Kp*DnaB) used for the assay, 3 mM $MgCl_2$, 5 mM ATP, 10 μM flavonol, and 20–50 ng of *Kp*DnaB were chosen for analysis of inhibition of *Kp*DnaB ATPase activity by the flavonol. In the absence of the flavonol and ϕX-ssDNA, the specific activity of *Kp*DnaB was $0.42 \pm 0.09\,\mu\text{mol}\cdot\text{min}^{-1}\cdot\text{mg}^{-1}$. In the presence of ϕX-ssDNA, the specific activity of *Kp*DnaB was increased to $5.5 \pm 0.6\,\mu\text{mol}\cdot\text{min}^{-1}\cdot\text{mg}^{-1}$. These data are similar to reported values for *Ec*DnaB; the activity of *Ec*DnaB is 3.3×10^5 (without M13 ssDNA) and 6.4×10^6 $\text{pmol}\cdot\text{min}^{-1}\cdot\text{mg}^{-1}$ (with M13 ssDNA), respectively, [33]. Thus, the ATPase activity of *Kp*DnaB was stimulated by ssDNA, a property common to all DnaB helicases.

3.3. ATPase Activity of KpDnaB Is Inhibited by Flavonols. Previously, we showed that the binding of *Kp*DnaB to dNTP is inhibited by the flavonols Myr, Kae, Gal, and Que [13]. Here, as shown in Figure 4(b), the ATP hydrolysis activity of *Kp*DnaB was also inhibited by the flavonols. In the presence of Myr, Que, Kae, or Gal, the specific activity of *Kp*DnaB was decreased to 59%, 75%, 65%, and 57%, respectively, meaning that Gal exhibited the strongest inhibitory effect on the ATP hydrolysis of *Kp*DnaB in the presence of ϕX-ssDNA.

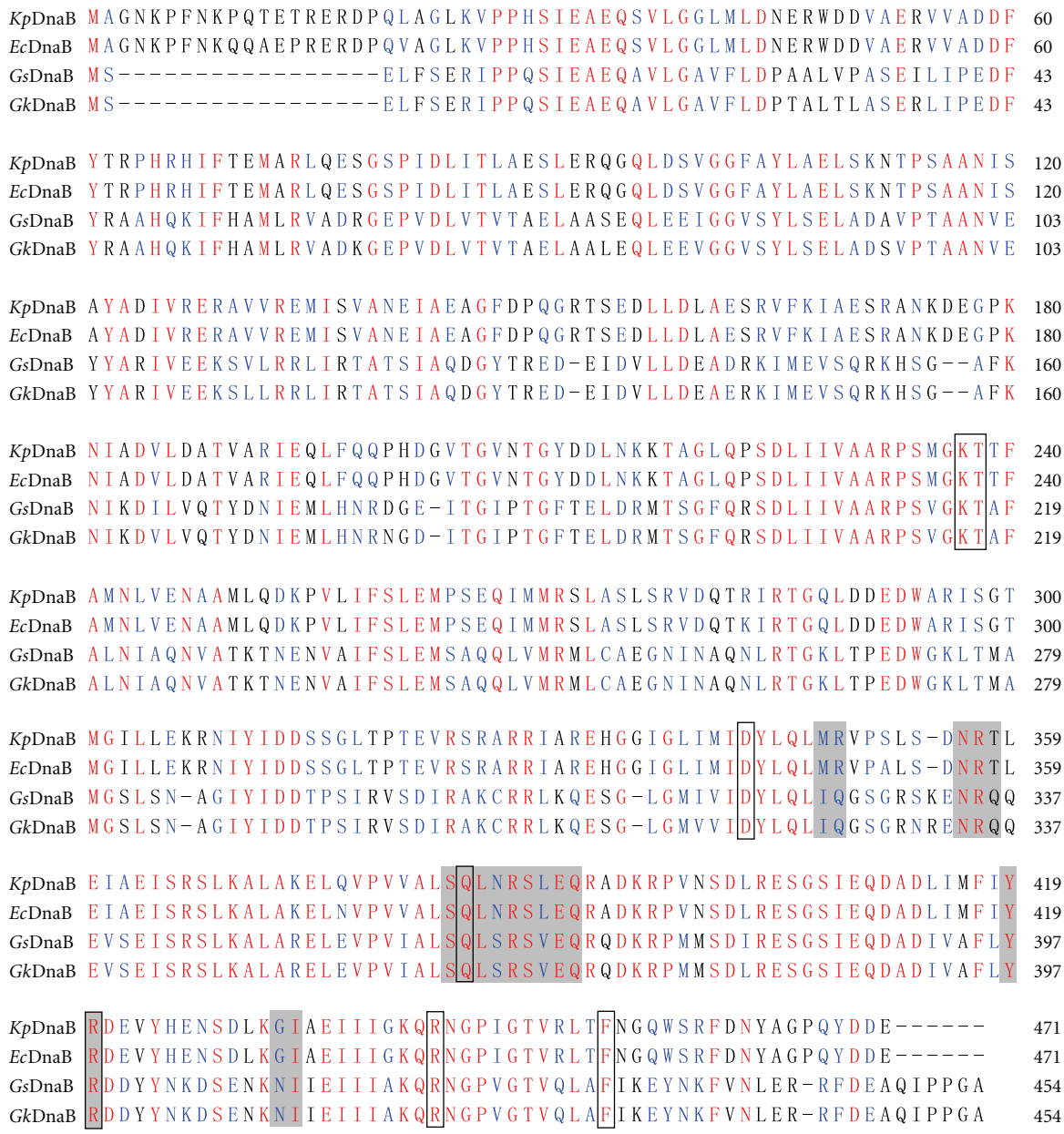

Figure 3: Multiple amino acids sequence alignment of DnaB helicases. Alignment was carried out using CLUSTALW2. Amino acid residues displaying 100% homology are highlighted in red, and those displaying similarity are highlighted in blue. The amino acids that are involved in ATP binding are boxed. The amino acids that are involved in ssDNA binding are shaded in gray. For clarity, only 4 bacterial stains are shown. Abbreviations: *Kp*, *K. pneumoniae*; *Ec*, *E. coli*; *Gs*, *Geobacillus stearothermophilus* [32]; *Gk*, *Geobacillus kaustophilus* [7].

3.4. Inhibitory Effects of Flavonols on ssDNA Binding of KpDnaB. To investigate whether the ssDNA-binding ability of *Kp*DnaB is inhibited by the flavonol, we used EMSA to study the binding of *Kp*DnaB to dT30 (Figure 5) when mixed with Myr, Que, Kae, or Gal. In the absence of any flavonol, *Kp*DnaB formed a stable complex with dT30, as shown by electrophoresis (Figure 5(a)). In the presence of 16.7 μM Gal (Figure 5(b)), Kae (Figure 5(c)), Que (Figure 5(d)), or Myr (Figure 5(e)), *Kp*DnaB still bound to dT30, but the binding activity was slightly decreased. The apparent dissociation constant ($K_{d,app}$) values of *Kp*DnaB bound to dT30 in the absence of any flavonol or presence of Myr, Que, Kae, or Gal, as determined from the titration curves, were 0.97 ± 0.07, 1.11 ± 0.05, 1.03 ± 0.07, 1.10 ± 0.05, and 1.03 ± 0.06 μM, respectively. It should be noted that the observed inhibition was dependent on protein concentration (Figure 5(f)); the disruption of formation of the *Kp*DnaB-dT30 complex did disappear when its concentration was increased to 2.72 μM, a value that the [flavonol]/[*Kp*DnaB monomer] ratio is ~6.1 (16.7/2.73 = 6.14).

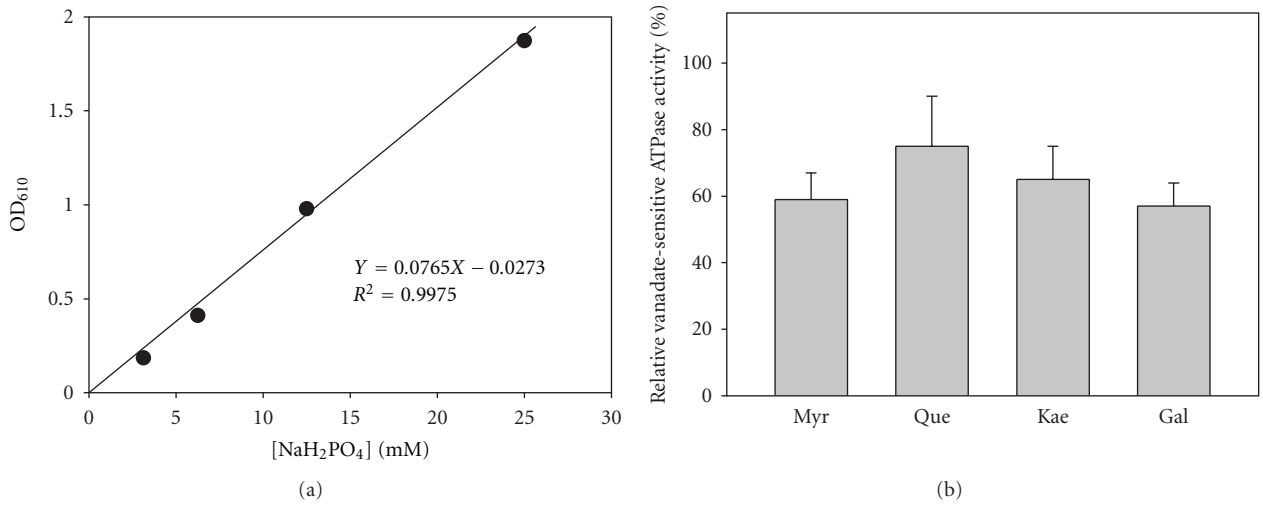

Figure 4: ssDNA-dependent ATPase activity of *Kp*DnaB. (a) The vanadate-sensitive colorimetric determination of inorganic phosphate released by the hydrolysis of ATP. A standard linear regression curve was generated by plotting the optical density (OD) at 610 nm against the concentrations of sodium phosphate (NaH_2PO_4). (b) ATPase activity of *Kp*DnaB is inhibited by flavonols. In the presence of Myr, Que, Kae, or Gal, the specific activity of *Kp*DnaB was decreased to 59%, 75%, 65%, and 57%, respectively.

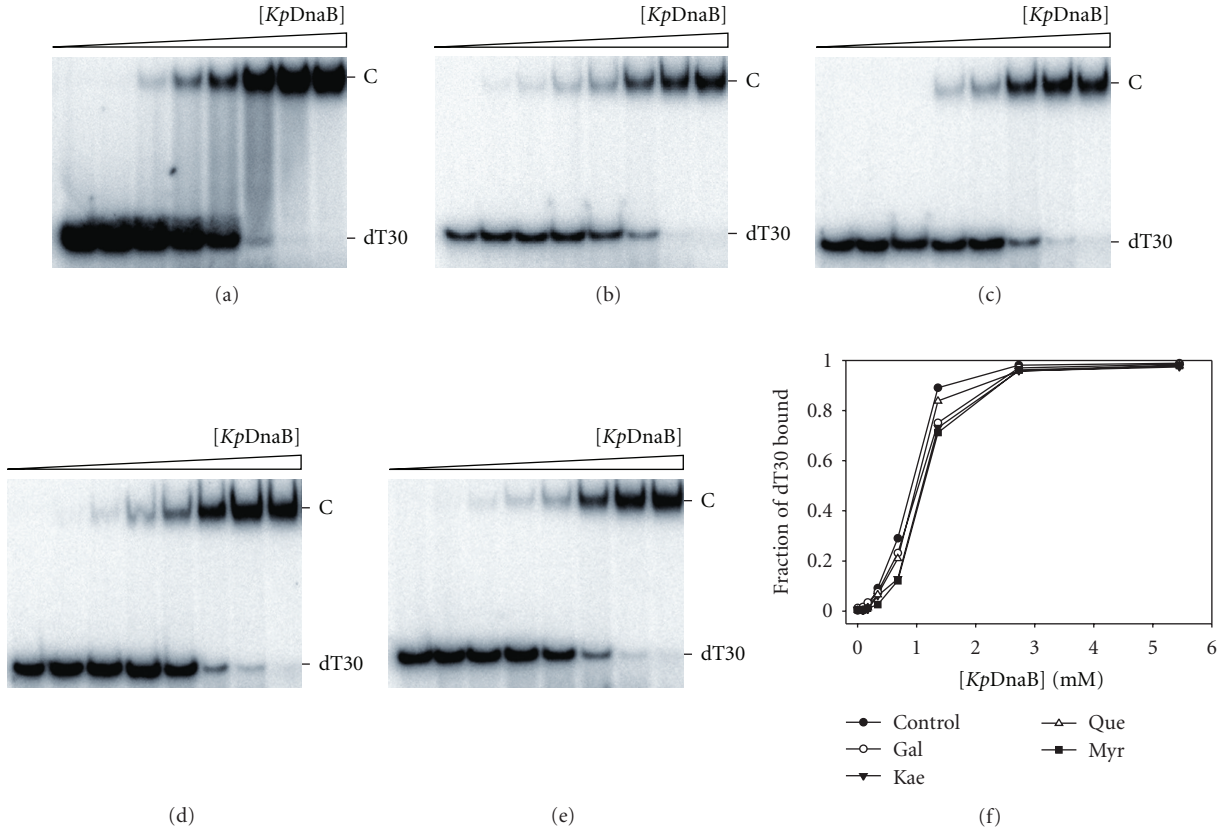

Figure 5: Inhibitory effects of flavonols on ssDNA binding of *Kp*DnaB. EMSA of *Kp*DnaB bound to dT30 (a) in the absence of any flavonol or presence of (b) Gal, (c) Kae, (d) Que, or (e) Myr. (f) The titration curves for ssDNA binding of *Kp*DnaB. The apparent dissociation constant ($K_{d,app}$) values of *Kp*DnaB bound to dT30 in the absence of any flavonol or presence of Myr, Que, Kae, or Gal, as determined from the titration curves, were 0.97 ± 0.07, 1.11 ± 0.05, 1.03 ± 0.07, 1.10 ± 0.05, and 1.03 ± 0.06 μM, respectively.

Table 1: Docking results of *Kp*DnaB with Myr and Que from PatchDock.

Solution number	Score	
	Myr	Que
1	4142	4170
2	3938	4096
3	3802	3994
4	3796	3962
5	3752	3766
6	3722	3694

3.5. Real-Time Monitoring of KpDnaB Helicase Activity Based on FRET. To investigate whether the helicase activity of *Kp*DnaB is also inhibited by flavonols, the fluorescence helicase assay was carried out in the absence or presence of Myr or Gal. This assay, modified from that for HCV NS3 3′-5′ RNA helicase [34], was found to be useful for *Kp*DnaB. The dsDNA substrate was prepared by annealing 2 oligonucleotides, a 5′ fluorophore-labeled (Alexa Fluor 488) 22-nucleotide donor and a 3′ quencher-labeled (BHQ1) 36-nucleotide quencher (Figure 6(a)). When the dsDNA substrate is unwound by the helicase, the fluorophore (F) emits upon its release from the quencher (Q). The fluorescence quenching efficiency (signal-to-background ratio) for this substrate was >90%, suggesting high sensitivity for monitoring helicase activity, similar to that for HCV NS3 RNA helicase [34].

Because of its high inhibitory effects on the ATPase activity of *Kp*DnaB (Figure 4(b)), Myr and Gal were selected for this assay. When *Kp*DnaB was added, fluorescence was continuously emitted, whereas no increase in fluorescence occurred in the absence of *Kp*DnaB (as the negative control). These results indicate that the observed fluorescence emission arose from the unwinding of the dsDNA substrate by purified *Kp*DnaB (Figure 6(b)). When assaying the helicase activity of *Kp*DnaB in the presence of Myr or Gal, a linear increase in fluorescence emission was also observed. In addition, the initial velocity for *Kp*DnaB helicase activity was nearly identical with or without flavonol ($\sim 1 \times 10^{-3}$ fluorescence intensity/s). In contrast, unlike fluorescence emission of *Kp*DnaB that continued to increase, the fluorescence emission of *Kp*DnaB assayed in the presence of the flavonol Myr or Gal soon reached its maximal point. The magnitude of fluorescence activity for *Kp*DnaB was in the following order: no flavonol added > Myr present > Gal present.

3.6. Homology Modeling. The most thoroughly studied replicative DnaB helicase from bacteria is that of *E. coli*. Although *Kp*DnaB shows a high degree of sequence identity with *Ec*DnaB, its crystal structure is not yet reported. To deeply understand the structure-function relationship of the flavonol-*Kp*DnaB-ssDNA complex(es), we decided to model its three-dimensional structure by homology modeling. The model of *Kp*DnaB was built from the coordinates of 2R6D (crystal structure of *Gs*DnaB), 2VYF (crystal structure of *Gk*DnaB) and 2VYE (crystal structure of *Gk*DnaB in complex with ssDNA) by using SWISS-MODEL, http://swissmodel.expasy.org/ [28]. *Kp*DnaB and *Gk*DnaB share 47% identity and 69%, similarity, and *Kp*DnaB and *Gs*DnaB share 46% identity and 69% similarity, respectively, in the amino acid sequences level. The three-dimensional model of the hexameric *Kp*DnaBs all forms a ring structure (Figure 7(a)), of which the loop I position in *Gk*DnaB-ssDNA complex based model was different. We propose that, as in the *Gk*DnaB complexes [7], loop I of *Kp*DnaB undergoes a conformational change, and thereby playing an important role in stabilizing DNA binding. It should be noted that the NTP-binding site, Walker A and B motifs, is adjacent to the DNA interaction site loop I (Figure 7(b)).

3.7. Docking Study Using PatchDock. The flavonol, found in DrugBank, was individually computationally docked into the three-dimensional models of *Kp*DnaB by using PatchDock, http://bioinfo3d.cs.tau.ac.il/PatchDock/ [30]. After uploading the coordinate and topology file of the flavonol and *Kp*DnaB, the docking was automatically performed. The docking results for *Kp*DnaB (*Gk*DnaB based model) interacting with Myr or Que are shown in Figure 8 and Table 1. Myr (Figure 8(a)) and Que (Figure 8(b)) were found to be docked in the ATP-binding pocket of *Kp*DnaB; however, there were also a few binding poses docked outside the pocket (Figure 8(b)). Despite a similar structure, these flavonols were found to be docked with distinct binding poses in the ATP-binding pocket of both DNA-unbound and DNA-bound models of *Kp*DnaB. For example, the binding pose of *Kp*DnaB to Myr is different from that of Que (Figure 9(a)). Que, the compound with 2 hydroxyl groups on the B ring, interacts with L214 and N215, whereas Myr (3 hydroxyl groups) interacts with L214, N247, and F460. In addition, the same compound is also found to be docked in different positions of the ATP-binding pocket of both DNA-unbound and DNA-bound models of *Kp*DnaB. For instance, Myr interacts with L214, N247, and F460 in the DNA-unbound model, and interacts with L214 and N462 in the DNA-bound model of *Kp*DnaB, respectively (Figure 9(b)). Generally, L214 is a key residue in all DNA-unbound and DNA-bound modeled structures regardless of which flavonol was used.

4. Discussion

The development of clinically useful small molecule antibiotics has been a seminal event in the world of infectious diseases [35]. DNA replication is one of the most basic biological functions and should be a prime target in antibiotic development. For example, some novel inhibitors were discovered to target topoisomerase [36, 37], DNA gyrase [38], RNA polymerase [39], helicase-primase [40], and retroviral reverse transcriptase [41, 42]. Since DNA helicases are important components of the cellular replication machinery in all organisms, inhibition of helicase activity would be detrimental to bacterial survival as well. Previously, we have shown that some flavonoid compounds can directly bind to *Kp*DnaB and inhibit its binding ability

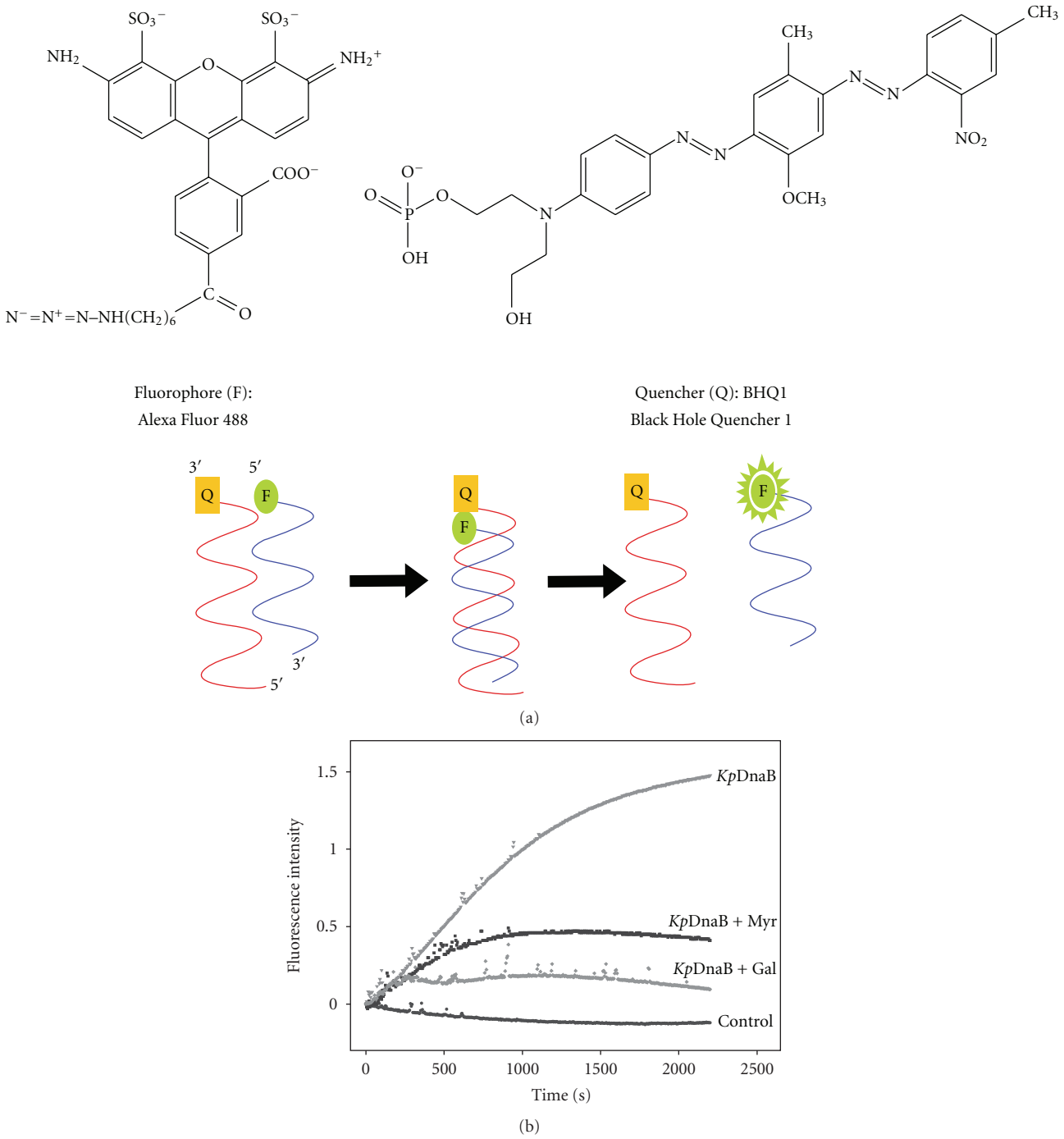

Figure 6: Real-time monitoring of *Kp*DnaB helicase activity. (a) Schematic representation of fluorescence helicase assay based on FRET. The dsDNA substrate was prepared by annealing 2 oligonucleotides, a 5′ fluorophore-labeled (Alexa Fluor 488) 22-nucleotide donor, and a 3′ quencher-labeled (BHQ1) 36-nucleotide quencher. When the dsDNA substrate is unwound by the helicase, the fluorophore (F) emits upon its release from the quencher (Q). (b) Inhibitory effects of flavonols on *Kp*DnaB helicase activity. Myr and Gal were selected for this assay.

to nucleotides, thus interfering with the growth of *K. pneumoniae* [13]. Flavonoids [14] are the most common group of plant polyphenols with antioxidant [16], antiradical [17], and antibacterial activities [18]. It is now clear that some flavonoids are ATP-inhibiting agents as competitors for ATP-binding proteins. For example, several flavonoid derivatives have been developed as therapeutic agents for cancer [43]. In this study, we used several assays to analyze the effects of 4 flavonols, namely, Myr, Que, Kae, and Gal—which contain different numbers of hydroxyl substituents on the aromatic rings—on the ssDNA binding, ATP hydrolysis, and dsDNA unwinding abilities of *Kp*DnaB. For the first

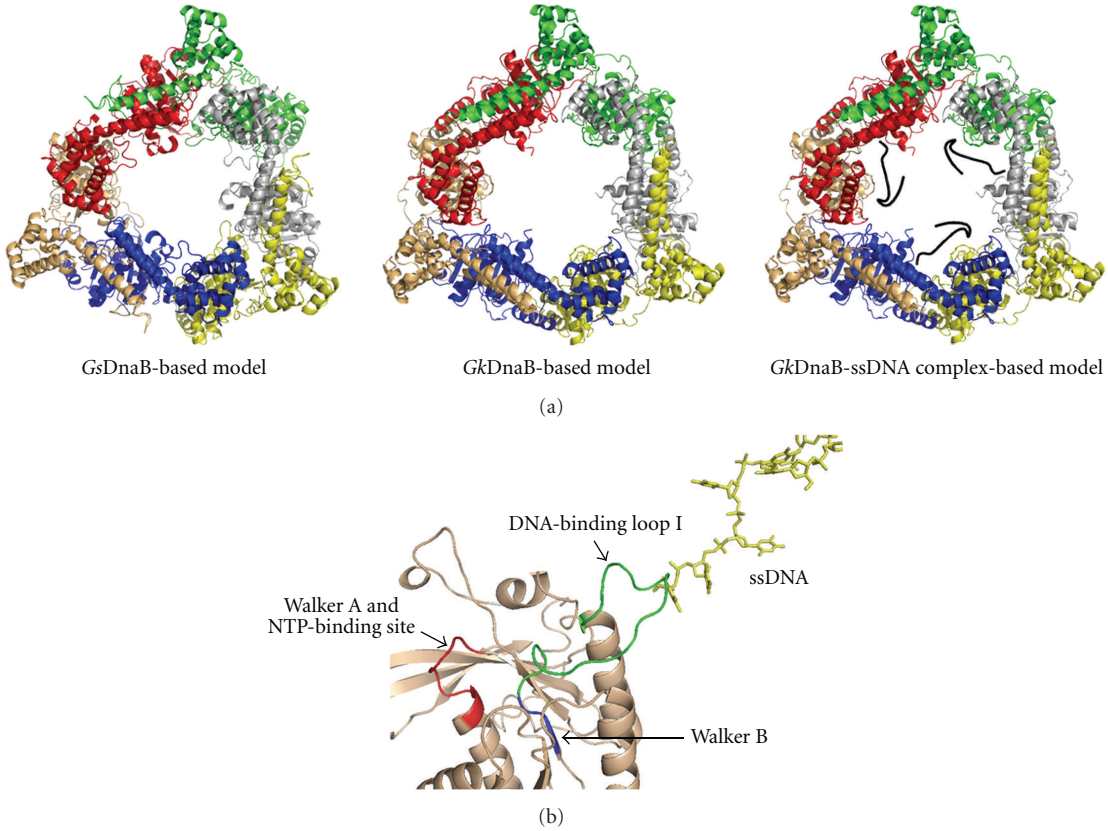

Figure 7: Homology modeling. (a) The three-dimensional models of the hexameric *Kp*DnaB form a ring structure. The monomers are colored differently. ssDNA is colored in black. (b) The structural model of the *Kp*DnaB-ssDNA complex. The NTP-binding site, Walker A and B motifs, is adjacent to the DNA interaction site loop I (green). There are synergistic effects between the nucleotide and ssDNA binding [7]. The Walker A and B motifs are colored in red and blue, respectively. ssDNA is colored in gold.

time, our results demonstrated that these flavonols were capable of inhibiting the unwinding activity of the helicase.

DnaB helicase is an ssDNA-dependent ATPase. Previously, we showed that the binding of *Kp*DnaB to dNTP is inhibited by the flavonols Myr, Kae, Gal, and Que. This study further investigated the flavonol-mediated inhibition of *Kp*DnaB binding to dNTP, which may have led to the associated decrease in ATPase activity in the presence of ssDNA (Figure 4). The ATP-hydrolyzing activity of *Kp*DnaB was inhibited by flavonols in the following order of decreasing efficiency: Gal > Myr > Kae > Que. Although it is well established that flavonoids have several hydroxyl groups, and thus have marked potentials to bind any protein, the strength of inhibition of *Kp*DnaB ATP-hydrolyzing activity did not correlate with the number of hydroxyl substituents on the flavonol aromatic rings. In addition, the structural model of *Kp*DnaB shows that these flavonols bind to *Kp*DnaB with distinct binding poses in the ATP-binding pocket (Figure 9). This situation is also found in several ATP-binding proteins that bind to different flavonoids. Crystal structures of PIM1 kinase in complex with quercetagetin and Myr reveal 2 distinct binding poses in the ATP-binding pocket, namely, orientations I and II [44]. Myr, adopting orientation II, has flipped 180° in PIM1 kinase, in contrast to quercetagetin (orientation I), such that the B ring is oriented toward the entrance of the ATP pocket. These orientations in PIM1 are also found to closely resemble those of Que and Myr in phosphatidylinositol 3-kinase [45]. Although the ATP-binding pocket in these proteins, including *Kp*DnaB, is different, cases of PIM1 and phosphatidylinositol 3-kinase with different binding poses, are very similar to that of *Kp*DnaB. Despite a very similar structure, flavonols may bind to *Kp*DnaB by using different mechanisms, as shown in the structural models (Figures 8 and 9). This may explain why the strength of inhibition in *Kp*DnaB ATPase activity was not correlated with the number of hydroxyl substituents on the flavonol aromatic rings.

Other studies showed that Myr noncompetitively inhibits *E. coli* DnaB helicase with an IC_{50} of approximately 10 μM [46]; however, we have recently discovered that Gal, Kae, Que, and Myr can inhibit dNTP binding to *Kp*DnaB, indicating a specific inhibitory process. Furthermore, these flavonols can be docked into the *Kp*DnaB ATP-binding pocket. It is not known whether this disparity is due to the inherent differences among the species, or an alternative (allosteric) binding site(s) in DnaB helicase. However, the docking results also show that a few binding poses of the flavonol outside the ATP-binding pocket

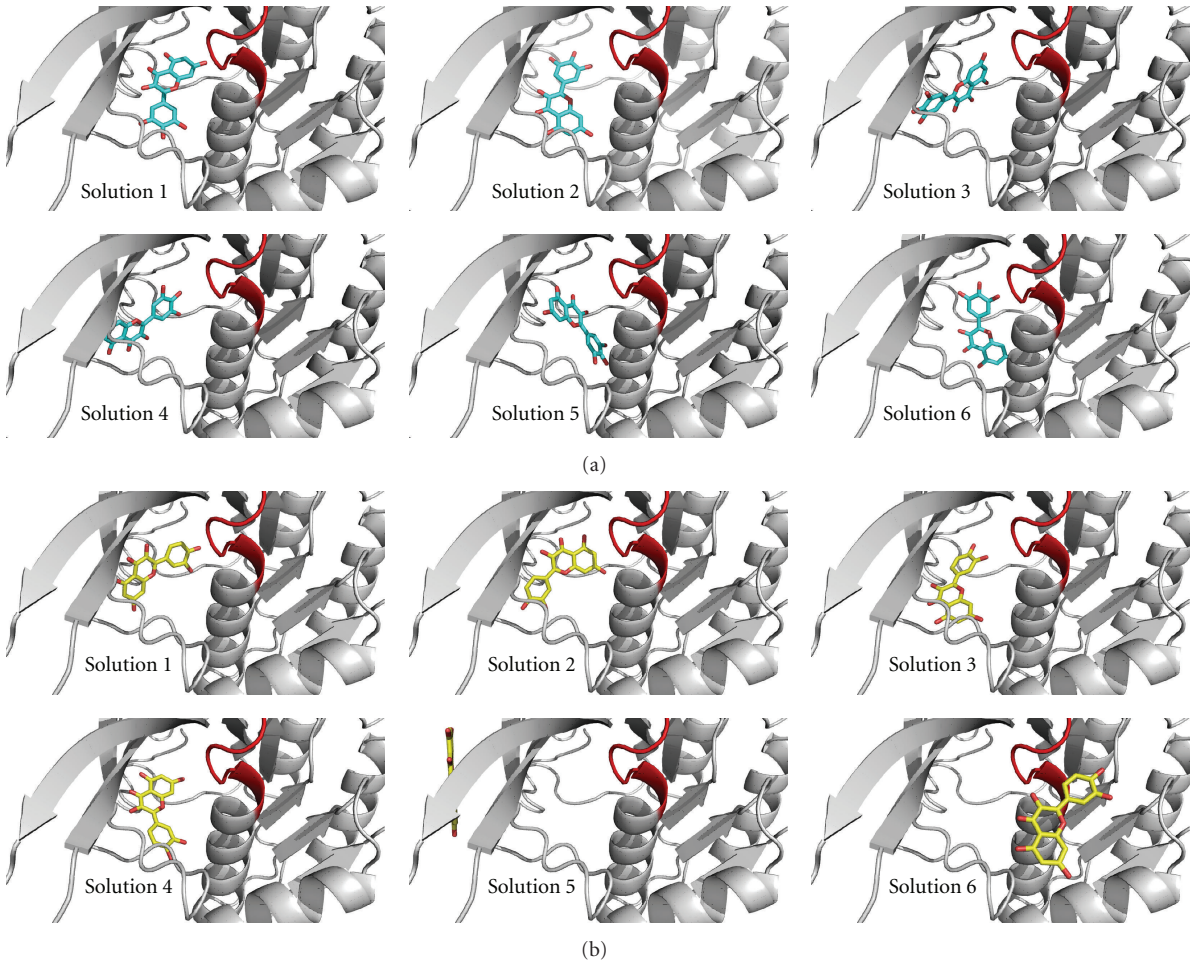

FIGURE 8: Representation of the docking models from PatchDock. The six docking models with the highest score for *Kp*DnaB (*Gk*DnaB-based model) interacting with (a) Myr and (b) Que are shown. The Walker A motif (aa 232–238), a nucleotide binding site, is colored in red.

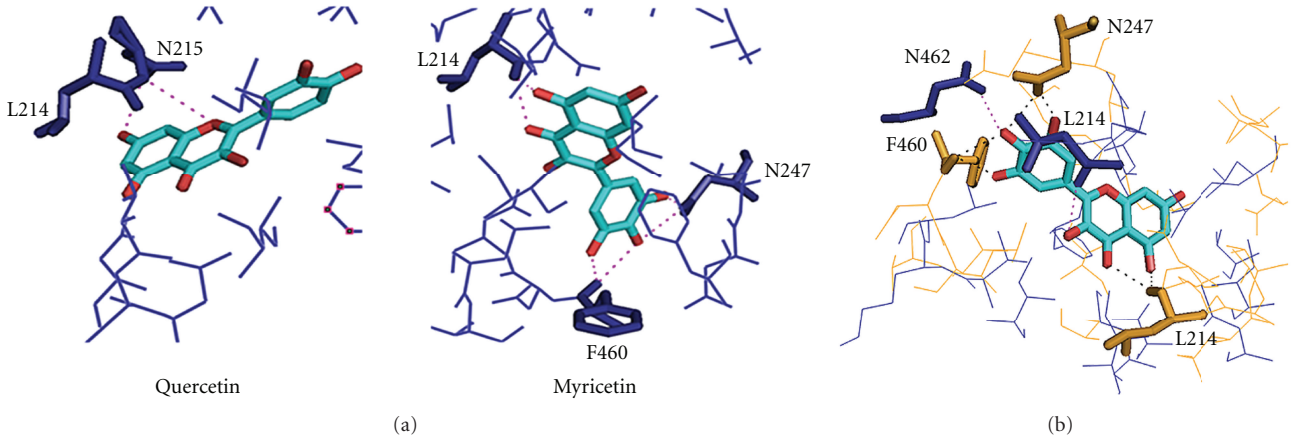

FIGURE 9: (a) The binding pose of *Kp*DnaB to Myr is different from that of Que. Que interacts with L214 and N215, whereas Myr interacts with L214, N247, and F460. (b) Myr was docked in different positions of the ATP-binding pocket of both DNA-unbound and DNA-bound models of *Kp*DnaB. Myr interacts with L214, N247, and F460 in the DNA-unbound model, and interacts with L214 and N462 in the DNA-bound model of *Kp*DnaB, respectively.

(Figure 8), suggesting that there may be more than one site for flavonol binding in the DnaB helicase. This may explain why Myr non-competitively inhibits *Ec*DnaB. In addition, we also showed flavonol-mediated inhibition of *Kp*DnaB-ssDNA complex formation, which depended on the [flavonol]/[*Kp*DnaB monomer] ratio; at a ~6 fold ratio, the inhibitory effect did disappear (Figure 5). Since these flavonols inhibited not only the ATPase activity of *Kp*DnaB but also the ssDNA-binding ability, we believe that there may be more than one site in *Kp*DnaB for flavonol binding. However, this speculation must be confirmed by further biochemical experiments.

In this study, we describe a new in vitro fluorescence assay for measuring 5′-3′ DNA helicase activity by using dsDNA substrate (Figure 6). Alexa Fluor 488 and BHQ1 were selected as the fluorophore-quencher pair. This assay enables the real-time, high-throughput measurement of DNA helicase activity, and does not require time-consuming procedures like the conventional gel-based assays. For example, on the basis of this assay, we observed that the initial velocity of *Kp*DnaB for the unwinding activity assayed in the absence of the flavonol, or with Myr or Gal were very similar; however, their maximal activities were different. While fluorescence was continuously emitted without the addition of flavonol to the *Kp*DnaB solution, the fluorescence increase stopped at ~300 s and ~600 s for Myr and Gal, respectively (Figure 6(b)). This real-time unwinding kinetics of the DNA helicase cannot be easily observed by the conventional gel-based assays. Our laboratory is currently screening DNA helicase inhibitors using this high-throughput method.

All DNA-unbound and DNA-bound modeled structures showed flavonols binding to *Kp*DnaB with distinct poses. However, these models all displayed a key residue involved in the flavonol binding, namely, L214. The L214 residue in DnaB helicases is highly conserved (Figure 3), but its role has not yet been determined. On the basis of these results, we propose that these flavonols may inhibit *Kp*DnaB in 2 possible ways. First, since DnaB helicase binding to dNTP causes a large conformational change [31, 47, 48] to become a translocase [7], these flavonols may partially occupy the ATP-binding pocket of the DnaB helicase and inhibit conformational change, thereby causing varying degrees of inhibition. This is a possible inhibition mechanism because the L214 residue of *Kp*DnaB is not involved in ATP binding (Figure 3), but most structural models indicate its importance in binding flavonols (Figure 9). Second, more than one flavonol binds to *Kp*DnaB; 1 is at the active site, and the other(s) is at an unknown site. The overall inhibition possibly results from the interactions between the flavonols and the enzyme. This may be a reason why flavonols not only bind at the ATP pocket of the DNA helicase, but can also non-competitively inhibit the ATPase activity of the DNA helicase [46]. Our crystal structure of *Gk*DnaB in complex with ssDNA previously suggested that ATP hydrolysis may drive the movement of the helicase toward the 3′ end of the lagging strand [7]. In addition, the dNTP-binding site of the helicase at loop I, part of the Walker B motif, is adjacent to the DNA interaction site. In conclusion, the flavonol likely inhibits the DNA helicase (translocase) activity by affecting the ATP binding of *Kp*DnaB, to ultimately shut down and lock the enzyme in the ATP-unbound state.

Acknowledgments

The authors thank Ms. Yen-Hua Huang for structural modeling and docking. This research was supported by a grant from the National Research Program for Genome Medicine, Taiwan (NSC 100-3112-B-040-001 to C.-Y. Huang).

References

[1] R. Reyes-Lamothe, D. J. Sherratt, and M. C. Leake, "Stoichiometry and architecture of active DNA replication machinery in *Escherichia coli*," *Science*, vol. 328, no. 5977, pp. 498–501, 2010.

[2] M. L. Mott and J. M. Berger, "DNA replication initiation: mechanisms and regulation in bacteria," *Nature Reviews Microbiology*, vol. 5, no. 5, pp. 343–354, 2007.

[3] K. J. Marians, "Prokaryotic DNA replication," *Annual Review of Biochemistry*, vol. 61, pp. 673–719, 1992.

[4] T. A. Baker and S. P. Bell, "Polymerases and the replisome: machines within machines," *Cell*, vol. 92, no. 3, pp. 295–305, 1998.

[5] M. R. Singleton, M. S. Dillingham, and D. B. Wigley, "Structure and mechanism of helicases and nucleic acid translocases," *Annual Review of Biochemistry*, vol. 76, pp. 23–50, 2007.

[6] S. S. Patel and K. M. Picha, "Structure and function of hexameric helicases," *Annual Review of Biochemistry*, vol. 69, pp. 651–697, 2000.

[7] Y. H. Lo, K. L. Tsai, Y. J. Sun, W. T. Chen, C. Y. Huang, and C. D. Hsiao, "The crystal structure of a replicative hexameric helicase DnaC and its complex with single-stranded DNA," *Nucleic Acids Research*, vol. 37, no. 3, pp. 804–814, 2009.

[8] H. W. Boucher, G. H. Talbot, J. S. Bradley et al., "Bad bugs, no drugs: no ESKAPE! An update from the Infectious Diseases Society of America," *Clinical Infectious Diseases*, vol. 48, no. 1, pp. 1–12, 2009.

[9] K. K. Kumarasamy, M. A. Toleman, T. R. Walsh et al., "Emergence of a new antibiotic resistance mechanism in India, Pakistan, and the UK: a molecular, biological, and epidemiological study," *The Lancet Infectious Diseases*, vol. 10, no. 9, pp. 597–602, 2010.

[10] K. Bush, "Alarming β-lactamase-mediated resistance in multidrug-resistant *Enterobacteriaceae*," *Current Opinion in Microbiology*, vol. 13, no. 5, pp. 558–564, 2010.

[11] R. Podschun and U. Ullmann, "*Klebsiella* spp. as nosocomial pathogens: epidemiology, taxonomy, typing methods, and pathogenicity factors," *Clinical Microbiology Reviews*, vol. 11, no. 4, pp. 589–603, 1998.

[12] P. Soultanas, "The bacterial helicase-primase interaction: a common structural/functional module," *Structure*, vol. 13, no. 6, pp. 839–844, 2005.

[13] C. C. Chen and C. Y. Huang, "Inhibition of *Klebsiella pneumoniae* dnab helicase by the flavonol galangin," *Protein Journal*, vol. 30, no. 1, pp. 59–65, 2011.

[14] J. A. Ross and C. M. Kasum, "Dietary flavonoids: bioavailability, metabolic effects, and safety," *Annual Review of Nutrition*, vol. 22, pp. 19–34, 2002.

[15] F. Teillet, A. Boumendjel, J. Boutonnat, and X. Ronot, "Flavonoids as RTK inhibitors and potential anticancer agents," *Medicinal Research Reviews*, vol. 28, no. 5, pp. 715–745, 2008.

[16] K. L. Wolfe and R. H. Liu, "Structure-activity relationships of flavonoids in the cellular antioxidant activity assay," *Journal of Agricultural and Food Chemistry*, vol. 56, no. 18, pp. 8404–8411, 2008.

[17] S. Burda and W. Oleszek, "Antioxidant and antiradical activities of flavonoids," *Journal of Agricultural and Food Chemistry*, vol. 49, no. 6, pp. 2774–2779, 2001.

[18] T. P. T. Cushnie and A. J. Lamb, "Antimicrobial activity of flavonoids," *International Journal of Antimicrobial Agents*, vol. 26, no. 5, pp. 343–356, 2005.

[19] C. C. Wang, H. W. Tsau, W. T. Chen, and C. Y. Huang, "Identification and characterization of a putative dihydroorotase, KPN01074, from *Klebsiella pneumoniae*," *Protein Journal*, vol. 29, no. 6, pp. 445–452, 2010.

[20] H. C. Jan, Y. L. Lee, and C. Y. Huang, "Characterization of a single-stranded DNA-binding protein from *Pseudomonas aeruginosa* PAO1," *Protein Journal*, vol. 30, no. 1, pp. 20–26, 2011.

[21] Y. H. Huang, Y. L. Lee, and C. Y. Huang, "Characterization of a single-stranded DNA binding protein from *Salmonella* enterica serovar typhimurium LT2," *Protein Journal*, vol. 30, no. 2, pp. 102–108, 2011.

[22] Y. H. Huang and C. Y. Huang, "Characterization of a single-stranded DNA binding protein from *Klebsiella pneumoniae*: mutation at either Arg73 or Ser76 causes a less cooperative complex on DNA," *Genes to Cells*, vol. 17, pp. 146–157, 2012.

[23] H. C. Hsieh and C. Y. Huang, "Identification of a novel protein, PriB, in *Klebsiella pneumoniae*," *Biochemical and Biophysical Research Communications*, vol. 404, no. 1, pp. 546–551, 2011.

[24] C. Y. Huang, C. H. Hsu, Y. J. Sun, H. N. Wu, and C. D. Hsiao, "Complexed crystal structure of replication restart primosome protein PriB reveals a novel single-stranded DNA-binding mode," *Nucleic Acids Research*, vol. 34, no. 14, pp. 3878–3886, 2006.

[25] J. H. Liu, T. W. Chang, C. Y. Huang et al., "Crystal structure of PriB, a primosomal DNA replication protein of *Escherichia coli*," *Journal of Biological Chemistry*, vol. 279, no. 48, pp. 50465–50471, 2004.

[26] P. P. Van Veldhoven and G. P. Mannaerts, "Inorganic and organic phosphate measurements in the nanomolar range," *Analytical Biochemistry*, vol. 161, no. 1, pp. 45–48, 1987.

[27] M. A. Larkin, G. Blackshields, N. P. Brown et al., "Clustal W and Clustal X version 2.0," *Bioinformatics*, vol. 23, no. 21, pp. 2947–2948, 2007.

[28] K. Arnold, L. Bordoli, J. Kopp, and T. Schwede, "The SWISS-MODEL workspace: a web-based environment for protein structure homology modelling," *Bioinformatics*, vol. 22, no. 2, pp. 195–201, 2006.

[29] C. Knox, V. Law, T. Jewison et al., "DrugBank 3.0: a comprehensive resource for 'Omics' research on drugs," *Nucleic Acids Research*, vol. 39, no. 1, pp. D1035–D1041, 2011.

[30] D. Schneidman-Duhovny, Y. Inbar, R. Nussinov, and H. J. Wolfson, "PatchDock and SymmDock: servers for rigid and symmetric docking," *Nucleic Acids Research*, vol. 33, no. 2, pp. W363–W367, 2005.

[31] A. Roychowdhury, M. R. Szymanski, M. J. Jezewska, and W. Bujalowski, "Mechanism of NTP hydrolysis by the *Escherichia coli* primary replicative helicase DnaB protein. 2. Nucleotide and nucleic acid specificities," *Biochemistry*, vol. 48, no. 29, pp. 6730–6746, 2009.

[32] S. Bailey, W. K. Eliason, and T. A. Steitz, "Structure of hexameric DnaB helicase and its complex with a domain of DnaG primase," *Science*, vol. 318, no. 5849, pp. 459–463, 2007.

[33] E. E. Biswas and S. B. Biswas, "Mechanism of DnaB helicase of *Escherichia coli*: structural domains involved in ATP hydrolysis, DNA binding, and oligomerization," *Biochemistry*, vol. 38, no. 34, pp. 10919–10928, 1999.

[34] H. Tani, O. Fujita, A. Furuta et al., "Real-time monitoring of RNA helicase activity using fluorescence resonance energy transfer in vitro," *Biochemical and Biophysical Research Communications*, vol. 393, no. 1, pp. 131–136, 2010.

[35] A. Koul, E. Arnoult, N. Lounis, J. Guillemont, and K. Andries, "The challenge of new drug discovery for tuberculosis," *Nature*, vol. 469, no. 7331, pp. 483–490, 2011.

[36] B. D. Bax, P. F. Chan, D. S. Eggleston et al., "Type IIA topoisomerase inhibition by a new class of antibacterial agents," *Nature*, vol. 466, no. 7309, pp. 935–940, 2010.

[37] M. T. Black and K. Coleman, "New inhibitors of bacterial topoisomerase GyrA/ParC subunits," *Current Opinion in Investigational Drugs*, vol. 10, no. 8, pp. 804–810, 2009.

[38] K. L. Hopkins, R. H. Davies, and E. J. Threlfall, "Mechanisms of quinolone resistance in *Escherichia coli* and *Salmonella*: recent developments," *International Journal of Antimicrobial Agents*, vol. 25, no. 5, pp. 358–373, 2005.

[39] A. Srivastava, M. Talaue, S. Liu et al., "New target for inhibition of bacterial RNA polymerase: 'switch region'," *Current Opinion in Microbiology*, vol. 14, no. 5, pp. 532–543, 2011.

[40] K. Chono, K. Katsumata, T. Kontani et al., "ASP2151, a novel helicase-primase inhibitor, possesses antiviral activity against varicella-zoster virus and herpes simplex virus types 1 and 2," *Journal of Antimicrobial Chemotherapy*, vol. 65, no. 8, Article ID dkq198, pp. 1733–1741, 2010.

[41] S. Li, T. Hattori, and E. N. Kodama, "Epigallocatechin gallate inhibits the HIV reverse transcription step," *Antiviral Chemistry and Chemotherapy*, vol. 21, no. 6, pp. 239–243, 2011.

[42] S. C. Chu, Y. S. Hsieh, and J. Y. Lin, "Inhibitory effects of flavonoids on moloney murine leukemia virus reverse transcriptase activity," *Journal of Natural Products*, vol. 55, no. 2, pp. 179–183, 1992.

[43] M. K. Chahar, N. Sharma, M. P. Dobhal, and Y. C. Joshi, "Flavonoids: a versatile source of anticancer drugs," *Pharmacognosy Reviews*, vol. 5, no. 9, pp. 1–12, 2011.

[44] S. Holder, M. Zemskova, C. Zhang et al., "Characterization of a potent and selective small-molecule inhibitor of the PIM1 kinase," *Molecular Cancer Therapeutics*, vol. 6, no. 1, pp. 163–172, 2007.

[45] E. H. Walker, M. E. Pacold, O. Perisic et al., "Structural determinants of phosphoinositide 3-kinase inhibition by wortmannin, LY294002, quercetin, myricetin, and staurosporine," *Molecular Cell*, vol. 6, no. 4, pp. 909–919, 2000.

[46] M. A. Griep, S. Blood, M. A. Larson, S. A. Koepsell, and S. H. Hinrichs, "Myricetin inhibits *Escherichia coli* DnaB helicase but not primase," *Bioorganic and Medicinal Chemistry*, vol. 15, no. 22, pp. 7203–7208, 2007.

[47] M. J. Jezewska, U. S. Kim, and W. Bujalowski, "Interactions of *Escherichia coli* primary replicative helicase DnaB protein with nucleotide cofactors," *Biophysical Journal*, vol. 71, no. 4, pp. 2075–2086, 1996.

[48] M. J. Jezewska and W. Bujalowski, "Global conformational transitions in *Escherichia coli* primary replicative helicase DnaB protein induced by ATP, ADP, and single-stranded DNA binding: multiple conformational states of the helicase hexamer," *Journal of Biological Chemistry*, vol. 271, no. 8, pp. 4261–4265, 1996.

Genes to Cells

Characterization of a single-stranded DNA-binding protein from *Klebsiella pneumoniae*: mutation at either Arg73 or Ser76 causes a less cooperative complex on DNA

Yen-Hua Huang[1] and Cheng-Yang Huang[1,2]*

[1]*Department of Biomedical Sciences, Chung Shan Medical University, No.110, Sec.1, Chien-Kuo N. Rd., Taichung City, Taiwan*
[2]*Department of Medical Research, Chung Shan Medical University Hospital, No.110, Sec.1, Chien-Kuo N. Rd., Taichung City, Taiwan*

Single-stranded DNA-binding protein (SSB) plays an important role in DNA metabolism, such as in processes like DNA replication, repair and recombination, and is essential for cell survival. Here, we characterized the ssDNA-binding properties of *Klebsiella pneumoniae* SSB (*Kp*SSB) by using fluorescence-quenching measurements, electrophoretic mobility shift analysis (EMSA) and site-directed mutagenesis. Analysis of purified *Kp*SSB by gel-filtration chromatography showed a stable tetramer in solution. In fluorescence titrations, *Kp*SSB bound to 25–40 nucleotides (nt) per tetramer depending on the salt concentration. Using EMSA, we characterized the stoichiometry of *Kp*SSB complexed with a series of ssDNA homopolymers, and the size of the binding site was determined to be 26 ± 1 nt. Mutation at either Arg73 or Ser76 of *Kp*SSB caused a less cooperative complex on DNA. Arg73 forms an intermolecular hydrogen bond with Ser76, and this appears to be a likely driving force that directs the self-assembly of SSB on DNA.

Introduction

Single-stranded DNA-binding protein (SSB) plays an important role in DNA replication, repair and recombination (Shereda *et al.* 2008; Roy *et al.* 2009; Reyes-Lamothe *et al.* 2010). During these reactions, SSB binds to and protects susceptible single-stranded DNA (ssDNA) from nucleolytic digestion and also prevents secondary structure formation. Most bacterial and human mitochondrial SSBs (Yang *et al.* 1997) are active as homotetramers where 4 oligonucleotide-/oligosaccharide-binding folds (OB-folds) form a DNA-binding domain (Murzin 1993; Raghunathan *et al.* 2000; Chan *et al.* 2009). However, SSB from the bacterial phylum *Deinococcus-Thermus* functions as a homodimer in which each monomer contains 2 OB-folds linked by a conserved spacer sequence (Dabrowski *et al.* 2002; Witte *et al.* 2005; Fedorov *et al.* 2006). SSB from *Sulfolobus solfataricus* is a monomer that includes 1 OB-fold, which differentiates it from the bacterial form, and is likely a more ancestral 'simple' SSB (Haseltine & Kowalczykowski 2002; Kerr *et al.* 2003). A recent study showed that the DdrB protein from *Deinococcus radiodurans* is an alternative SSB and functions as a pentamer (Sugiman-Marangos & Junop 2010).

Bacterial SSBs consist of two domains, namely, an N-terminal ssDNA-binding/oligomerization domain and a flexible C-terminal protein–protein interaction domain (Shereda *et al.* 2008). The N-terminal domain is separated from the highly conserved acidic tail of the last 10 C-terminal amino acids of SSB by a long proline- (Olszewski *et al.* 2010) or glycine-rich hinge (Lohman & Ferrari 1994). The C-terminal domain of SSB interacts with other auxiliary proteins that are essential for cell survival (Curth *et al.* 1996). The binding of SSB to ssDNA makes the glycine-rich region more easily accessible to other proteins such as proteases and DNA polymerase III (Curth *et al.* 1996; Witte *et al.* 2003).

The most thoroughly studied SSB is that of *Escherichia coli* (*Ec*SSB), which binds cooperatively to ssDNA (Lohman & Ferrari 1994). The estimated size of the

Communicated by: Hisao Masai
**Correspondence*: cyhuang@csmu.edu.tw

DOI: 10.1111/j.1365-2443.2011.01577.x

binding sites of SSBs is dependent on the salt concentration in fluorescence titrations with poly(dT). *Ec*SSB mainly binds to 35- and 65-nucleotide (nt)-long ssDNA, using the $(SSB)_{35}$- and $(SSB)_{65}$-binding modes, respectively. In the $(SSB)_{35}$-binding mode, two subunits of the *Ec*SSB tetramer interact with ssDNA, whereas in the $(SSB)_{65}$-binding mode, all four subunits participate in ssDNA binding. These different binding modes of SSB may be required during different stages of DNA metabolism (Roy *et al.* 2007, 2009).

In this study, we examined the electrophoretic mobility shift patterns of *Klebsiella pneumoniae* SSB (*Kp*SSB) bound to ssDNA of different lengths. Furthermore, we also studied the binding properties of *Kp*SSB between low- and high-salt conditions using fluorescence-quenching measurements. Site-directed mutagenesis of the putative self-assembly site of *Kp*SSB was also carried out. On the basis of these biophysical analyses, the ssDNA-binding mode of *Kp*SSB proteins is discussed.

Results

Sequence analysis

The gene *KPN04446*, encoding *K. pneumoniae* SSB, was initially found using a database search through the National Center for Biotechnology Information (NCBI). On the basis of the known nucleotide sequence, the predicted *Kp*SSB monomer protein has a length of 174 amino acid residues and a molecular mass of 19 kDa. Analysis of the primary structure of *Kp*SSB by RPS-BLAST (Madden *et al.* 1996) showed the presence of a putative OB-fold domain that is common in all known SSBs. Figure 1 shows an alignment of the amino acid sequences of *K. pneumoniae*, *Salmonella enterica* Serovar Typhimurium LT2 (Huang *et al.* 2011), *Pseudomonas aeruginosa* (Jan *et al.* 2011), *Helicobacter pylori* (Chan *et al.* 2009), *E. coli* (Savvides *et al.* 2004), *Mycobacterium tuberculosis* (Saikrishnan *et al.* 2003) and *Mycobacterium smegmatis* (Saikrishnan *et al.* 2005) SSBs. In the *Ec*SSB–ssDNA complex (Raghunathan *et al.* 2000), four essential aromatic residues, Trp40, Trp54, Phe60 and Trp88, participate in ssDNA binding via stacking interactions. These residues are conserved in most SSB families as Phe/Tyr/Trp, and the corresponding residues in *Kp*SSB are Trp41, Trp55, Phe61 and Trp89. The important motif in the C-terminal tail of *Ec*SSB, DDDIPF residues, is also conserved in *Kp*SSB. In contrast to those motifs, two glycine residues found in the glycine-rich hinge of *Ec*SSB (Gly125 and Gly128) are not found in *Kp*SSB.

Oligomerization of *Kp*SSB in solution

Analysis of purified protein by gel-filtration chromatography showed a single peak (Fig. 2). Assuming that

```
KpSSB  MASRGVNKVILVGNLGQDPEVRYMPSGGAVANFTLATSESWRDKQTGEMKE-QTEWHRVVLFG   62
StSSB  MASRGVNKVILVGNLGQDPEVRYMPSGGAVANLTLATSESWRDKQTGEMKE-QTEWHRVVMFG   62
PaSSB  -MARGVNKVILVGNVGGDPETRYMPNGNAVTNITLATSESWKDKQTGQQQE-RTEWHRVVFFG   61
HpSSB  ----MFNKVIMVGRLTRNVELKYLPSGSAAATIGLATSRRFK-KQDGTLGE-EVCFIDARLFG   57
EcSSB  MASRGVNKVILVGNLGQDPEVRYMPNGGAVANITLATSESWRDKATGEMKE-QTEWHRVVLFG   62
MtSSB  --MAGDTTITIVGNLTADPELRFTPSGAAVANFTVASTPRIYDRQTGEWKDGEALFLRCNIWR   61
MsSB   --MAGDTTITVVGNLTADPELRFTPSGAAVANFTVASTPRMFDRQSGEWKDGEALFLRCNIWR   61

KpSSB  KLAEVAGEYLRKGSQVYIEGQLRTRKWTDQSGQDKYTTEV-VVNVGGTMQMLGGRQGGGAPAG  124
StSSB  KLAEVAGEYLRKGSQVYIEGQLRTRKWTDQSGQERYTTEINVPQIGGVMQMLGGRQGGGAPAG  125
PaSSB  RLAEIAGEYLRKGSQVYVEGSLRTRKWQGQDGQDRYTTEI-VVDINGNMQLLGGR-----PSG  121
HpSSB  RTAEIANQYLSKGSSVLIEGRLTYESWMDQTGKKNSRHTITADSLQFMDKKSDNPQANAMQDS  120
EcSSB  KLAEVASEYLRKGSQVYIEGQLRTRKWTDQSGQDRYTTEV-VVNVGGTMQMLGGRQGGGAPAG  124
MtSSB  EAAENVAESLTRGARVIVSGRLKQRSFETREGEKRTVIEVEVDEIGPSLRYATAKVNKASRSG  124
MsSB   EAAENVAESLTRGSRVIVTGRLKQRSFETREGEKRTVVEVEVDEIGPSLRYATAKVNKASRSG  124

KpSSB  ------GGQQQQGGWGQPQQPQ---GGNQFSGGAQSRPQQQAPAAPSNEPPMD-FDDDIPF   174
StSSB  -------GQQQQGGWGQPQQPQQPQGGNQFSGGAQSRPQQSAP-APSNEPPMD-FDDDIPF   176
PaSSB  -------DDSQRAPREPMQRP------QQAPQQQSRPAPQQQPAPQPAQDYDSFDDDIPF   165
HpSSB  IMHENSNNAYPANHNAPSQDPFN-QAYAQNAYAKENLQAQPSKYQNSVPEINIDEEEIPF   179
EcSSB  GNI--GGGQPQGGWGQPQQPQ---GGNQFSGGAQSRPQQSAPAAPSNEPPMD-FDDDIPF   178
MtSSB  ------------GFGSGSRPA-------PAQTS-SASGDDPWGSAPASGSFGGGDDEPPF   164
MsSB   ------------GGGGGFGSG-------GGGSRQSEPKDDPWGSAPASGSFSGADDEPPF   165
```

Figure 1 Multiple amino acid sequence alignment of SSB proteins. Sequence alignment of *Kp*SSB, with other SSB proteins from *Salmonella enterica serovar Typhimurium LT2* (*St*SSB), *Escherichia coli* (*Ec*SSB), *Mycobacterium tuberculosis* (*Mt*SSB), *Mycobacterium smegmatis* (*Ms*SSB), *Helicobacter pylori pylori* (*Hp*SSB) and *Pseudomonas aeruginosa* (*Pa*SSB), was generated by CLUSTALW2 (Larkin *et al.* 2007). Amino acid residues displaying 100% identity are highlighted in bold black, and those displaying similarity are highlighted in black.

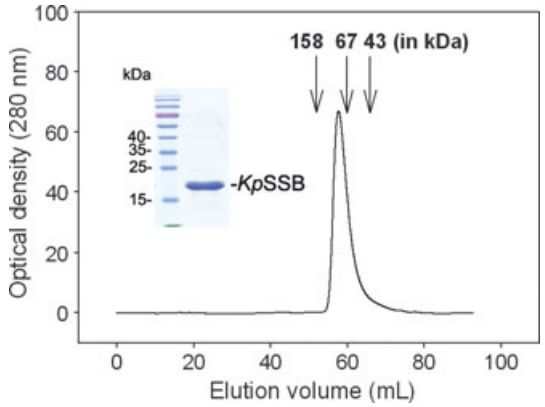

Figure 2 Gel-filtration chromatographic analysis of *Kp*SSB. Purified *Kp*SSB protein in buffer (0.1 M NaCl and 20 mM Tris–HCl at pH 8.0) was applied to a Superdex 200 HR 10/30 column equilibrated with the same buffer. The proteins were detected by measuring absorbance at 280 nm. The column was calibrated with proteins of known molecular masses: γ-globulin (158 kDa), albumin (67 kDa), ovalbumin (43 kDa), chymotrypsinogen A (25 kDa) and ribonuclease A (13.7 kDa). The sizes of the molecular mass markers (in kDa) are indicated at the top. The corresponding peak shows the eluted *Kp*SSB. Coomassie Blue-stained SDS-PAGE (12%) of the purified *Kp*SSB and molecular mass standards are also shown. The sizes of the standard proteins, from the top down, are as follows: 170, 130, 100, 70, 55, 40, 35, 25 and 15 kDa. The purified *Kp*SSB migrated between the 25 and 15 kDa standards on the SDS-PAGE.

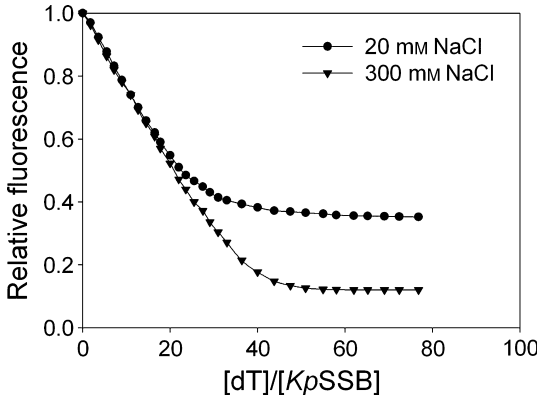

Figure 3 Fluorescence titration of *Kp*SSB with ssDNA dT50. Tryptophan fluorescence quenching of *Kp*SSB in the presence of 20 or 300 mM NaCl is shown. The excitation and emission of tryptophan fluorescence were detected at 295 and 348 nm, respectively. The *Kp*SSB solution (0.1 μM; tetramer) in 2 mL Tris–HCl buffer (20 mM Tris–HCl and pH 8.0) containing 20 or 300 mM NaCl was titrated with rising quantities of dT50 oligonucleotide. After the addition of the ssDNA, the complex solution was equilibrated for 300 s until no fluorescence change could be observed.

*Kp*SSB has a shape and partial-specific volume similar to the standard proteins, the native molecular mass of *Kp*SSB was estimated to be approximately 80 kDa. The native molecular mass for *Kp*SSB is approximately 4.1 times the molecular mass of a *Kp*SSB monomer (19 kDa). Thus, we concluded that *Kp*SSB in solution is a stable tetramer, similar to *Ec*SSB.

DNA binding monitored by quenching of intrinsic tryptophan fluorescence

It is well established that the fluorescence quenching and the estimated size of the binding sites of SSBs depend on the salt concentration of the SSB solution (Lohman & Ferrari 1994). *Kp*SSB has three tryptophan residues (Trp41, Trp55 and Trp89) in the OB-fold domain, allowing an analysis of ssDNA binding by tryptophan fluorescence quenching (Fig. 3). The protein displayed strong intrinsic fluorescence with a peak wavelength of 348 nm when excited at 295 nm, consistent with tryptophan fluorescence (data not shown). As dT50 was titrated into the *Kp*SSB solution, the intrinsic fluorescence of the protein was progressively quenched. On addition of a saturating quantity of ssDNA in the presence of 20 and 300 mM NaCl, the intrinsic fluorescence at 348 nm was quenched by 65% and 89%, respectively. The estimated binding-site sizes of *Kp*SSB in 20 and 300 mM NaCl were approximately of 27 ± 2 and 38 ± 2 nt, respectively.

*Kp*SSB binding to dT25–50 forms a single complex

To investigate the length of nucleotides sufficient for the formation of the *Kp*SSB–ssDNA complex and the ssDNA-binding ability of *Kp*SSB, we studied the binding of *Kp*SSB to dT20 (Fig. 4A), dT25 (Fig. 4B), dT30 (Fig. 4C), dT35 (Fig. 4D), dT40 (Fig. 4E), dT45 (Fig. 4F) and dT50 (Fig. 4G) with different protein concentrations using EMSA. As shown in Fig. 4A, no significant band shift was observed when *Kp*SSB was incubated with dT20, indicating that *Kp*SSB could not form a stable complex with this homopolymer. In contrast to dT20, longer dT homopolymers, dT25–50, bind to *Kp*SSB and form a single complex (Fig. 4B–G). Thus, the EMSA results suggest that the length of ssDNA required for *Kp*SSB binding ranges between 20 and 25 nt.

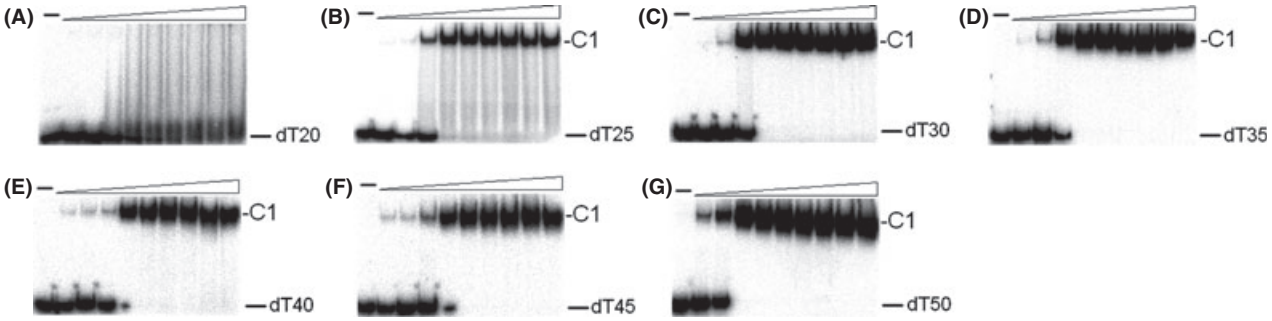

Figure 4 Binding of *Kp*SSB to dT20–50. *Kp*SSB (0, 19, 37, 77, 155, 310, 630, 1250, 2500 and 5000 nM) was incubated for 30 min at 25 °C with 1.7 nM of (A) dT20, (B) dT25, (C) dT30, (D) dT35, (E) dT40, (F) dT45 or (G) dT50 in a total volume of 10 μL in 20 mM Tris–HCl pH 8.0 and 100 mM NaCl. Aliquots (5 μL) were removed from each reaction solution and added to 2 μL of gel-loading solution (0.25% bromophenol blue and 40% sucrose). The resulting samples were resolved on a native 8% polyacrylamide gel at 4 °C in TBE buffer (89 mM Tris borate and 1 mM EDTA) for 1 h at 100 V and visualized by autoradiography.

Two different complexes are formed when *Kp*SSB binds to dT55–75

To examine the minimal nucleotide length necessary for the binding of a second *Kp*SSB tetramer to ssDNA prebound to *Kp*SSB, we studied the binding of *Kp*SSB to longer dT homopolymers of 55–75 nt (Fig. 5). Although dT55 is only 5 nt longer than dT50, the pattern of the *Kp*SSB–ssDNA complexes observed using EMSA is very different. At lower protein concentrations, *Kp*SSB forms a single complex with dT55 (Fig. 5A), similar to that observed with dT50 (Fig. 4G); however, when the *Kp*SSB concentration is increased, another slower-migrating complex appears. The appearance of the second complex results from the increasing *Kp*SSB concentration, which suggests that it may contain at least two *Kp*SSB tetramers per oligonucleotide. As the minimal length of ssDNA required for *Kp*SSB binding ranges between 20 and 25 nt (see above), the presence of an extra 5 nt in dT55, as compared with dT50, provides enough interaction space for the binding of a second *Kp*SSB tetramer, which occupies approximately 27 nt ssDNA. Furthermore, the stoichiometry of the two *Kp*SSB tetramers bound per ssDNA does not change when the length of the dT homopolymers is further increased to 75 nt (Fig. 5E). These results from EMSA suggest that the length of ssDNA required for efficient binding of *Kp*SSB is 26 ± 1 nt (Fig. 6).

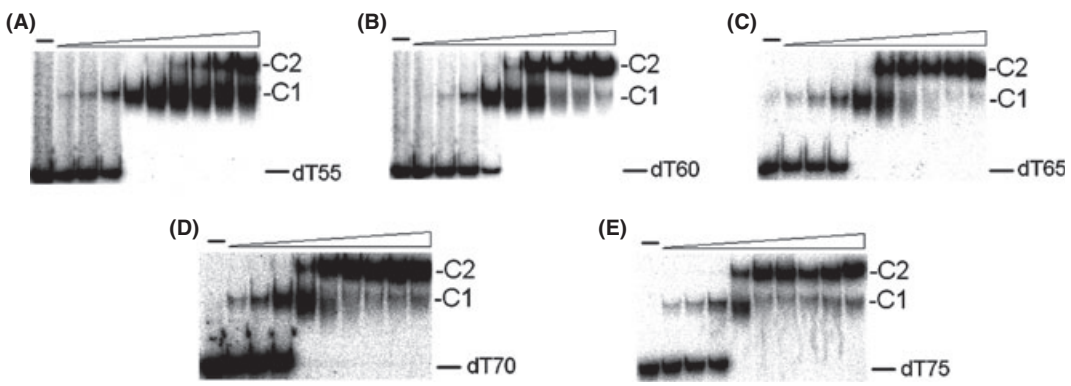

Figure 5 Binding of *Kp*SSB to dT55–75. *Kp*SSB (0, 19, 37, 77, 155, 310, 630, 1250, 2500 and 5000 nM) was incubated for 30 min at 25 °C with 1.7 nM of (A) dT55, (B) dT60, (C) dT65, (D) dT70 or (E) dT75 in a total volume of 10 μL in 20 mM Tris–HCl pH 8.0 and 100 mM NaCl. Aliquots (5 μL) were removed from each reaction solution and added to 2 μL of gel-loading solution (0.25% bromophenol blue and 40% sucrose). The resulting samples were resolved on a native 8% polyacrylamide gel at 4 °C in TBE buffer (89 mM Tris borate and 1 mM EDTA) for 1 h at 100 V and visualized by autoradiography.

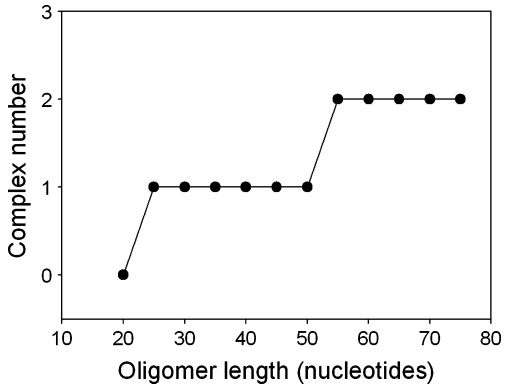

Figure 6 Summary of the complex number of *Kp*SSB. Complex number of *Kp*SSB as a function of the length of the ssDNA determined using electrophoretic mobility shift analysis (EMSA).

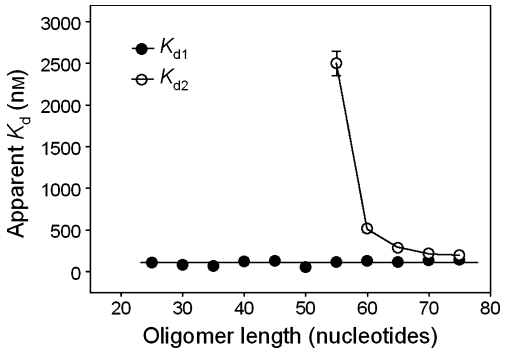

Figure 7 Summary of the apparent K_d values of *Kp*SSB. Apparent K_d values of *Kp*SSB as a function of the length of the ssDNA; K_{d1}, K_d for the formation of the first complex (C1); K_{d2}, K_d for the formation of the second complex (C2).

Binding constants of the *Kp*SSB–ssDNA complexes

The binding constants of the *Kp*SSB–ssDNA complexes (K_d values) are summarized in Table 1. The formation of the *Kp*SSB–ssDNA complex 1 (C1) was nearly ssDNA-length-independent (Fig. 7), suggesting that the protein–DNA contact for each C1 is similar. In contrast, the ability of a second *Kp*SSB tetramer (K_{d2}) to bind to ssDNA that is already bound to the *Kp*SSB tetramer was length-dependent (Fig. 7). In fact, increases in ssDNA length were associated with higher binding abilities (lower K_{d2} values), indicating that the second *Kp*SSB prefers to bind to long ssDNA segments to which *Kp*SSB tetramer(s) is already bound.

Table 1 ssDNA-binding parameters of *Kp*SSB

	*Kp*SSB	
	The apparent K_{d1} (nM)	The apparent K_{d2} (nM)
dT20		
dT25	108 ± 8	
dT30	78 ± 10	
dT35	67 ± 6	
dT40	118 ± 15	
dT45	123 ± 10	
dT50	51 ± 7	
dT55	112 ± 12	2500 ± 150
dT60	123 ± 10	513 ± 46
dT65	109 ± 14	282 ± 22
dT70	134 ± 15	214 ± 24
dT75	140 ± 18	196 ± 15

Each K_d is calculated as the average of at least three measurements ± SD.
*Kp*SSB, *Klebsiella pneumoniae* SSB.

Functional role of Arg73 in *Kp*SSB

According to the sequence and crystal structural alignments, it is known that Arg72 plays an important role in the formation of higher aggregates of *Ec*SSB (Witte *et al.* 2008). The corresponding residue in *Kp*SSB is Arg73. To investigate the role of Arg73 in the binding of a second *Kp*SSB to ssDNA prebound to *Kp*SSB, mutants were created with Gly (Fig. 8A), Ala (Fig. 8B), Thr (Fig. 8C), Asn (Fig. 8D), Asp (Fig. 8E) and Phe (Fig. 8F) substitutions, and binding of the Arg mutant protein of *Kp*SSB to dT25 or dT55 was assessed. As shown in Fig. 8, although these mutant proteins, namely, R73G, R73A, R73T, R73N, R73D and R73F, could bind to dT25 and dT55, they did not form C2 as in the case of the wild-type protein; however, R73D and R73F could weakly form a C2 only at a protein concentration of 5 μM. We also noted that most of these mutant proteins bound dT55 well; the dT55 binding ability for some of them was even better than that of the wild-type protein. For example, the apparent K_{d1} values for dT55 binding are 112 ± 12 and 70 ± 5 nM for the wild-type (Fig. 5A) and the R73A mutant protein (Fig. 8B), respectively, suggesting that the R73 mutation may not directly affect ssDNA binding. This is an indication of a less cooperative complex compared with that of the wild-type *Kp*SSB (Fig. 5). Thus, these results show that Arg73 may play a functional

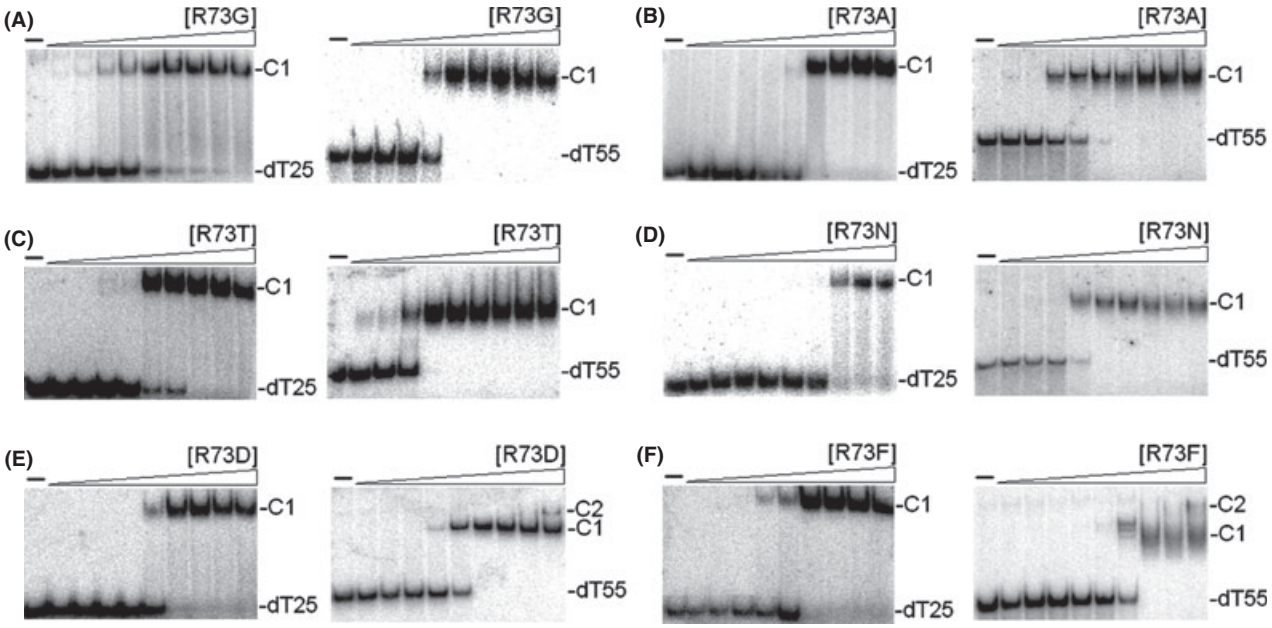

Figure 8 Analysis of Arg73 mutant proteins. Binding of Arg73 mutant proteins, (A) R73G, (B) R73A, (C) R73T, (D) R73N, (E) R73D and (F) R73F of *Kp*SSB to dT25 and dT55. The mutant protein (0, 19, 37, 77, 155, 310, 630, 1250, 2500 and 5000 nM) was incubated for 30 min at 25 °C with 1.7 nM of dT25 or dT55 in a total volume of 10 μL in 20 mM Tris–HCl pH 8.0 and 100 mM NaCl. Aliquots (5 μL) were removed from each reaction solution and added to 2 μL of gel-loading solution (0.25% bromophenol blue and 40% sucrose). The resulting samples were resolved on a native 8% polyacrylamide gel at 4 °C in TBE buffer (89 mM Tris borate and 1 mM EDTA) for 1 h at 100 V and visualized by autoradiography.

role in the interaction between *Kp*SSB tetramers on ssDNA.

Functional role of Ser76 in *Kp*SSB

Ser75 is thought to play an important role in the formation of higher aggregates of *Ec*SSB via hydrogen bonding to Arg72 (Witte *et al.* 2008). The corresponding residue to Ser75 in *Kp*SSB is Ser76. To further examine the effect of the Ser76 mutation on the binding of a second *Kp*SSB to ssDNA prebound to *Kp*SSB, mutants were created with Gly (Fig. 9A), Ala (Fig. 9B), Thr (Fig. 9C), Lys (Fig. 9D) and Asp (Fig. 9E) substitutions, similarly to our study on Arg73. For the first time, the ssDNA-binding properties of Ser76 mutant proteins of *Kp*SSB were assessed. As shown in Fig. 9, like R73, these mutant proteins, namely, S76G, S76A, S76T, S76K and S76D, could bind to dT25 and dT55, but they did not or only weakly formed C2 (S76K). Thus, like in the case of R73 mutants, these results suggest that Ser76 in *Kp*SSB is involved in the contact between *Kp*SSB tetramers on ssDNA, probably via the Arg73-mediated interaction with Ser76. However, this hypothesis must be confirmed by further biochemical experiments.

Discussion

In this study, we described the cloning, expression, purification and characterization of SSB from *K. pneumoniae*, which is a ubiquitous opportunistic pathogen that colonizes the mucosal surfaces in humans, causing severe diseases. In addition, many clinical strains of *K. pneumoniae* are highly resistant to antibiotics (Bush 2010; Tempe 2010). Sequence analysis (Fig. 1) indicates that the *Kp*SSB monomer possesses an OB-fold domain at its N-terminus and a flexible tail at its C-terminus, as in *Ec*SSB. Analysis of *Kp*SSB by gel-filtration chromatography showed that the protein forms a tetramer in solution (Fig. 2).

Here, we showed that the binding of *Kp*SSB to dT50 results in tryptophan fluorescence quenching (Fig. 3). In the presence of 20 and 300 mM NaCl, the binding-site sizes of *Kp*SSB were 27 ± 2 and 38 ± 2 nt per tetramer, respectively. In addition, two distinct binding modes could be observed between low- and high-salt conditions, as observed in *Ec*SSB.

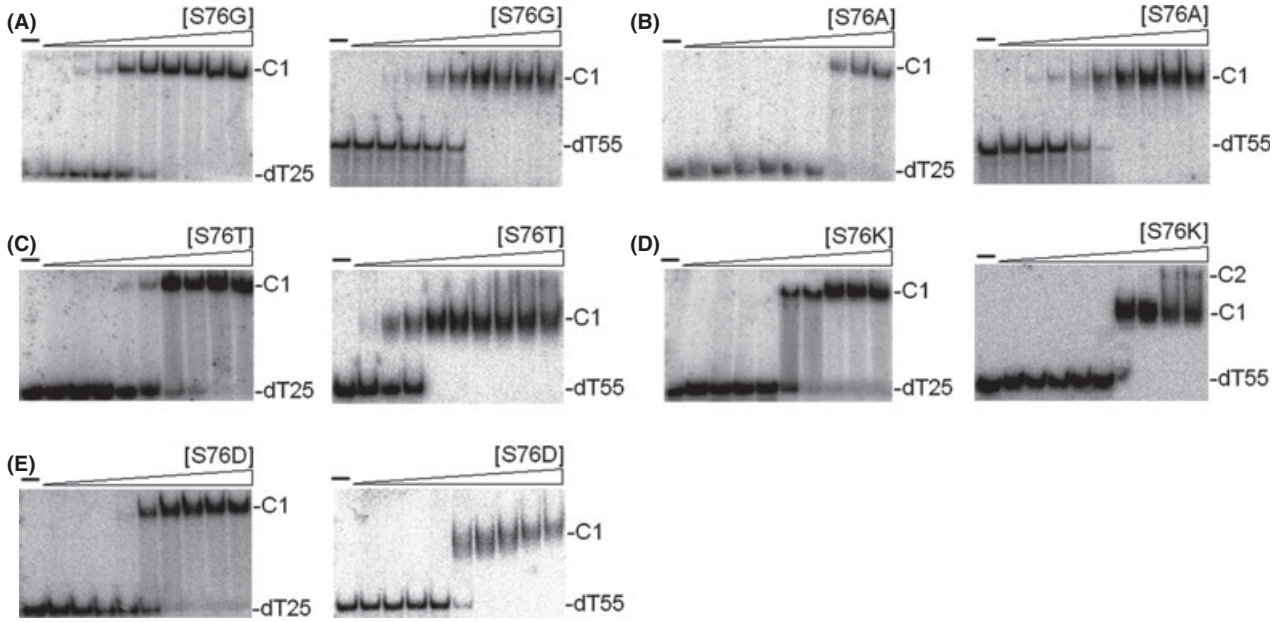

Figure 9 Analysis of Ser76 mutant proteins. Binding of Ser76 mutant proteins, (A) S76G, (B) S76A, (C) S76T, (D) S76K and (E) S76D of *Kp*SSB to dT25 and dT55. The mutant protein (0, 19, 37, 77, 155, 310, 630, 1250, 2500 and 5000 nM) was incubated for 30 min at 25 °C with 1.7 nM of dT25 or dT55 in a total volume of 10 μL in 20 mM Tris–HCl pH 8.0 and 100 mM NaCl. Aliquots (5 μL) were removed from each reaction solution and added to 2 μL of gel-loading solution (0.25% bromophenol blue and 40% sucrose). The resulting samples were resolved on a native 8% polyacrylamide gel at 4 °C in TBE buffer (89 mM Tris borate and 1 mM EDTA) for 1 h at 100 V and visualized by autoradiography.

In case of *Ec*SSB, under high-salt conditions, a 65-nt ssDNA binds to each *Ec*SSB tetramer with almost 90% quenching of fluorescence, whereas under low-salt conditions, a 35-nt ssDNA exhibits 53% quenching of fluorescence. In case of *Hp*SSB, the stoichiometry is 25 ± 2 nt per homotetramer (Chan *et al.* 2009), but the salt effect on its ssDNA-binding mode(s) remains unclear. Human replication protein A (hRPA), a eukaryotic SSB, binds to DNA in two different steps. The first binding step is noncooperative, where hRPA70-A and B bind ssDNA in a linear arrangement (approximately 8 nt), but the next two OB-fold domains bind cooperatively during the second stage of interaction where approximately 25 nt are bound per heterotrimer. (Wold 1997; Oakley & Patrick 2010). The constant binding mode (or 'salt-independent' binding mode) of SSBs determined using fluorescence quenching at high- and low-salt concentrations has also been previously reported in SSBs from the *Deinococcus-Thermus* group (Witte *et al.* 2005), *Thermotoga maritima* (Olszewski *et al.* 2010), *Thermotoga neapolitana* (Olszewski *et al.* 2010), *Thermoanaerobacter tengcongensis* (Olszewski *et al.* 2008) and *P. aeruginosa* PAO1 (Jan *et al.* 2011), possibly because of low flexibility and/or low number of glycine residues (Olszewski *et al.* 2010; Jan *et al.* 2011). In fact, eight glycine residues in the glycine-rich hinge that are found in *Ec*SSB are not found in *Pa*SSB (Fig. 1). The amino acid sequences of *Kp*SSB and *Ec*SSB are found to share >80% identity, suggesting the presence of multiple binding modes, even though two glycine residues in the glycine-rich hinge of *Ec*SSB (Gly125 and Gly128) are not found in *Kp*SSB. However, this speculation must be confirmed by further biochemical experiments.

Many SSBs bind to ssDNA with some degree of positive cooperativity. Cooperativity can result from direct protein–protein interactions between the nearest neighbors, such as the LAST motif in the T4 gene-32 protein (Casas-Finet *et al.* 1992) and the arginine-mediated interaction motif in *Thermus* SSB (Fedorov *et al.* 2006; Witte *et al.* 2008). Cooperativity can also result from the protein-induced distortion of adjacent DNA as shown by *Sulfolobus* SSB, PriB and FOXK1a proteins (Kerr *et al.* 2003; Huang *et al.* 2006; Tsai *et al.* 2006; Hsieh & Huang 2011). In case of *Kp*SSB, binding appeared to be nearly noncooperative for several DNAs, because essentially, all DNA shifts into the first complex (C1) before the appearance of the second complex (C2). In addition, the

apparent K_d values were of the first and second complex, as expected for noncooperative binding (Table 1 and Fig. 7); for positive cooperative binding, K_{d2} should be less than K_{d1}. Increasing the length of C2 caused its K_d value to match that of C1 (Fig. 7), suggesting that length dependence reflects the minimal amount of spacing that is optimal for steric considerations.

The EMSA approach used here allowed us to observe the formation of distinct complexes and to determine the ssDNA-binding mode of *Kp*SSB. A *Kp*SSB tetramer was shown to bind with other *Kp*SSB tetramer(s), thereby forming a cooperative complex on DNA. The ordered assembly of *Kp*SSB on DNA may be directed through the intermolecular Arg-Ser hydrogen bond (Witte *et al.* 2008). This hydrogen bond leads to a protein–protein interaction between *Kp*SSB tetramers. A mutation at either Arg73 (Fig. 8) or Ser76 (Fig. 9) to other residues caused a less cooperative complex on the DNA, suggesting that the formation of a hydrogen bond between these two residues may be a driving force to promote the cooperative binding of SSB to long ssDNA. However, it should be noted that this force is not a requirement for C2 formation of *Kp*SSB. In fact, if the ssDNA length was longer than dT55 (e.g., dT60), or a higher protein concentration of R73A (e.g., 12 μM; 10-fold concentrations required for the appearance of C2 for the wild-type protein) was used, the C2 could still be observed (data not shown). Thus, here, we only identified that the intermolecular Arg-Ser hydrogen bond in SSB is important, but not required, for the correct binding of a second protein to a SSB prebound DNA. Other questions concerning this are whether a DNA-induced process exists and how many subunits of a SSB are involved in this self-assembly. Furthermore, does this binding cause a specific conformational change on the C-terminal flexible region of SSB? At this point, these questions remain to be elucidated experimentally.

In addition, we found that if only 1 *Kp*SSB bound to ssDNA, the minimal nucleotide length necessary for a *Kp*SSB tetramer binding was approximately 25 nt; however, for two *Kp*SSB tetramers binding, the minimal nucleotide length was approximately 55, 22–23 nt per *Kp*SSB. This reduced binding-site size for two *Kp*SSB tetramers suggests that a conformational change during the participation of second *Kp*SSB tetramer may be occurring. Previous data showed that the binding of *Ec*SSB to long ssDNA results in a conformational change in the protein, making the glycine-rich region more easily accessible

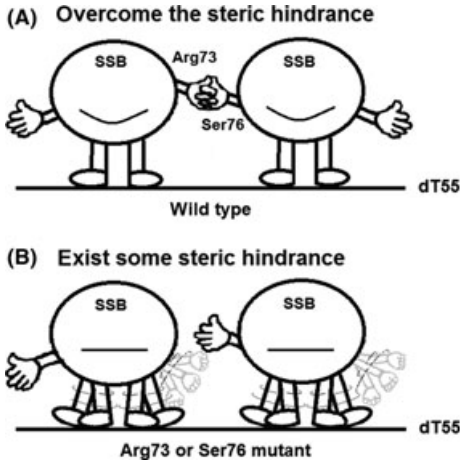

Figure 10 Proposed working model for the sequential assembly of bacterial SSB proteins. On the basis of electrophoretic mobility shift analysis (EMSA) results, the two highly conserved residues in bacterial SSB, namely, R73 and S76, may facilitate the assembly of SSB proteins on DNA by establishing an intermolecular Arg-Ser hydrogen bond. (A) The wild-type protein of SSB. The two SSB tetramers can bind to dT55 together and form a cooperative complex on DNA. (B) The R73 or S76 mutant protein of SSB. According to the sequence and crystal structural alignments (Witte *et al.* 2008), R73 and S76 play an important role in the formation of higher aggregates of SSB. Along with our mutational analysis, the intermolecular Arg-Ser hydrogen bond in SSB may serve as an anchor to pull each SSB protein closer on DNA. This model may explain why the mutant proteins could not form a cooperative complex but could bind DNA well. Shown is a working model of the Arg-Ser hydrogen bond in SSB based on these EMSA observations. Please note that if the ssDNA length is longer than dT55 or if a higher R73A protein concentration is used, the cooperative complex (C2) can still be observed.

to the action of proteases (Curth *et al.* 1996). We speculate that this phenomenon may also be applied to SSB itself; when SSB binds to long ssDNA, the resultant conformational change may make the glycine-rich region and some ssDNA-binding region of SSB more accessible to the binding of a second SSB. Therefore, some steric hindrance (e.g., the C-terminal regions) would be overcome, causing closer binding of two SSB proteins on DNA. The intermolecular Arg-Ser hydrogen bond in SSB may serve as an anchor to pull each SSB protein binding closer on DNA (Fig. 10). If SSB does not have this Arg-Ser hydrogen bond, SSB proteins may bind to DNA randomly without a specific sequence. This may explain the reason for a reduced size of the binding site for the two *Kp*SSB tetramers from EMSA data.

SSB plays an important role in DNA metabolism, including DNA replication, repair and recombination, and is absolutely essential for cell survival. The cooperative binding of SSB proteins leads to clustering of SSB protein tracts to form protein filaments on long DNA (Shereda *et al.* 2008). In this study, we identified that the highly conserved Arg73 and Ser76 in bacterial SSBs are crucial for forming the cooperative complex on DNA. The Arg73 and Ser76 are both located in a flexible loop (the $L_{\alpha 4}$) of the OB-fold domain, and thus, are possibly suitable to mediate this dynamic process. Furthermore, in other proteins, such as AAA+ proteins, the Arg residue, called arginine finger, is also found to be involved in oligomerization and inter-subunit communication in the proteins (Sauer & Baker 2011). Whether the intermolecular interaction, like between the Arg-Ser pair in bacterial SSB, is found in other proteins involved in DNA metabolism remains to be elucidated. Figure 11 shows the structurally corresponding residues, namely, Arg73 and Ser76 of *Kp*SSB, in an OB-fold domain of *Ec*SSB (R73 and S76), *Ss*SSB (K64 and Q67), hRPA70-A (E250 and K253), hRPA70-B (S371 and P374), *Ta*SSB (R190 and D193), *Dr*RecO (N51 and H54), *Tt*RecJ (L499 and E502) and *Ec*PriB (S70 and T73). On comparing the aforementioned residues, we found that only *Ta*SSB has an Arg residue like *Kp*SSB; this residue with its partner, D193, has already been proven to be structurally important for the formation of the cooperative complex (Fedorov *et al.* 2006). We also noted that hRPA70-A, but not hRPA70-B, has a potential pair, E250-K253, like that of *Kp*SSB. However, unlike *Kp*SSB forming homotetramers, hRPA functions as heterotrimers. It is still unclear whether the cooperative binding of hRPA to ssDNA in the second step is involved in the intermolecular interaction pair of E250-K253 of hRPA70-A subunits or even K253 of hRPA70-A with S371 of hRPA70-B. Possibly, these issues could be addressed by using mutational analyses like in this study.

The EMSA results indicate that *Kp*SSB binds to short ssDNAs (dT25–50) to form a complex in which a single tetramer is bound to the ssDNA (Fig. 4), and two tetramers are bound to dT55–75 (Fig. 5). Thus, the apparent size of the binding site of *Kp*SSB is 26 ± 1 nt (Fig. 7). Recently, we have determined using EMSA that the binding-site sizes of *Pa*SSB and *St*SSB are 29 ± 1 and 22 ± 1 nt, respectively (Huang *et al.* 2011; Jan *et al.* 2011). The amino acid sequence of the N-terminal ssDNA-binding/oligomerization domain in these pathogenic SSBs is highly conserved, but their apparent binding-site sizes are quite different: this suggests that the C-terminal protein–protein interaction domain may also contribute to ssDNA binding (Kozlov *et al.* 2010).

Conclusion

In this study, we characterized the ssDNA-binding properties of SSB from *K. pneumoniae* and proposed a

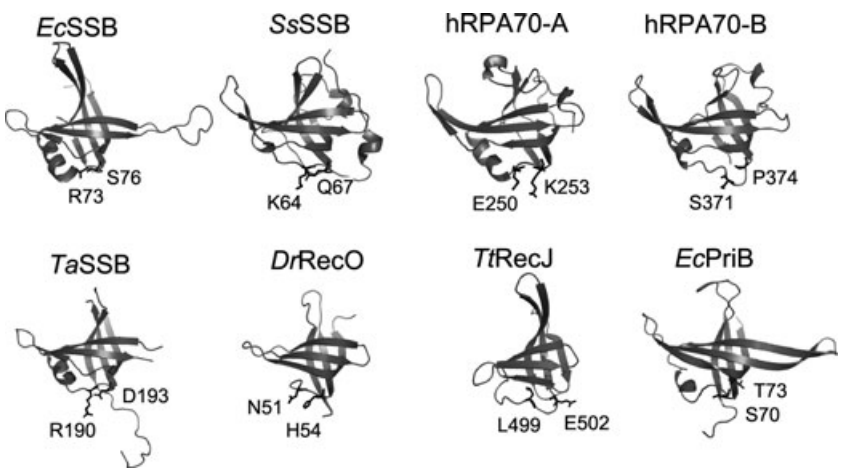

Figure 11 Molecular representation comparing potential cooperative binding sites among some OB-fold proteins involved in DNA metabolism. The structurally corresponding residues, namely, Arg73 and Ser76, of *Kp*SSB, in an OB-fold domain of the proteins, are shown. The PDB codes for *Escherichia coli* (*Ec*SSB), *Sulfolobus solfataricus* (*Ss*SSB), hRPA70-A (human), hRPA70-B, *Thermus aquaticus* (*Ta*SSB), *Deinococcus radiodurans* (*Dr*RecO), *Thermus thermophilus* (*Tt*RecJ) and *Ec*PriB are 1EYG, 1O7I, 1JMC, 1JMC, 2IHE, 1W3S, 2ZXO and 1V1Q, respectively.

putative working model for the self-assembly of SSB from EMSA results. The two highly conserved residues in bacterial SSB, R73 and S76, may facilitate the assembly of SSB proteins on DNA by establishing an intermolecular Arg-Ser hydrogen bond.

Experimental procedures

Materials

All restriction enzymes and DNA-modifying enzymes were purchased from New England Biolabs (Ipswich, MA, USA) unless explicitly stated otherwise. All chemicals were purchased from Sigma-Aldrich (St. Louis, MO, USA) unless explicitly stated otherwise. The *E. coli* strains TOP10F' (Invitrogen, USA) and BL21(DE3) pLysS (Novagen, UK) were used for genetic construction and protein expression, respectively.

Cloning, expression and purification

The gene *KPN04446* encoding the *Kp*SSB was PCR-amplified from *K. pneumoniae* subsp. *pneumoniae* MGH 78578 (Wang *et al.* 2010). The forward (5′-GGGAATTCCATATGGCCAGCAGAGGCGTAAACAAG-3′) and the reverse (5′-CCCGCTCGAGGAACGGGATGTCGTCGTCGAAGTCCAT-3′) primers were designed to introduce unique *Nde*I and *Xho*I restriction sites (underlined) into *Kp*SSB, permitting the insertion of the amplified gene into the pET21b vector (Novagen Inc., Madison, WI, USA) for the protein expression in *E. coli*. *E. coli* cells were transformed with the expression vector and grown to OD_{600} of 0.9 at 37 °C in Luria-Bertani medium containing 250 μg/mL ampicillin. Overexpression of *Kp*SSB construct was induced with 1 mM isopropyl thiogalactoside for 3 h at 37 °C. The cells overexpressing the protein were chilled on ice, harvested by centrifugation, resuspended in Buffer A (20 mM Tris–HCl, 5 mM imidazole, 0.5 M NaCl; pH 7.9) and disrupted by sonication with ice cooling between pulses. The *Kp*SSB protein was then purified from the soluble supernatant by Ni^{2+} affinity chromatography (HiTrap HP; GE Healthcare Bio-Sciences, Piscataway, NJ, USA). Protein purity remained >95% as determined by Coomassie-stained SDS-PAGE.

Gel-filtration chromatography

Gel-filtration chromatography was carried out by the same protocol as previously described for DnaD using an AKTA-FPLC system (Huang *et al.* 2008). Briefly, purified *Kp*SSB in buffer (0.1 M NaCl and 20 mM Tris–HCl at pH 8.0) was applied to a Superdex 200 HR 10/30 column (GE Healthcare Bio-Sciences) equilibrated with the same buffer. The column was operated at a flow rate of 0.5 mL/min, and 0.5-mL fractions were collected. The proteins were detected by measuring absorbance at 280 nm. The column was calibrated with proteins of known molecular masses: γ-globulin (158 kDa), albumin (67 kDa), ovalbumin (43 kDa), chymotrypsinogen A (25 kDa) and ribonuclease A (13.7 kDa).

Fluorescence measurement

Fluorescence titrations were carried out in a spectrofluorimeter (Hitachi F-2700; Hitachi High-Technologies, Tokyo, Japan) as described previously (Curth *et al.* 1993; Chan *et al.* 2009; Olszewski *et al.* 2010; Chen & Huang 2011; Huang *et al.* 2011; Jan *et al.* 2011). The excitation and emission of tryptophan fluorescence were detected at 295 and 348 nm, respectively. The *Kp*SSB solution (0.1 μM; tetramer) in 2 mL Tris–HCl buffer (20 mM Tris–HCl, and pH 8.0) containing 20 or 300 mM NaCl was titrated with rising quantities of dT50 oligonucleotide. After the addition of the ssDNA, the complex solution was equilibrated for 300 s until no fluorescence change could be observed. The tryptophan fluorescence quenching is used to measure the diminution of fluorescence between the ssDNA-free and the ssDNA-bound proteins. The ssDNA-binding-site size (n) was analyzed by the ssDNA-binding curve using the model of Schwarz & Watanabe (1983).

Gel shifts

Various lengths of ssDNA oligonucleotides were custom-synthesized by MdBio, Inc. (Frederick, MD, USA). Radiolabeling was carried out with [γ^{32}P]ATP (6000 Ci/mmol; PerkinElmer Life Sciences) and T4 polynucleotide kinase (Promega, Madison, WI, USA). *Kp*SSB (0, 19, 37, 77, 155, 310, 630, 1250, 2500 and 5000 nM) was incubated for 30 min at 25 °C with 1.7 nM DNA substrates (dT15–75) in a total volume of 10 μL in 20 mM Tris–HCl pH 8.0 and 100 mM NaCl. Aliquots (5 μL) were removed from each reaction solution and added to 2 μL of gel-loading solution (0.25% bromophenol blue and 40% sucrose). The resulting samples were resolved on a native 8% polyacrylamide gel at 4 °C in TBE buffer (89 mM Tris borate and 1 mM EDTA) for 1 h at 100 V and visualized by autoradiography. Complexed and free DNA bands were scanned and quantified. The binding dissociation constants for the *Kp*SSB–ssDNA complex 1 (K_{d1}) were estimated from the protein concentration that binds 50% of the input DNA (Liu *et al.* 2004; Huang *et al.* 2006, 2011; Tsai *et al.* 2006, 2007; Hsieh & Huang 2011; Jan *et al.* 2011); the binding dissociation constants for the *Kp*SSB–ssDNA complex 2 (K_{d2}) were estimated from the protein concentration that forms 50% of the complex 2. In this report, each K_d is calculated as the average of at least three measurements ± SD.

Site-directed mutagenesis

The *Kp*SSB mutants were generated according to the QuikChange Site-Directed Mutagenesis kit protocol (Stratagene, LaJolla, CA, USA), using the wild-type plasmid pET21b-*Kp*SSB as a template and the forward (5′-TGGTGAGTATCTGNNNAAAGGCTCTCA-3′) and the reverse (5′-TGAGAGCCTTTNNNCAGATACTCACCA-3′) primers

for the R73 mutants, and the forward (5′-CTGCGTAAA GGCNNNCAGGTGTACATT-3′) and the reverse (5′-AAT GTACACCTGNNNGCCTTTACGCAG-3′) primers for the S76 mutants, respectively. The presence of the mutation was verified by DNA sequencing.

Acknowledgements

We would like to thank two anonymous reviewers and the editor for their comments. This research was supported by a grant from the National Research Program for Genome Medicine (NSC 100-3112-B-040-001 to C.Y. Huang).

References

Bush, K. (2010) Alarming beta-lactamase-mediated resistance in multidrug-resistant *Enterobacteriaceae*. *Curr. Opin. Microbiol.* **13**, 558–564.

Casas-Finet, J.R., Fischer, K.R. & Karpel, R.L. (1992) Structural basis for the nucleic acid binding cooperativity of bacteriophage T4 gene 32 protein: the $(Lys/Arg)_3(Ser/Thr)_2$ (LAST) motif. *Proc. Natl Acad. Sci. USA* **89**, 1050–1054.

Chan, K.W., Lee, Y.J., Wang, C.H., Huang, H. & Sun, Y.J. (2009) Single-stranded DNA-binding protein complex from *Helicobacter pylori* suggests an ssDNA-binding surface. *J. Mol. Biol.* **388**, 508–519.

Chen, C.C. & Huang, C.Y. (2011) Inhibition of *Klebsiella pneumoniae* DnaB helicase by the flavonol galangin. *Protein J.* **30**, 59–65.

Curth, U., Genschel, J., Urbanke, C. & Greipel, J. (1996) In vitro and in vivo function of the C-terminus of *Escherichia coli* single-stranded DNA binding protein. *Nucleic Acids Res.* **24**, 2706–2711.

Curth, U., Greipel, J., Urbanke, C. & Maass, G. (1993) Multiple binding modes of the single-stranded DNA binding protein from *Escherichia coli* as detected by tryptophan fluorescence and site-directed mutagenesis. *Biochemistry* **32**, 2585–2591.

Dabrowski, S., Olszewski, M., Piatek, R., Brillowska-Dabrowska, A., Konopa, G. & Kur, J. (2002) Identification and characterization of single-stranded-DNA-binding proteins from *Thermus thermophilus* and *Thermus aquaticus* – new arrangement of binding domains. *Microbiology* **148**, 3307–3315.

Fedorov, R., Witte, G., Urbanke, C., Manstein, D.J. & Curth, U. (2006) 3D structure of *Thermus aquaticus* single-stranded DNA-binding protein gives insight into the functioning of SSB proteins. *Nucleic Acids Res.* **34**, 6708–6717.

Haseltine, C.A. & Kowalczykowski, S.C. (2002) A distinctive single-strand DNA-binding protein from the Archaeon *Sulfolobus solfataricus*. *Mol. Microbiol.* **43**, 1505–1515.

Hsieh, H.C. & Huang, C.Y. (2011) Identification of a novel protein, PriB, in *Klebsiella pneumoniae*. *Biochem. Biophys. Res. Commun.* **404**, 546–551.

Huang, C.Y., Chang, Y.W. & Chen, W.T. (2008) Crystal structure of the N-terminal domain of *Geobacillus kaustophilus* HTA426 DnaD protein. *Biochem. Biophys. Res. Commun.* **375**, 220–224.

Huang, C.Y., Hsu, C.H., Sun, Y.J., Wu, H.N. & Hsiao, C.D. (2006) Complexed crystal structure of replication restart primosome protein PriB reveals a novel single-stranded DNA-binding mode. *Nucleic Acids Res.* **34**, 3878–3886.

Huang, Y.H., Lee, Y.L. & Huang, C.Y. (2011) Characterization of a single-stranded DNA binding protein from *Salmonella enterica* Serovar Typhimurium LT2. *Protein J.* **30**, 102–108.

Jan, H.C., Lee, Y.L. & Huang, C.Y. (2011) Characterization of a single-stranded DNA-binding protein from *Pseudomonas aeruginosa* PAO1. *Protein J.* **30**, 20–26.

Kerr, I.D., Wadsworth, R.I., Cubeddu, L., Blankenfeldt, W., Naismith, J.H. & White, M.F. (2003) Insights into ssDNA recognition by the OB fold from a structural and thermodynamic study of *Sulfolobus* SSB protein. *EMBO J.* **22**, 2561–2570.

Kozlov, A.G., Cox, M.M. & Lohman, T.M. (2010) Regulation of single-stranded DNA binding by the C termini of *Escherichia coli* single-stranded DNA-binding (SSB) protein. *J. Biol. Chem.* **285**, 17246–17252.

Larkin, M.A., Blackshields, G., Brown, N.P., Chenna, R., McGettigan, P.A., McWilliam, H., Valentin, F., Wallace, I.M., Wilm, A., Lopez, R., Thompson, J.D., Gibson, T.J. & Higgins, D.G. (2007) Clustal W and Clustal X version 2.0. *Bioinformatics* **23**, 2947–2948.

Liu, J.H., Chang, T.W., Huang, C.Y., Chen, S.U., Wu, H.N., Chang, M.C. & Hsiao, C.D. (2004) Crystal structure of PriB, a primosomal DNA replication protein of *Escherichia coli*. *J. Biol. Chem.* **279**, 50465–50471.

Lohman, T.M. & Ferrari, M.E. (1994) *Escherichia coli* single-stranded DNA-binding protein: multiple DNA-binding modes and cooperativities. *Annu. Rev. Biochem.* **63**, 527–570.

Madden, T.L., Tatusov, R.L. & Zhang, J. (1996) Applications of network BLAST server. *Methods Enzymol.* **266**, 131–141.

Murzin, A.G. (1993) OB(oligonucleotide/oligosaccharide binding)-fold: common structural and functional solution for non-homologous sequences. *EMBO J.* **12**, 861–867.

Oakley, G.G. & Patrick, S.M. (2010) Replication protein A: directing traffic at the intersection of replication and repair. *Front. Biosci.* **15**, 883–900.

Olszewski, M., Grot, A., Wojciechowski, M., Nowak, M., Mickiewicz, M. & Kur, J. (2010) Characterization of exceptionally thermostable single-stranded DNA-binding proteins from *Thermotoga maritima* and *Thermotoga neapolitana*. *BMC Microbiol.* **10**, 260.

Olszewski, M., Mickiewicz, M. & Kur, J. (2008) Two highly thermostable paralogous single-stranded DNA-binding proteins from *Thermoanaerobacter tengcongensis*. *Arch. Microbiol.* **190**, 79–87.

Raghunathan, S., Kozlov, A.G., Lohman, T.M. & Waksman, G. (2000) Structure of the DNA binding domain of *E. coli* SSB bound to ssDNA. *Nat. Struct. Biol.* **7**, 648–652.

Reyes-Lamothe, R., Sherratt, D.J. & Leake, M.C. (2010) Stoichiometry and architecture of active DNA replication machinery in *Escherichia coli*. *Science* **328**, 498–501.

Roy, R., Kozlov, A.G., Lohman, T.M. & Ha, T. (2007) Dynamic structural rearrangements between DNA binding modes of *E. coli* SSB protein. *J. Mol. Biol.* **369**, 1244–1257.

Roy, R., Kozlov, A.G., Lohman, T.M. & Ha, T. (2009) SSB protein diffusion on single-stranded DNA stimulates RecA filament formation. *Nature* **461**, 1092–1097.

Saikrishnan, K., Jeyakanthan, J., Venkatesh, J., Acharya, N., Sekar, K., Varshney, U. & Vijayan, M. (2003) Structure of *Mycobacterium tuberculosis* single-stranded DNA-binding protein. Variability in quaternary structure and its implications. *J. Mol. Biol.* **331**, 385–393.

Saikrishnan, K., Manjunath, G.P., Singh, P., Jeyakanthan, J., Dauter, Z., Sekar, K., Muniyappa, K. & Vijayan, M. (2005) Structure of *Mycobacterium smegmatis* single-stranded DNA-binding protein and a comparative study involving homologous SSBs: biological implications of structural plasticity and variability in quaternary association. *Acta Crystallogr. D Biol. Crystallogr.* **61**, 1140–1148.

Sauer, R.T. & Baker, T.A. (2011) AAA+ proteases: ATP-fueled machines of protein destruction. *Annu. Rev. Biochem.* **80**, 587–612.

Savvides, S.N., Raghunathan, S., Futterer, K., Kozlov, A.G., Lohman, T.M. & Waksman, G. (2004) The C-terminal domain of full-length *E. coli* SSB is disordered even when bound to DNA. *Protein Sci.* **13**, 1942–1947.

Schwarz, G. & Watanabe, F. (1983) Thermodynamics and kinetics of co-operative protein-nucleic acid binding. I. General aspects of analysis of data. *J. Mol. Biol.* **163**, 467–484.

Shereda, R.D., Kozlov, A.G., Lohman, T.M., Cox, M.M. & Keck, J.L. (2008) SSB as an organizer/mobilizer of genome maintenance complexes. *Crit. Rev. Biochem. Mol. Biol.* **43**, 289–318.

Sugiman-Marangos, S. & Junop, M.S. (2010) The structure of DdrB from *Deinococcus*: a new fold for single-stranded DNA binding proteins. *Nucleic Acids Res.* **38**, 3432–3440.

Tempe, D.K. (2010) New Delhi metallo-beta-lactamase 1. *Lancet Infect. Dis.* **10**, 750–751; author reply 752–754.

Tsai, K.L., Huang, C.Y., Chang, C.H., Sun, Y.J., Chuang, W.J. & Hsiao, C.D. (2006) Crystal structure of the human FOXK1a-DNA complex and its implications on the diverse binding specificity of winged helix/forkhead proteins. *J. Biol. Chem.* **281**, 17400–17409.

Tsai, K.L., Sun, Y.J., Huang, C.Y., Yang, J.Y., Hung, M.C. & Hsiao, C.D. (2007) Crystal structure of the human FOXO3a-DBD/DNA complex suggests the effects of post-translational modification. *Nucleic Acids Res.* **35**, 6984–6994.

Wang, C.C., Tsau, H.W., Chen, W.T. & Huang, C.Y. (2010) Identification and characterization of a putative dihydroorotase, KPN01074, from *Klebsiella pneumoniae*. *Protein J.* **29**, 445–452.

Witte, G., Fedorov, R. & Curth, U. (2008) Biophysical analysis of *Thermus aquaticus* single-stranded DNA binding protein. *Biophys. J.* **94**, 2269–2279.

Witte, G., Urbanke, C. & Curth, U. (2003) DNA polymerase III chi subunit ties single-stranded DNA binding protein to the bacterial replication machinery. *Nucleic Acids Res.* **31**, 4434–4440.

Witte, G., Urbanke, C. & Curth, U. (2005) Single-stranded DNA-binding protein of *Deinococcus radiodurans*: a biophysical characterization. *Nucleic Acids Res.* **33**, 1662–1670.

Wold, M.S. (1997) Replication protein A: a heterotrimeric, single-stranded DNA-binding protein required for eukaryotic DNA metabolism. *Annu. Rev. Biochem.* **66**, 61–92.

Yang, C., Curth, U., Urbanke, C. & Kang, C. (1997) Crystal structure of human mitochondrial single-stranded DNA binding protein at 2.4 A resolution. *Nat. Struct. Biol.* **4**, 153–157.

Received: 20 September 2011
Accepted: 12 November 2011

Biosci. Biotechnol. Biochem., **76** (6), 1110–1115, 2012

A Single Residue Determines the Cooperative Binding Property of a Primosomal DNA Replication Protein, PriB, to Single-Stranded DNA

Yen-Hua HUANG,[1] Hsin-Hsien LIN,[1] and Cheng-Yang HUANG[1,2,†]

[1]*Department of Biomedical Sciences, Chung Shan Medical University, No. 110, Sec. 1, Chien-Kuo North Road, Taichung City, Taiwan*
[2]*Department of Medical Research, Chung Shan Medical University Hospital, No. 110, Sec. 1, Chien-Kuo North Road, Taichung City, Taiwan*

Received December 7, 2011; Accepted February 29, 2012; Online Publication, June 23, 2012
[doi:10.1271/bbb.110938]

PriB is a primosomal protein required for re-initiation of replication in bacteria. We characterized and compared the DNA-binding properties of PriB from *Salmonella enterica* serovar Typhimurium LT2 (*St*PriB) and *Escherichia coli* (*Ec*PriB). Only one residue of *Ec*PriB, V6, was different in *St*PriB (replaced by A6). Previous structural information revealed that this residue is located on the putative dimer-dimer interface of PriB and is not involved in single-stranded DNA (ssDNA) binding. The cooperative binding mechanism of *St*PriB to DNA is, however, very different from that of *Ec*PriB. Unlike *Ec*PriB, which forms a single complex with ssDNAs of various lengths, *St*PriB forms two or more distinct complexes. Based on these results, as well as information on structure, binding modes for forming a stable complex of PriB with ssDNA of 25 nucleotides (nt), $(EcPriB)_{25}$, and $(StPriB)_{25}$ are proposed.

Key words: PriB; PriA; primosome; single-stranded DNA (ssDNA) binding; ssDNA-binding protein (SSB)

In the maintenance of genetic integrity after DNA damage, reactivation of stalled DNA replication at the forks, mediated by a replication restart primosome, is essential for bacterial survival.[1–4] In *Escherichia coli*, the replication restart primosome includes seven essential proteins (PriA helicase, PriB, PriC, DnaB helicase, DnaC, DnaT, and DnaG primase).[5,6] There are two overlapping mechanisms for reassembly of the replication forks: initiation is induced by either PriA helicase or PriC.[7,8] In a PriA-PriB-DnaT-dependent reaction, PriB is the second protein to be assembled in the protein-DNA complex, where it then stimulates PriA helicase activity.[9,10] Recent studies have indicated that there may be more than one PriA-PriB complex involved in the initiation of primosome formation, and that the effect of PriB on the PriA-DNA association is dependent on DNA structure.[11] PriB also facilitates the association of DnaT with PriA.[12] How PriA-PriB-DnaT participates in reloading the DnaC-DnaB complex and the formation of the DnaB-DnaG complex at the forks remains unclear.

PriB is a homodimer with 104-amino acid (aa) polypeptide chains,[13–16] in which each PriB monomer has an oligonucleotide/oligosaccharide-binding (OB) fold structure.[17,18] PriB shares structural similarity with the DNA-binding domain of the *Escherichia coli* single-stranded DNA (ssDNA)-binding protein (*Ec*SSB),[15,16,19,20] but they probably differ in their ssDNA-binding modes.[21,22] PriB can bind to ssDNA,[21–23] ssRNA,[16] and double-stranded DNA (dsDNA).[9] The N-terminal 1–49 aa region of PriB is crucial for dimerization, while the C-terminal 50–104 aa region is crucial for ssDNA binding.[23] Although a dimer, PriB has only one DNA-binding site,[22] located in loop L_{45} centrally within the dimer, and this site occupies 12 ± 1 nucleotides (nt) of the total site size.[21] This is just enough to fill a single DNA binding pocket of one monomer, but not long enough to wrap the nucleic acid around the protein dimer.[21,22]

Previously, we described the crystal structure of *Ec*PriB[16] and its complex with ssDNA dT15.[22] Although a single dT15 periodically interacts with two OB folds from two symmetrically related PriB dimers in the crystal, we proposed that the *in vitro* assembled cooperative complex of PriB-ssDNA-PriB mimics the ternary structure of the PriA-ssDNA-PriB complex. In fact, the positive cooperative binding of the PriB dimer to ssDNA of various lengths has been studied by comparing their Hill coefficients.[22] However, for PriB-ssDNA complexes, a cooperativity transition was found to be significant between dA25 and dA30, and not at dT15 and dA15, as in the crystal. Since the DNA used for the complex structure is short, it is not yet completely clear whether the PriB dimer can form a stable complex with dT15 in solution, or how PriB dimers cooperatively bind to and form long clusters on the nucleic acid lattice.

In the present study, we characterized and compared the ssDNA-binding properties of *Salmonella enterica* serovar Typhimurium LT2 PriB (*St*PriB) and *Ec*PriB. These two proteins share >99% aa identity: only one residue of *Ec*PriB, V6, is different in *St*PriB (replaced with A6). That is, *St*PriB can be considered a single point mutation of *Ec*PriB (V6A). One might conclude that they must be similar in structure and function,[13] but we found that their ssDNA-binding modes were very different. On the basis of the results in this study, and

† To whom correspondence should be addressed. Tel: +886-4-24730022 ext 11472; Fax: +886-4-23248187; E-mail: cyhuang@csmu.edu.tw
Abbreviations: ssDNA, single-stranded DNA; SSB, ssDNA-binding protein; EMSA, electrophoretic mobility shift analysis; nt, nucleotides; aa, amino acids; OB, oligonucleotide/oligosaccharide binding; GA, glutaraldehyde

10

Determination of the Binding Site-Size of the Protein-DNA Complex by Use of the Electrophoretic Mobility Shift Assay

Cheng-Yang Huang
Department of Biomedical Sciences, Chung Shan Medical University,
Department of Medical Research, Chung Shan Medical University Hospital,
Taichung City,
Taiwan

1. Introduction

In this chapter we describe how to perform an electrophoretic mobility shift assay (EMSA), also known as the band shift or gel retardation assay, to determine the binding site-size of the DNA binding protein using a series of DNA polymers. The binding site-size information of the DNA binding protein is a prerequisite for formulating any model of the proteins' function in DNA replication. EMSA is simple and quick, and if needed, the use of radioactive DNA make it highly sensitive and allow us to "see" the formation of distinct complexes of the DNA binding protein. The expectation of EMSA is that, once the length of the nucleotides is sufficient for the binding of protein, the protein-DNA complex remains intact and migrates as distinct band during gel electrophoresis. In addition, once the length of the nucleotides is sufficient for the binding of two or more proteins, the protein-DNA complexes migrate as distinct bands, usually referred to as a super shift: the higher the oligomeric protein-DNA complex, the lower the electrophoretic mobility. This technique can be used for both highly sequence-specific (e.g., transcription factor) (1,2) and non-specific proteins (e.g., single-stranded DNA binding protein) (3-7).

2. Some general considerations

1. Although EMSA was originally used in the detection of DNA-binding proteins in the crude cell extracts, it is thought that cell extracts contain many other DNA-binding proteins (and their regulatory proteins), and some small molecules (such as ATP and DNA metabolites), that are also able to interact with the DNA and the target protein; these molecules may cause some unpredictable effects on the reaction. Therefore, it is highly recommended to use purified protein(s) for EMSA.
2. When the studied protein has low DNA-binding activity, needs other loading factors, or binds to DNA in a strong sequence-specific way, a relatively high concentration of protein (in μM range) may be required to facilitate protein-DNA complex formation.
3. Protein binding to DNA usually needs to be in the "suitable" condition for optimal complex formation and stabilization. The conditions for the DNA binding process may

vary significantly in terms of pH, ionic strength, and necessary factors (such as metal ions or ATP).

4. When the protein-DNA interaction is highly cooperative, a particular care must be taken for determining its binding site-size by use of EMSA. If only one protein-DNA complex is visible when the DNA length is further increased (for example, to dT60 or more), it is likely inappropriate to determine its binding site-size using EMSA.

3. Experimental systems

1. Polyacrylamide gels. Differences in the size, aggregation state and pI of protein-DNA complexes will affect the choice of conditions used for EMSA. Generally, the lower percent of polyacrylamide gel will be considered for the bigger protein. Polyacrylamide gels, usually in 6-12% w/v, are made using an acrylamide to bisacrylamide weight ratio of 19:1 and TBE as the buffer in the gel and for electrophoresis.
2. Electrophoresis buffers. The process of electrophoretic separation may destabilize protein-DNA complexes, and thus the ionic strength, pH and composition of electrophoresis buffers should be adjusted to fit the need of the protein-DNA complex formation. If the binding condition for the formation of the protein-DNA complex is known, the electrophoresis buffer can be kept similar to the binding buffer. The most common buffer used in both polyacrylamide and agarose gels is TBE buffer. However, some metal-containing or metal-binding proteins should be analyzed in a buffer without EDTA. Sometimes the use of low ionic strength electrophoresis buffers at the same pH value can improve the stability of the protein-DNA complexes and the resolutions between bands; TE (10 mM Tris–HCl, 0.1 mM EDTA) or HE (10 mM HEPES, 0.1 mM EDTA) might be used in this case.
3. Sample buffers. Protein-DNA complexes are loaded on the polyacrylamide gel usually in the presence of 5-10% glycerol or sucrose. This can be included in the binding buffer or added before the protein-DNA complexes loading to the gel. Bromophenol blue and/or xylene cyanol (0.02% w/v) is usually used as an electrophoresis marker.
4. Visualization of gels. After electrophoresis, the gels are placed on filter paper, dried under vacuum at 80 ^{o}C, and then visualized by either autoradiography (exposed to X-ray film) or using a phosphorimager (exposed to the phosphor storage plate). Phosphorimaging is much more sensitive and the dynamic range is much greater than that of X-ray film. For phosphorimaging, the phosphor storage plate is scanned, and the data are digitized for quantitative analysis.

4. Determination of the binding site-size of the protein-DNA complex by use of the electrophoretic mobility shift assay: Single-stranded DNA binding protein (SSB)

Step 1. Use of a purified protein

As mentioned above, cell extracts contain many other proteins and some small molecules, able to interact with the target DNA and protein, which may cause some unpredictable effects on the DNA-binding reaction. Therefore, it is highly recommended to use purified protein(s) for EMSA. More and more proteins have become available in a pure form now, especially by using recombinant technology. The overexpression of DNA-binding proteins or their domains is essential for their purification, characterization and structure

determination. The bacterial host *E. coli* is the first choice of expression system; it is simple to use and inexpensive to culture. For example, the gene encoding the single-stranded DNA binding protein (SSB) from *Pseudomonas aeruginosa* PAO1 can be PCR-amplified from the genomic DNA (3), inserted into the pET21b vector, and the gene can be expressed in transformed *E. coli* cell by using the inducer isopropyl thiogalactoside (IPTG). *P. aeruginosa* SSB can be then purified from the soluble supernatant by Ni^{2+}-affinity chromatography (HiTrap HP; GE Healthcare Bio-Sciences, Piscataway, NJ, USA). Protein purity can be determined by Coomassie-stained SDS-PAGE.

Step 2. Preparation of protein-DNA complexes

Binding mode is not always the same for several DNA-binding proteins. For example, differences in the binding condition, such as the ionic strength, pH and some small molecules included in the reaction mixture, can affect the binding mode of SSB (8). These factors also influence the stability of the SSB-DNA complexes in the binding reaction. For determination of the binding site-size of SSB using EMSA, various lengths of ssDNA oligonucleotides or other series of ssDNA homopolymers will be needed; radiolabeling can be carried out with [γ^{32}P]ATP (6000 Ci/mmol; PerkinElmer Life Sciences) and T4 polynucleotide kinase (Promega, Madison, WI, USA). The SSB-DNA complexes will be formed with different protein concentrations, usually at range of 10^{-9}–10^{-7} M. For *P. aeruginosa* PAO1 SSB, 0, 19, 37, 77, 155, 310, 630, 1250, 2500, and 5000 nM protein was used for the complexes formation, respectively. *P. aeruginosa* PAO1 SSB was incubated for 30 min at 25°C with 1.7 nM radioactive DNA substrates (dT15, 20, 25, 30, 35, 40, 45, 50, 55, 60, 65, 70, 75, and 80) in a total volume of 10 µL in 20 mM Tris-HCl pH 8.0 and 100 mM NaCl. The composition of the binding buffer may be adjusted to fit the need of study or the nature of the protein of interest.

Step 3. Fractionation of the SSB-DNA complexes using EMSA

Polyacrylamide or agarose gels can be used to fractionate mixture of protein-DNA complexes prior to further analysis. For *P. aeruginosa* PAO1 SSB, the complexes were formed in a total volume of 10 µL (see above), and aliquots (5 µL) were removed from each reaction solution and added to 2 µL of gel-loading solution (0.25% bromophenol blue and 40% sucrose). The resulting samples can be resolved on a native 8% polyacrylamide gel at 4 °C in TBE buffer for 1 h at 100 V and visualized by autoradiography or phosphorimaging.

Step 4. Determination of the binding site-size of protein-DNA complexes

After fractionating and phosphorimaging, complexed and free DNA bands can be visualized and quantified, and the binding site-size of DNA-protein complex can be determined. For example, various lengths of radioactive ssDNA oligonucleotides d(T5)n were complexed with SSB and with different protein concentrations. If the DNA space (length) is enough, the second or third studying protein will bind to the same complex where one protein of interest has been already pre-bound. Therefore, we can calculate the length of DNA required for the second joining protein (Figure 1). For example, SSB from *Klebsiella pneumoniae* binds to short ssDNAs (dT30–50) to form a complex in which a single protein is bound to the ssDNA (Figure 2), and two proteins could bind to dT55–75 (Figure 3). The presence of an extra 5 nt in dT55, as compared with dT50, provides enough interaction space for the binding of a second SSB protein, which occupies around 27 nt ssDNA (55/2=27.5). Furthermore, three SSB proteins could bind to dT80–85 (Figure 4), which occupies around 26 nt ssDNA per SSB protein (80/3=26.7). Thus, combining together

the EMSA results with the number of the SSB-DNA (dT30–85) complexes, it can be found that the binding-site size of SSB from *Klebsiella pneumoniae* is 27 ± 1 nt, as determined using EMSA under this binding condition (Figure 5).

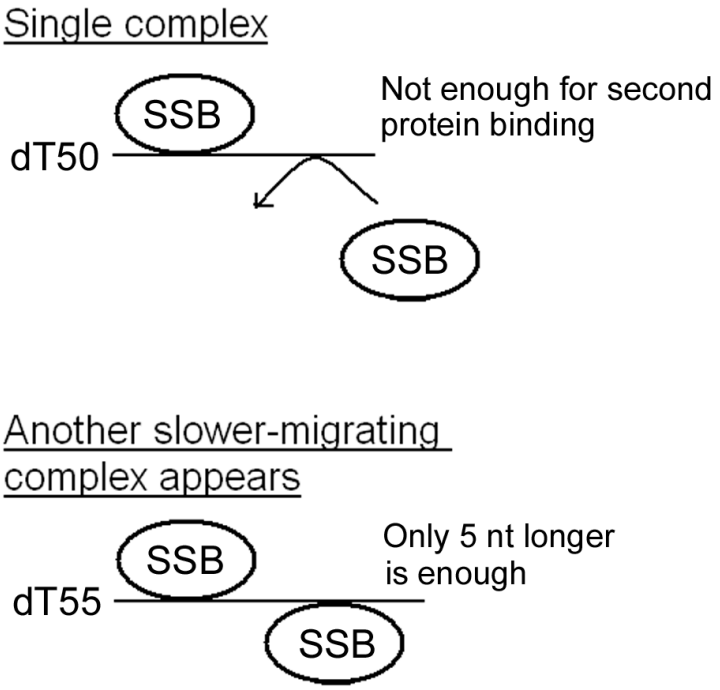

Fig. 1. Schematic model for the supershift of the SSB binding to the ssDNA. If the DNA provides enough interaction space for the binding of a second protein, we can observe another slower-migrating complex from EMSA when the protein concentration is increased.

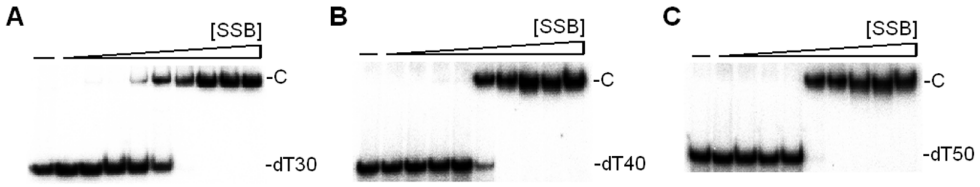

Fig. 2. Binding of *Klebsiella pneumoniae* SSB to dT30–50. The reaction solutions contained DNA substrate dT30, dT40, or dT50 and the SSB (0–5.0 μM). SSB (0, 19, 37, 77, 155, 310, 630, 1250, 2500, and 5000 nM) was incubated for 30 min at 25 °C with 1.7 nM of (A) dT30, (B) dT40, or (C) dT50 in a total volume of 10 μL in 20 mM HEPES pH 7.0 and 500 mM NaCl. Aliquots (5 μL) were removed from each reaction solution and added to 2 μL of gel-loading solution (0.25% bromophenol blue and 40% sucrose). The resulting samples were resolved on a native 8% polyacrylamide gel at 4 °C in TBE buffer (89 mM Tris borate and 1 mM EDTA) for 1 h at 100 V and visualized by autoradiography. This SSB binding to dT30–50 forms a single complex.

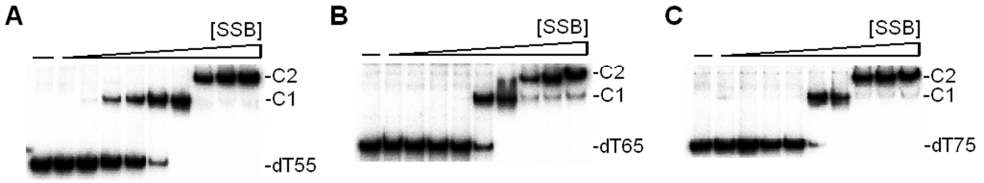

Fig. 3. Binding of *Klebsiella pneumoniae* SSB to dT55–75. The reaction solutions contained DNA substrate dT55, dT65, or dT75 and the SSB (0–5.0 μM). SSB (0, 19, 37, 77, 155, 310, 630, 1250, 2500, and 5000 nM) was incubated for 30 min at 25 °C with 1.7 nM of (A) dT55, (B) dT65, or (C) dT75 in a total volume of 10 μL in 20 mM HEPES pH 7.0 and 500 mM NaCl. Aliquots (5 μL) were removed from each reaction solution and added to 2 μL of gel-loading solution (0.25% bromophenol blue and 40% sucrose). The resulting samples were resolved on a native 8% polyacrylamide gel at 4 °C in TBE buffer (89 mM Tris borate and 1 mM EDTA) for 1 h at 100 V and visualized by autoradiography. This SSB binding to dT55–75 forms two different complexes.

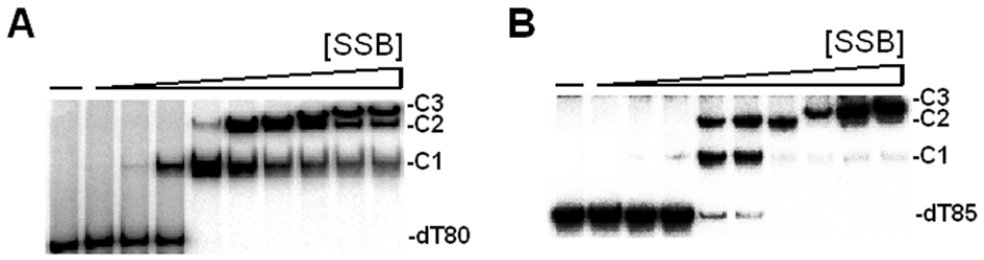

Fig. 4. Binding of *Klebsiella pneumoniae* SSB to dT80–85. The reaction solutions contained DNA substrate dT80 or dT85 and the SSB (0–5.0 μM). SSB (0, 19, 37, 77, 155, 310, 630, 1250, 2500, and 5000 nM) was incubated for 30 min at 25 °C with 1.7 nM of (A) dT80 or (B) dT85 in a total volume of 10 μL in 20 mM HEPES pH 7.0 and 500 mM NaCl. Aliquots (5 μL) were removed from each reaction solution and added to 2 μL of gel-loading solution (0.25% bromophenol blue and 40% sucrose). The resulting samples were resolved on a native 8% polyacrylamide gel at 4 °C in TBE buffer (89 mM Tris borate and 1 mM EDTA) for 1 h at 100 V and visualized by autoradiography. This SSB binding to either dT80 or dT85 forms three different complexes.

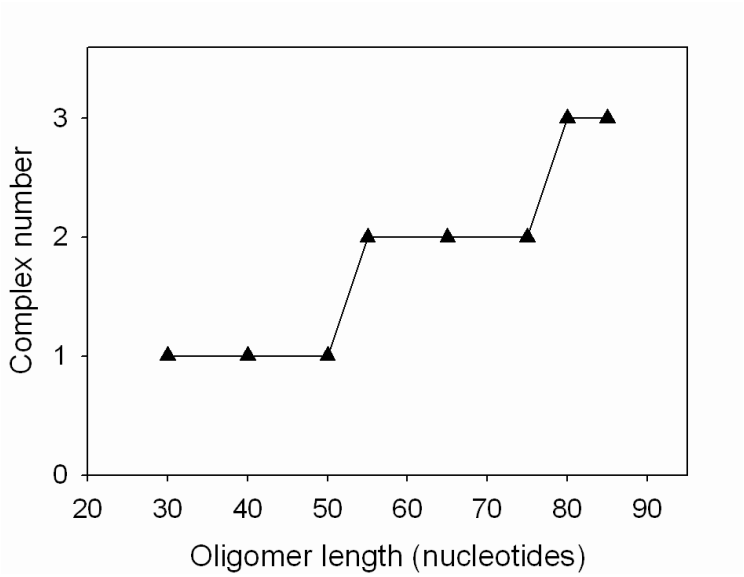

Fig. 5. Complex number of *Klebsiella pneumoniae* SSB as a function of the length of the ssDNA determined using EMSA. The binding site-size of other DNA-binding protein may also be determined using a similar protocol.

Step 5. Estimation of the apparent dissociation constants

In addition to the binding site-size, EMSA can also be used to estimate the apparent dissociation constants for the protein-DNA complexes when the protein concentration is known accurately and the used DNA is at low concentrations. If the DNA concentration is much lower than the apparent dissociation constant, its value will be equal to the protein concentration needed to have 50% of protein-DNA complex formed. The radio-intensity of free DNA and each protein-DNA complex, with increasing amounts of the protein, can be scanned and quantified by using phosphorimaging. For example, using *Salmonella enterica* serovar Typhimurium LT2 SSB (4), the apparent dissociation constant for the SSB-ssDNA complex 1 (K_{d1}) was estimated from the protein concentration that binds 50% of the input DNA; the apparent dissociation constant for the SSB-ssDNA complex 2 (K_{d2}) was estimated from the protein concentration that forms 50% of the complex 2, and K_{dn} could be also calculated in a similar manner if multiple complexes are formed.

Step 6. Analysis of oligomeric state by gel filtration chromatography

We have previously described how to determine the binding-site size of DNA-binding protein like SSB. Information about the oligomeric state of protein of interest may also be important for analysis of its binding mode. Assuming that the protein has a shape and partial specific volume similar to the standard proteins, the native molecular mass of the protein can be estimated and compared with its predicted mass in monomer from the amino acid sequence. For example, the native molecular mass for *S. enterica* serovar Typhimurium LT2 SSB is approximately 4.1 times the molecular mass of a *St*SSB monomer, and thus *S. enterica* serovar Typhimurium LT2 SSB in solution is a tetramer.

5. Conclusion

Development of more targeted drugs or antibiotics against many pathogenic bacteria has been hampered due to the lack of knowledge of DNA replication and the overall molecular biology of the organisms. For example, *K. pneumoniae* used here is a ubiquitous opportunistic pathogen that colonizes at the mucosal surfaces in humans and causes severe diseases; many clinical strains of *K. pneumoniae* are highly resistant to antibiotics. Since SSB is required for DNA replication, blocking the activity of SSB would be detrimental to bacterial survival. A characteristic of any protein-nucleic acid complex is its "site size", i.e. the average number of nucleotide residues occluded by the bound protein. Here we describe how to determine the binding-site size of DNA-binding protein using EMSA in different binding conditions. The information obtained through the use of this methodology may be very helpful in studying the binding mode(s) of DNA-binding protein. However, a particular care must be taken when the DNA-binding protein of interest binds to DNA with high cooperativity, as like PriB. If only one protein-DNA complex is visible when the length of the DNA is further increased (for example, to dT60 or more), it is likely inappropriate to determine its binding site-size using EMSA.

6. Acknowledgement

This work was supported by a grant from the National Research Program for Genome Medicine (NSC 100-3112-B-040-001 to C.Y. Huang).

7. Experimental protocol

Determination of the binding site-size of SSB (or other DNA-binding protein)

Equipment and reagents

- 30% acrylamide/bis- acrylamide stock solution
- Binding buffer: 20 mM Tris–HCl, pH 8.0, 100 mM NaCl. The composition of the binding buffer may be adjusted to fit the particular study or the nature of the studied protein
- Various lengths of ssDNA homopolymers. The duplex DNA can be used for other DNA-binding protein
- [γ^{32}P]ATP solution at 10mCi/mL, specific activity 3000 Ci/mmol
- T4 polynucleotide kinase
- Purified SSB protein
- Loading buffer: 0.25% bromophenol blue and 40% sucrose
- TBE buffer (89 mM Tris borate and 1 mM EDTA)
- Vertical electrophoresis system and a power pack

Experimental method

1. Phosphorylate the ssDNA homopolymers of varying length in 10 µL of T4 polynucleotide kinase buffer (70 mM Tris–HCl, pH 7.6, 10 mM $MgCl_2$, 5 mM dithiothreitol) supplemented with 1 µL of [γ^{32}P]ATP and 1 µL of T4 polynucleotide kinase. Incubate at 37 ^{o}C for 1 h.
2. Dilute radiolabeled DNA substrates to suitable concentration (for example, 1–10 nM; for determination of the apparent dissociation constant) using binding buffer.

3. Incubate radiolabeled DNA substrates with different concentrations of protein, respectively, for 30 min at 25 °C, in a total volume of 10 μL in binding buffer.
4. Remove aliquots (5 μL) from each reaction solution and add it to 2 μL of loading buffer and load on a native 8% polyacrylamide gel at 4°C in TBE buffer for 1–2 h at 100 V, depending on the length of DNA.
5. Dry the gel under vacuum and autoradiograph.
6. Summarize the number of DNA-protein complexes formation for each length of DNA used.
7. Evaluate DNA length required for two and three complexes formation.
8. Calculate the length (the binding site-size) needed for one protein binding.

8. References

[1] Tsai, K. L., Sun, Y. J., Huang, C. Y., Yang, J. Y., Hung, M. C., and Hsiao, C. D. (2007) *Nucleic Acids Res* 35, 6984-6994
[2] Tsai, K. L., Huang, C. Y., Chang, C. H., Sun, Y. J., Chuang, W. J., and Hsiao, C. D. (2006) *J Biol Chem* 281, 17400-17409
[3] Jan, H. C., Lee, Y. L., and Huang, C. Y. (2011) *Protein J* 30, 20-26
[4] Huang, Y. H., Lee, Y. L., and Huang, C. Y. (2011) *Protein J* 30, 102-108
[5] Hsieh, H. C., and Huang, C. Y. (2011) *Biochem Biophys Res Commun* 404, 546-551
[6] Huang, C. Y., Hsu, C. H., Sun, Y. J., Wu, H. N., and Hsiao, C. D. (2006) *Nucleic Acids Res* 34, 3878-3886
[7] Liu, J. H., Chang, T. W., Huang, C. Y., Chen, S. U., Wu, H. N., Chang, M. C., and Hsiao, C. D. (2004) *J Biol Chem* 279, 50465-50471
[8] Lohman, T. M., and Ferrari, M. E. (1994) *Annu Rev Biochem* 63, 527-570

國科會補助專題研究計畫項下出席國際學術會議心得報告

日期：101 年 10 月 30 日

計畫編號	NSC 100－3112－B－040－001		
計畫名稱	抑制克雷伯氏菌複製叉重啟活性之研究		
出國人員 姓名	黃晟洋	服務機構 及職稱	中山醫學大學/生物醫學科學系/ 副教授
會議時間	101 年 06 月 20 日 至 101 年 06 月 22 日	會議地點	日本/名古屋
會議名稱	（中文）第 12 回日本蛋白質科學年會 （英文）The 12th Annual Meeting of the Protein Science Society of Japan		
發表論文 題目	(中文)克雷白氏肺炎桿菌的 PriB 蛋白質：驗證、結晶結構以及 DNA 結合模式 (英文) The *Klebsiella pneumoniae* primosomal PriB protein: identification, crystal structure, and DNA binding mode		

一、參加會議經過

The 12th Annual Meeting of the Protein Science Society of Japan was held from Jun 20 to 22, 2012 in Nagoya, Japan. As the meeting is mainly based on biophysics for the main shaft, so lots of the participating researchers are in the fields of macromolecular interactions in which I am rather interested. In the lecture sections of Prof. Toshiya Endo, Prof. Hidekazu Hiroaki, and Prof. Nobutoshi Ito, I am deeply attracted to learn more about new and efficient strategies to develop my research scenario. I also contributed a post presentation (1P-023) at Day 1 (June 20). The title is “The *Klebsiella pneumoniae* primosomal PriB protein: identification, crystal structure, and DNA binding mode.”

二、與會心得

I would briefly elucidate those summaries of my most impressive lectures as following:

1). The talk by Dr. Toshiya Endo, entitled “Protein dynamics and cellular functions”, discusses the latest topics of in vivo protein science in perspective of dynamic cellular protein systems. Proteins mediate cellular functions by forming functional networks involving membranes. Conventional in vitro protein science on purified proteins is developing into in vivo protein science aiming at understanding protein biogenesis, traffic, and quality control in contexts of organelles and cells.

2). The talk by Dr. Daisuke Kohda, entitled “Structural biology in the YouTube Era”, discusses how YouTube affects the studies of structural biology. In efforts to create vivid pictures of biomolecules in cells, the observation of a single molecule along a time axis, or the structural data as a function of time in the case of an ensemble of Avogadro’s number molecules is highly desirable. The talk focuses on a next generation of structural biology in the “YouTube” era.

3). The talk by Dr. Takeshi Iwatsubo, entitled “The alpha-helical structure of the hydrophilic loop 1 of presenilin 1 contributes to the formation of the substrate binding site.”, mainly focuses on a molecular insight into the hydrophilic loop 1 forming the active site within of presenilin 1 (PS1). gamma-Secretase is an intramembrane-cleaving aspartyl protease that endoproteolyzes a scissile bond within the transmembrane domain (TMD) of the substrates. They have analyzed the structure of PS1, the catalytic subunit of gamma-secretase, by substituted cysteine accessibility method (SCAM). PS1 harbors a hydrophilic catalytic pore structure formed by TMD1, 6, 7, and 9 within membrane. In this talk, they analyzed the structure and function of the hydrophilic loop 1 of PS1 by SCAM. Essentially all residues in hydrophilic loop 1 reside in the hydrophilic environment. However, residues at C-terminal region of hydrophilic loop 1 showed low or high water accessibility in every three or four residues. Circular dichroism spectrometric analysis revealed that hydrophilic loop 1contained the alpha-helix structure. Intriguingly, introduction of proline substitutions to disrupt the helix structure of hydrophilic loop 1 diminished the formation of the substrate binding site in PS1. These data suggest that hydrophilic loop 1 of PS1 forms a short alpha-helical structure that contributes to the formation of the substrate binding site of the gamma-secretase.

4). The talk by Dr. 荒牧 峻彦, a direct competitive researcher with our project, emphasizes PriC can bind to not only ssDNA, but also dsDNA. I did not understand his whole study, because his talk was in Japanese. Since his team has investigated PriC’s function, we must avoid to studying the same story as those. I think that PriC possesses this novel DNA binding activity that would rewrite the mechanism of the primosome assembly.

5). The talk by Dr. Wataru Nishii, entitled “Redox switch of Lon protease in a facultative anaerobe”, provides the information about how the redox switch regulates the activity of Lon protease. The E. coli ATP-dependent Lon protease rapidly degrades damaged proteins and certain regulatory proteins, thus playing pivotal roles in cellular stress responses. However, the enzyme is harmful unless controlled due to its unwanted activity toward cellular proteins. In this talk, they showed that the enzyme activity is posttranslationally controlled by redox. Under reducing conditions, the enzyme adopts the reduced form, of which activity is weak and strictly regulated by the amount of ATP and protein substrate. When oxidative stress is elevated, the enzyme reversibly transforms into the oxidized form having much higher (5-19 times) and rather deregulated activity through the intramolecular disulfide bond formation.

三、攜回資料名稱及內容

The 12th Annual Meeting of the Protein Science Society of Japan abstracts book.

所發表之論文全文或摘要

ID: 1P-023

The Klebsiella pneumoniae primosomal PriB protein: identification, crystal structure, and DNA binding mode

Huang, Cheng-Yang*, Huang, Yen-Hua
Biomed. Sci., Chung Shan Med. Univ.

PriB is a primosomal protein required for the re-initiation of replication in bacteria. Previously, we characterized the 55-aa PriB in *Klebsiella pneumoniae* (KPN04595), which is much shorter in length than the well-studied *Escherichia coli* PriB (EcPriB). In the present study, gene expression of the real PriB (104 aa) in *K. pneumoniae* (KpPriB) was identified, and the gene product was characterized by crystal structural and functional analyses. Quantitative-polymerase chain reaction analysis indicated that the 104-aa *priB* was expressed in *K. pneumoniae* with the C_T value of 22.40. Crystal structure of KpPriB, determined at a resolution of 2.1, was similar to that of EcPriB; the largest difference was found in their L_{45} loops. KpPriB formed a single complex with ssDNA of different lengths, suggesting a highly cooperative process. Furthermore, we also found that KpPriB can bind dsDNA and dsDNA containing either $5'$ or $3'$ ssDNA overhang. Structure-based mutational analysis revealed that substitution at K18, F42, R44, W47, K82, K84, or K89 (but not R34) in KpPriB had a great effect on ssDNA binding. On the basis of these findings, the structure-function relationships and DNA binding mode of PriB was proposed and discussed.

cyhuang

寄件者: "第12回日本蛋白質科学会年会事務局" <pssj2012@aeplan.co.jp>
收件者: <cyhuang@csmu.edu.tw>
傳送日期: 2012年4月26日 上午 09:06
主旨: 【蛋白質科学会 PSSJ2012】採択通知/Acceptance notice
Huang Cheng-Yang 先生

このたびは本年会に演題をご投稿いただき
大変ありがとうございました。
Thank you for your abstract submission for PSSJ2012

登録番号/Registration Number：20032
演題名/Title：The Klebsiella pneumoniae primosomal PriB protein: identification, crystal structure, and DNA binding mode

上記演題は採択されましたので、ご連絡申し上げます。
You have been selected as a speaker of Poster.
Please confirm the following information.

【発表要項/Poster Presentation】
●ポスター番号/Poster Number： 1P-023
(ポスター番号の見方：例 2P-001 年会2日目（6/21）の1番目のパネル)
(How to read the Poster Number: ex. 2P-001 is No.1 on Day 2(June 21))

●発表日時/ポスター作成要項
Schedule for Set-up, Display and Removal of Posters
演題番号を元に、以下のページより自身のポスター発表時間をご確認下さい。
Please confirm the schedule for your poster presentation at the website below;

【日本語ページ】
http://www.aeplan.co.jp/pssj2012/happyo.html
【English page】
http://www.aeplan.co.jp/pssj2012/en/instruction.html

●会場/Place：
4号館 白鳥ホール内/ Shirotori Hall, Bldg. 4

全体プログラムは5月下旬に、年会HPにて公開いたします。
Program will be updated on the PSSJ2012 Website in late May.

御不明な点がありましたら、ご連絡頂けますと幸いです。
以上、どうぞよろしくお願い申し上げます。
If you have any questions, please feel free to contact me.

Thank you.
Sincerely yours,

****
第12回日本蛋白質科学会年会事務局
株式会社 エー・イー企画 大阪オフィス内
〒532-0003 大阪市淀川区宮原4-4-63 新大阪千代田ビル別館9階
Tel：06-6350-7163 Fax： 06-6350-7164
e-mail:pssj2012@aeplan.co.jp
****

國科會補助計畫衍生研發成果推廣資料表

日期:2012/11/02

國科會補助計畫	計畫名稱: 抑制克雷伯氏菌複製叉重啟活性之研究
	計畫主持人: 黃晟洋
	計畫編號: 100-3112-B-040-001- 學門領域: 基因體醫學國家型研究計畫

無研發成果推廣資料

100 年度專題研究計畫研究成果彙整表

計畫主持人：黃晟洋	計畫編號：100-3112-B-040-001-
計畫名稱：抑制克雷伯氏菌複製叉重啟活性之研究	

成果項目			量化			單位	備註（質化說明：如數個計畫共同成果、成果列為該期刊之封面故事...等）
			實際已達成數（被接受或已發表）	預期總達成數(含實際已達成數)	本計畫實際貢獻百分比		
國內	論文著作	期刊論文	0	0	100%	篇	
		研究報告/技術報告	0	0	100%		
		研討會論文	4	4	100%		
		專書	0	0	100%		
	專利	申請中件數	0	0	100%	件	
		已獲得件數	0	0	100%		
	技術移轉	件數	0	0	100%	件	
		權利金	0	0	100%	千元	
	參與計畫人力（本國籍）	碩士生	2	2	100%	人次	
		博士生	0	0	100%		
		博士後研究員	0	0	100%		
		專任助理	2	2	100%		
國外	論文著作	期刊論文	4	4	100%	篇	本人皆為通訊作者,第一作者皆為本實驗室學生；無任何共同貢獻作者
		研究報告/技術報告	0	0	100%		
		研討會論文	1	1	100%		
		專書	1	1	100%	章/本	一個章節； 本人為單一作者
	專利	申請中件數	0	0	100%	件	
		已獲得件數	0	0	100%		
	技術移轉	件數	0	0	100%	件	
		權利金	0	0	100%	千元	
	參與計畫人力（外國籍）	碩士生	0	0	100%	人次	
		博士生	0	0	100%		
		博士後研究員	0	0	100%		
		專任助理	0	0	100%		

其他成果 (無法以量化表達之成果如辦理學術活動、獲得獎項、重要國際合作、研究成果國際影響力及其他協助產業技術發展之具體效益事項等，請以文字敘述填列。)	無

	成果項目	量化	名稱或內容性質簡述
科教處計畫加填項目	測驗工具(含質性與量性)	0	
	課程/模組	0	
	電腦及網路系統或工具	0	
	教材	0	
	舉辦之活動/競賽	0	
	研討會/工作坊	0	
	電子報、網站	0	
	計畫成果推廣之參與（閱聽）人數	0	

國科會補助專題研究計畫成果報告自評表

請就研究內容與原計畫相符程度、達成預期目標情況、研究成果之學術或應用價值（簡要敘述成果所代表之意義、價值、影響或進一步發展之可能性）、是否適合在學術期刊發表或申請專利、主要發現或其他有關價值等，作一綜合評估。

1. 請就研究內容與原計畫相符程度、達成預期目標情況作一綜合評估

■達成目標

□未達成目標（請說明，以 100 字為限）

□實驗失敗

□因故實驗中斷

□其他原因

說明：

2. 研究成果在學術期刊發表或申請專利等情形：

論文：■已發表 □未發表之文稿 □撰寫中 □無

專利：□已獲得 □申請中 ■無

技轉：□已技轉 □洽談中 ■無

其他：(以 100 字為限)

3. 請依學術成就、技術創新、社會影響等方面，評估研究成果之學術或應用價值（簡要敘述成果所代表之意義、價值、影響或進一步發展之可能性）(以 500 字為限)

此計劃’’抑制克雷伯氏菌複製叉重啟活性之研究’’可能可以尋找出潛在的抗生素用於對抗各種細菌甚至是超級細菌,在這執行此一年期的計畫期間,目前已接受刊登 4 篇 SCI 論文與專書內章節一篇；參與的人員亦學習到各種不同層次的藥物設計法與蛋白質實驗流程；我們解出蛋白質結構,找到結合機制以及發現黃酮醇可能為一有效的 ATPase 的抑制劑